



HAL
open science

Electromagnetic modeling and characterization of anisotropic ferrite materials for microwave Isolators/Circulators

Vinod V K Thalakkatukulathil

► **To cite this version:**

Vinod V K Thalakkatukulathil. Electromagnetic modeling and characterization of anisotropic ferrite materials for microwave Isolators/Circulators. Electronics. Université de Bretagne occidentale - Brest, 2017. English. NNT: 2017BRES0134 . tel-01778053

HAL Id: tel-01778053

<https://theses.hal.science/tel-01778053>

Submitted on 25 Apr 2018

HAL is a multi-disciplinary open access archive for the deposit and dissemination of scientific research documents, whether they are published or not. The documents may come from teaching and research institutions in France or abroad, or from public or private research centers.

L'archive ouverte pluridisciplinaire **HAL**, est destinée au dépôt et à la diffusion de documents scientifiques de niveau recherche, publiés ou non, émanant des établissements d'enseignement et de recherche français ou étrangers, des laboratoires publics ou privés.



Université de Bretagne Occidentale

UNIVERSITE
BRETAGNE
LOIRE

THÈSE / UNIVERSITÉ DE BRETAGNE OCCIDENTALE

sous le sceau de l'Université Bretagne Loire

pour obtenir le titre de

DOCTEUR DE L'UNIVERSITÉ DE BRETAGNE OCCIDENTALE

Mention : Électronique

École Doctorale : Matière, Molécules et Matériaux (ED 3M)

présentée par

Vinod V K
Thalakkatukalathil

Préparée à Lab-STICC

Electromagnetic modeling and characterization of anisotropic ferrite materials for microwave Isolators/Circulators

Thèse soutenue le 15 December 2017

devant le jury composé de :

Geneviève MAZE-MERCEUR

Directeur de Recherche, CEA-CESTA, Le Barp / *Rapporteur*

Didier VINCENT

Professeur des Universités, UNIVERSITE JEAN MONNET,
Saint-Etienne / *Rapporteur*

Alexis CHEVALIER

Maître de conférences, UNIVERSITE DE BRETAGNE OCCIDENTALE,
Brest

Patrick QUEFFELEC

Professeur des Universités, UNIVERSITE DE BRETAGNE
OCCIDENTALE, Brest / *Directeur de thèse*

Acknowledgements

I would like to thank all the people who contributed in some way to the work described in this thesis. First and foremost, I would like to express my gratitude to my supervisors Patrick Qu  ff  lec and Alexis Chevalier for their trust and guidance during this thesis work. I am grateful to them for all their guidance, support and encouragement. During these years, they contributed to a rewarding doctoral school experience by giving me freedom in my work, engaging me with new ideas, and demanding high quality in all my research works. I am so glad to be part of the laboratory Lab-STICC and having the opportunity to work under their supervision.

I express my gratitude to all the members of the jury: Didier Vincent and Genevi  ve Maze-Merceur. I also extend my warmest thanks to Gregory Verissimo and July Paola for all our scientific exchanges and the work done together during these years. A big thank you to the members of the laboratory for all the support and for our various exchanges during these years. They provided a friendly and cooperative atmosphere at work and also useful feedback, and insightful comments on my work.

This research work was done under the frame work of EURIPIDES type project Low Cost Circulators for Microwave Modules (LOCCIMIM) and carried out within the MOM cluster of Lab-STICC (Laboratoire en sciences et techniques de l'information, de la communication et de la connaissance-UMR CNRS 6285) at Universit   de Bretagne Occidentale. All calculations in this thesis work were done on the high performance computing cluster WINCHYPS1. This cluster is managed by the TecHyp platform of the Lab-STICC.

Finally, I would like to acknowledge my friends and family who supported me during my time here. First and foremost I would like to thank Vipin, Rajju P Joseph, and Narasimha for their constant love, support and encouragement. Last, but not least, I would like to thank my family for their love, support and encouragement. This would not have been possible without their support and encouragement.

Contents

General Introduction	13
I EM Characterization of Anisotropic Ferrites - State Of The Art	17
I.1 Introduction	18
I.2 Ferrites	18
I.2.1 Static properties	20
I.2.2 Dynamic properties	25
I.2.3 Microwave behavior of ferrites	29
I.3 EM characterization of ferrite materials	31
I.3.1 Demagnetized state - Coaxial line method	33
I.3.2 Saturated state - Resonant cavity methods	35
I.3.2.1 Permeability measurement	36
I.3.2.2 Resonance linewidth measurements	36
I.3.3 Partially magnetized state	40
I.3.3.1 Nonreciprocal microstrip line – Quasi-TEM method	40
I.3.3.2 Partially filled waveguide method	43
I.3.3.3 Nonreciprocal strip line method	47
I.4 Motivation and Objectives	50
II A Coaxial Line Method For Damping Factor Measurement	57
II.1 Introduction	58
II.2 Permeability tensor models	58
II.2.1 Saturated state - Polder model	58
II.2.2 Demagnetized state - Schloemann model	60
II.2.3 Partially magnetized state	62
II.2.3.1 Permeability model by Rado	62
II.2.3.2 Green and Sandy model	63
II.2.3.3 Igarashi and Naito	63
II.2.4 Any magnetization state: Generalized permeability tensor model (GPT)	65
II.3 Measurement cell	70
II.4 General description of the method	72

II.5	Direct problem	73
II.5.1	Analytical functions for constituent parameters	74
II.5.2	EM analysis of the measurement cell	76
II.5.2.1	Theoretical solutions for propagation constant	79
II.5.2.2	Theoretical solutions for scattering parameters	82
II.5.3	Direct problem - Results	83
II.6	Validation of the direct problem	85
II.6.1	Dielectric material	86
II.6.2	Magnetic material	87
II.6.2.1	Demagnetized ferrites	87
II.6.2.2	Saturated ferrites	88
II.7	Conclusion	90
III	Inverse Problem- Experimental Results	95
III.1	Introduction	96
III.2	Inverse problem	96
III.2.1	Optimization procedure	97
III.2.2	Choice of the permittivity and permeability models	99
III.2.3	Optimization algorithm	100
III.3	Measurement setup	102
III.4	Measurement results	103
III.4.1	Composite ferrites	106
III.4.2	Bulk ferrites	110
III.4.3	Validation of results	116
III.5	Conclusion	118
IV	EM Modeling Of Anisotropic Ferrites - Application To Y-Junction Microstrip Circulators	123
IV.1	Introduction	124
IV.2	Anisotropic ferrites - Non-homogeneous internal fields	124
IV.2.1	Demagnetizing field effects	124
IV.2.2	Effect of non-uniform internal fields in the power absorption spectrum	128
IV.2.3	Commercial software solutions: Magneto-static simulations using Ansys Maxwell 3D	129
IV.3	Electromagnetic modeling tool	131
IV.3.1	Magneto-static solver (Lab-STICC)	132

IV.3.2 EM modeling of anisotropic ferrites – Ansys HFSS	136
IV.3.2.1 Integration of theoretical permeability tensor models with HFSS	137
IV.3.2.2 Ansys HFSS – Macro programming	138
IV.3.2.3 Validation of results	139
IV.3.2.4 Comparison with classical HFSS simulations	139
IV.3.2.5 Non-Uniform biasing – Comparison with Maxwell 3D sim- ulations	142
IV.4 Application - Microstrip Y-junction circulator	144
IV.4.1 Circulator Design	146
IV.4.2 Experimental results	147
IV.4.3 Non-uniform biasing fields- Electromagnetic analysis	149
IV.5 Conclusion	152
Conclusion and Perspectives	159
Bibliography	168

List of Figures

I.1	Magnetic moment distribution in materials.	18
I.2	Microscopic magnetic structure of ferrites.	20
I.3	Hysteresis loop.	21
I.4	Initial magnetization for easy and hard axis.	22
I.5	Precession of magnetic moment.	25
I.6	Polder-Smit effect.	27
I.7	Resonance linewidth.	28
I.8	Microwave devices based on ferrites.	30
I.9	EM characterization techniques.	31
I.10	Coaxial line method.	33
I.11	Cavity for ΔH measurement.	37
I.12	Cavity for ΔH_{eff} measurement at 9.1 GHz	39
I.13	Measurement cell	40
I.14	Equivalent electrical circuit model of loaded section	41
I.15	Equivalent model of the measurement cell loaded with sample	42
I.16	Rectangular waveguide measurement cell	43
I.17	Cross section of the rectangular waveguide-based measurement cell	44
I.18	Modal analysis of the measurement cell.	45
I.19	Asymmetrically loaded strip line	47
II.1	Spectra of the real and imaginary parts of the diagonal μ and off-diagonal κ components of the Polder tensor.	60
II.2	Schloemann model	60
II.3	GPTmodel- Principle.	66
II.4	Moment directions in polycrystalline ferrites.	67
II.5	Magnetized equilibrium direction of the domains	68
II.6	Coaxial line-based measurement cell and field pattern for the TEM dominant mode.	71
II.7	General description of the method.	72
II.8	Axially magnetized coaxial cell filled with ferrite sample.	76
II.9	Propagation constant	80

II.10	Permeability tensor components.	81
II.11	Propagation constant inside the ferrite material.	81
II.12	Measurement cell - discontinuities.	82
II.13	Spectra of real and imaginary parts of the diagonal and off-diagonal components of permeability tensor computed using GPT model	83
II.14	Theoretical S-parameters.	84
II.15	Power absorption in the system.	85
II.16	S-parameters calculated using EM analysis and Ansys HFSS. Dielectric sample: $\epsilon = 7.8 - j0.01$, thickness = 2.9 mm.	86
II.17	Real and imaginary parts of scalar permittivity, and permeability spectra measured using NRW method. Sample: YIG composite material	87
II.18	Measured and simulated S-parameters of demagnetized ferrite material	88
II.19	Real and imaginary parts of diagonal and off-diagonal components of the permeability tensor (Polder model) in saturated state.	89
II.20	S-parameters calculated using theoretical EM analysis, and Ansys HFSS for saturated ferrite material.	90
III.1	Inverse problem - Description	96
III.2	Broadband optimization procedure	97
III.3	Microwave behavior of permittivity- Cole-Cole model	99
III.4	Spectra of real and imaginary parts of the diagonal components of $\hat{\mu}$ tensor obtained using GPT model	100
III.5	Optimization algorithm. ($4\pi M_s$ is optional)	101
III.6	Measurement setup	103
III.7	Measured and optimized S-parameters of a Teflon sample of length 3 mm	104
III.8	Real and imaginary parts of effective permittivity ϵ of the dielectric sample- Teflon	104
III.9	Measured and optimized S-parameters of the demagnetized YIG 39 composite material in the high frequency region.	107
III.10	Real and imaginary parts of scalar permittivity, and permeability spectra in the demagnetized state. Sample: YIG 39 composite material	107
III.11	Optimized permeability spectrum and S-parameters of YIG39 composite material for different DC magnetic field (H_{dc}) values	108
III.12	YIG 39 sample- Optimized damping coefficient	109
III.13	Imaginary part of permeability μ'' of YIG 39 sample	110
III.14	YIG 39 sample- Domain wall relaxation and gyrotropic response.	111
III.15	Measured and optimized S-parameters of the demagnetized YIG 39 (EXXELIA TEMEX) ferrite sample of length 4 mm in the high frequency region.	113

III.16	Real and imaginary part of measured permittivity spectra, ϵ_f of the ferrite material of length 4 mm (considering the air gap correction using a layered capacitor model).	113
III.17	YIG 39 sample- Optimized damping coefficient	114
III.18	Optimized permeability spectrum and S-parameters of YIG 39 ferrite material for different DC magnetic field (H_{dc}) values	115
III.19	Measured resonance linewidth ΔH of Y39 ferrite material . 'x' - value provided by EXXELIA TEMEX	116
III.20	YIG 39 sample- Measured and calculated power absorption	117
IV.1	Evolution of the measured (-) and simulated (—) power absorption spectra of a coaxial line loaded with a YIG ferrite material (Y39 composite) as function of the applied DC magnetic field.	125
IV.2	Evolution of the maximum power absorbed by bulk ferrite materials (YIG 39- different thickness) with the applied magnetic field.	126
IV.3	Power absorption spectra of YIG 39 (EXXELIA TEMEX) samples of different thickness.	128
IV.4	Internal fields calculated inside a 2 mm YIG ferrite sample using the Maxwell 3D, when an external DC magnetic field $H_{DC}=1600$ Oe is applied uniformly on the ferrite material.	129
IV.5	Measured (-) and Simulated (- -) power absorption of 2 mm sample for various applied DC magnetic fields.	130
IV.6	Predictive electromagnetic modeling tool.	132
IV.7	Internal fields calculated inside a 3 mm YIG ferrite using the magneto-static analysis, when an external DC magnetic field $H_{DC}=1600$ Oe is applied uniformly on the ferrite material.	135
IV.8	Illustration of major and minor hysteresis loops- Stoner and Wohlfarth model.	135
IV.9	Material definition - Ansys HFSS.	136
IV.10	Definition of datasets in HFSS.	137
IV.11	Integration of GPT model with HFSS.	138
IV.12	Spectra of the real and imaginary parts of the diagonal μ and off-diagonal κ components of permeability tensor computed using GPT	140
IV.13	Simulated S-parameters of a coaxial line (APC7 standard) loaded with a magnetized ferrite (Polder model)	140
IV.14	Spectra of the real and imaginary parts of the diagonal μ and off-diagonal κ components of permeability tensor computed using GPT model	141
IV.15	Simulated S parameters (GPT model + HFSS). Sample properties: $4\pi M_s=800$ G, $H_a=54$ Oe, $N_z=0.42$ and $\Delta H=300$ Oe. Sample thickness = 2.9 mm.	141

IV.16	Internal DC magnetic fields calculated inside a 3 mm YIG ferrite using the magneto-static analysis, when a uniform DC magnetic field $H_{DC}=1600$ Oe is applied on the sample.	142
IV.17	Cross section of the ferrite sample- Definition of different regions where internal DC magnetic fields can be considered as uniform.	143
IV.18	Measured (-) and simulated power absorption spectra of 3 mm YIG ferrite (Maxwell 3D (...), GPT+HFSS (- -)).	144
IV.19	Symbol and S parameter matrix of an ideal circulator.	145
IV.20	Y-junction microstrip circulator- Design parameters. Quarter wavelength line	146
IV.21	Y-junction microstrip circulator- Experimental setup and cutting view. . .	148
IV.22	Measured (-) and simulated (-) S-parameters of Y-junction microstrip circulator: HFSS with uniform biasing fields assumption.	149
IV.23	Magneto-static analysis of a ferrite disk magnetized by a permanent magnet- Mesh settings.	150
IV.24	3D modeling of ferrite puck – Ferrite material is divided into different annulus sectors.	150
IV.25	Measured and simulated S-parameters of Y-junction microstrip circulator: Non-uniform biasing fields assumption.	151

General Introduction

Ferrite materials are widely used in microwave electronics for many telecommunication applications because of their high resistivity and their high saturation magnetization. When these materials are magnetized by a static magnetic field H_{dc} , they exhibit anisotropic properties and nonreciprocal behavior.

These characteristics are at the heart of the design of nonreciprocal devices and tunable devices. The first type includes devices such as insulators and circulators, in which the nonreciprocal nature of the wave propagation is paramount. Devices like tunable filters, delay lines, phase shifters, and variable attenuators exploit the non-linearity of the electromagnetic (EM) behavior of ferrites with respect to a static magnetic field.

For each of these devices, an external control is necessary to ensure their state of operation. The dynamic and static intrinsic properties of ferrites change as a function of magnetization state. In other words static and dynamic behavior of these devices can be controlled by an external magnetic field H_{dc} . Precise control over the performance of these components requires prior knowledge of the dynamic behavior of ferrite materials.

Dynamic behavior of ferrite material can be represented by the tensor permeability $\hat{\mu}$, each component of which has a double dependence with respect to the frequency and the static magnetic field H_{dc} . Consequently, design and optimization of microwave devices using ferrite materials requires a realistic knowledge of its dynamic response, namely permittivity and permeability and, on the other hand, control of wave propagation that condition their performance.

Experimentally, the EM characterization of ferrites is commonly carried out in demagnetized or saturated states, for example using the transmission/reflection technique in a coaxial line, and when in saturation using a resonant cavity. For partially magnetized states different characterization techniques have been developed in the laboratory (Lab-STICC) using microstrip lines, rectangular waveguides, and strip lines. The main advantage of these previously developed techniques is directly related to the fact that they provide access to the constituent material parameters, scalar permittivity ϵ and permeability tensor $\hat{\mu}$.

One of the specificities of the magnetic materials is the dependence of their dynamic response to the shape of the sample. The permeability of a sample ring is not the same as

that of a wafer. In addition, for non-ellipsoidal magnetic material which is the case most commonly encountered in ferrite devices, the internal static biasing field is not uniform. In a previous study, it is seen that in the most common microwave applications, unsaturated regions in ferrimagnetic materials still exist, even when strong DC fields are applied. This is due to the inhomogeneous nature of the demagnetizing fields within non-ellipsoidal samples. Under these conditions, characterization of material from an actual or average permeability does not constitute the most accurate solution to help the designer with ferrite devices.

The existing commercial simulation software use different theoretical models to describe the permeability tensor, according to the state of magnetization. These models use a number of physical parameters like saturation magnetization $4\pi M_s$, anisotropy field H_a , resonance linewidth ΔH , etc. as input parameters to describe the tensor permeability. With this procedure, one can describe the behavior of the ferrites in the saturated state in a very satisfactory manner. However, most of the EM simulators remain limited to certain states of magnetization, due to the simplified assumptions on which their permeability models are based upon. This limitation makes the design of devices laborious when the ferrite is neither in the saturated nor demagnetized state.

Designers often use two linewidth parameters, the resonance linewidth ΔH and the effective linewidth ΔH_{eff} to represent the ferromagnetic losses. These quantities are not physical parameters in the strict sense of the term, which appear in Maxwell's or Landau-Lifshitz-Gilbert equations like the damping factor α . These quantities are directly related to damping factor by Polder's formulations, which is only valid in the saturated state. Resonant cavity methods make it possible to measure ΔH and ΔH_{eff} at a given frequency (mono-frequency method). Measuring these parameters in a wide band of frequencies would involve too many cavities and sample sizes. Moreover, the representation of the magnetic losses by two values, one near the vicinity of the gyromagnetic resonance (ΔH) and the other outside this resonance (ΔH_{eff}), reduces the predictive character of the permeability model.

Design of the new classes of ferrite devices has to be based on the combination of experimental methods and theoretical tools capable of describing the dynamic EM behavior of the ferrites. We need experimental methods to find the physical parameters of the ferrites and theoretical models which will use these parameters to describe the dynamic behavior of ferrites in all magnetization states. In this context, the general objective of our research work is to improve the electromagnetic modeling of anisotropic ferrites in order to make the design procedure more predictive and accurate for any state of magnetization. In this line of research our objective is to develop a predictive EM simulation tool for accurate modeling of ferrite based devices.

Our first objective is to develop a simple and generalized broadband measurement method for the characterization of damping factor α of polycrystalline ferrites by overcoming the constraints of the standard linewidth measurements. This parameter, being the only dynamic input parameter of the theoretical permeability model, will be very useful for the designers of the microwave devices. It will allow us to predict the dynamic behavior of the ferrites more accurately at any magnetization state, and thus to optimize the design procedures.

The demagnetizing field effects due to the size and shape of the sample are prominent in non-ellipsoidal samples and accurate calculation of internal DC fields and understanding of the demagnetizing field effects are necessary to get better results with electromagnetic simulations. This brings us to our second objective, which is to improve the electromagnetic modeling of ferrite devices by integrating the magneto-static analysis and generalized permeability tensor model with a commercial simulation software like Ansys HFSS. A dynamic electromagnetic analysis of the structure, considering inhomogeneity of the internal fields and a generalized permeability tensor model would enable us to understand the inhomogeneous internal field distribution and the demagnetizing field effects on the performances of the ferrite based microwave devices.

In order to highlight the effectiveness of the developed EM simulation tool, and to demonstrate the need for a tool capable of realistically predicting their performance, it will then be used in the design of a ferrite device - a microwave ferrite circulator. Within the frame work of this thesis, we will work on the modeling and optimization of a microstrip Y-junction circulator.

This manuscript is organized in the following way: In the first chapter, we explain the current use of ferrites in the design of microwave device. We will present the intrinsic characteristics of ferrites which can influence their dynamic behavior. Then we will present the state of the art of the microwave material characterization methods and will highlight the problems that arise in the field of microwave characterization of ferrite materials.

In the second chapter, a simple and generalized measurement method to find a unique quantity representing the dynamic losses in ferrite material, the damping factor α will be presented. This unique dynamic property combined with the static characteristics (saturation magnetization $4\pi M_s$, anisotropy field H_a) would be the input parameters of theoretical tool describing the dynamic properties of the ferrite material. First, we will discuss the theoretical models of permeability existing in the literature for different states of magnetization. Secondly a general principle of the proposed coaxial line measurement method will be presented. Finally a description of quasi-TEM analysis of measurement cell will be presented and the EM analysis will be validated in the limit cases.

In third chapter, the inverse problem of the proposed coaxial line method and the experimental results will be discussed in detail. The inverse problem will optimize the damping factor α by matching theoretical S parameters with the measured S parameters. This dynamic quantity α will be one of the input parameter for the theoretical tool which we will present in detail in the fourth chapter. The inverse problem results will be validated by comparing optimized values with the supplier's data sheet. This method eliminates the constraints related to the cavity and sample dimensions imposed by standard measurement methods. Knowledge of a unique parameter representing dynamic losses would assist engineers in optimizing design and adjustment procedures for ferrite-based microwave devices.

Finally, in the fourth and last chapter, we will present a theoretical EM tool for accurately describing the dynamic behavior of ferrite based devices by taking into account the internal polarizing fields of anisotropic ferrite materials. This theoretical tool will combine a magneto-static analysis and the general permeability tensor model with a commercial EM simulation software Ansys HFSS. The input parameters of this theoretical tool will be the static properties of the ferrite material except the damping factor α which represents the dynamic losses. Static input parameters will be obtained using standard characterization measurements. Damping factor α will be determined using the coaxial line method developed in the first part of thesis.

We will discuss in detail about the non-homogeneity of the internal magnetic fields and its effect on the dynamic response of the anisotropic ferrite materials. By considering the inhomogeneity of the internal polarizing fields, proposed theoretical tool will be able to predict the dynamic behavior of ferrite devices more accurately, at all magnetization states. This theoretical tool will be validated in the limit case by modeling, and realizing a microstrip Y-junction circulator.

Chapter I

EM Characterization of Anisotropic Ferrites - State Of The Art

Contents

I.1	Introduction	18
I.2	Ferrites	18
I.2.1	Static properties	20
I.2.2	Dynamic properties	25
I.2.3	Microwave behavior of ferrites	29
I.3	EM characterization of ferrite materials	31
I.3.1	Demagnetized state - Coaxial line method	33
I.3.2	Saturated state - Resonant cavity methods	35
I.3.2.1	Permeability measurement	36
I.3.2.2	Resonance linewidth measurements	36
I.3.3	Partially magnetized state	40
I.3.3.1	Nonreciprocal microstrip line – Quasi-TEM method	40
I.3.3.2	Partially filled waveguide method	43
I.3.3.3	Nonreciprocal strip line method	47
I.4	Motivation and Objectives	50

I.1 Introduction

The initial chapter is devoted to the presentation of general context of our research. First, we will discuss in detail about the intrinsic properties of the ferrites and their microwave behavior. Then we will present the state of the art of the microwave material characterization methods and will highlight the problems that arise in the field of microwave characterization of ferrites, in order to define the objectives of our work.

I.2 Ferrites

In the atomic level, due to the angular momenta of electrons, individual atoms can have a net magnetic moment associated with them. The effective sum of these atomic magnetic moments results in the macroscopic magnetic field of the material. The magnetic materials can be classified according to their response to the internal magnetic field as diamagnetic, paramagnetic, antiferromagnetic, ferromagnetic, and ferrimagnetic materials. The latter two are of great interest due to their macroscopic magnetic properties [1].

A ferromagnetic material can retain a net magnetic moment even after the external magnetic field is removed. General theory of ferrimagnetism was developed by Neel in the 1940's. Ferrimagnetic materials behave like paramagnetic materials above Curie temperature and can retain spontaneous magnetization below the Curie temperature like ferromagnetic materials.

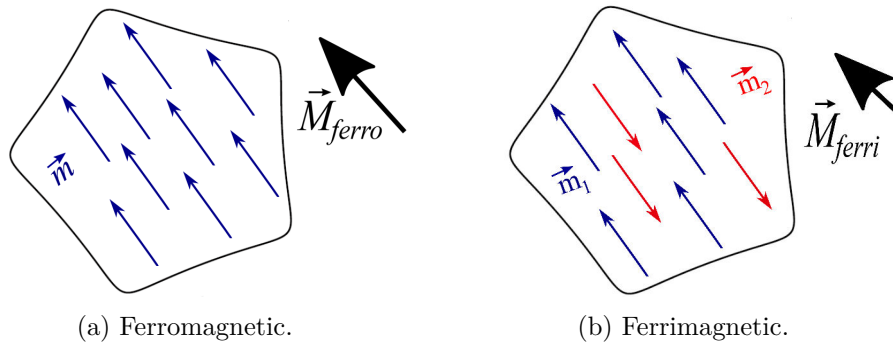


Figure I.1: Magnetic moment distribution in materials.

The ferromagnetic, and ferrimagnetic materials (ferrites) possess ions having permanent magnetic moments (\vec{m}) which are locally coupled by the exchange interactions. In the case of ferromagnetic materials, magnetic moments are aligned parallel resulting in a strong spontaneous magnetization (Figure I.1a). On the other hand, in the case of ferrimagnetic materials, the magnetic moments occupy two oppositely oriented sub-lattices with different densities (Figure I.1b). This arrangement of the magnetic moments leads to a much lower

spontaneous magnetization (M_{ferri}) than that of the ferromagnetic materials (M_{ferro}). This results in a non-zero spontaneous magnetization similar to the ferromagnetic magnetization but remains weaker than the latter.

Ferrites are ferrimagnetic materials with iron oxides (Fe^{3+}) as their main component. Ferrimagnetic substances are industrially important because they exhibit a substantial spontaneous magnetization at room temperature. Like ferromagnet, ferrimagnet also consists of self-saturated domains and they exhibit magnetic saturation and hysteresis phenomena. However, unlike ferromagnetic materials, ferrites have an insulating character with a high resistivity between 10^5 and $10^6 \Omega.m$, allowing their use in many microwave applications [2]. At high frequencies, the skin effect greatly limits the penetration of electromagnetic (EM) waves in the conductive materials [3]. On the contrary, the ferrimagnetic materials have a strong interaction with the EM waves due to their magnetic properties.

Other electromagnetic properties of the ferrites are relative dielectric constant ϵ_r , anisotropy field H_a , Curie temperature T_c , and saturation magnetization, $4\pi M_s$. The microwave ferrites have a relative dielectric constant in between 11 and 17 (little dispersive in frequency) with very low dielectric losses ($\tan \delta_e < 10^{-4}$).

The anisotropy field, H_a characterizes the rigidity with which the magnetization is maintained in the preferred directions and Curie temperature, T_C represents the maximum temperature up to which the ferrites can retain their magnetic properties. Finally the saturation magnetization, $4\pi M_S$ is the maximum possible value of the magnetization.

The ferrites are mainly divided into 3 sub-groups: spinel ferrites, garnets (soft ferrites) and hexaferrites (hard ferrites).

Spinel ferrites have a general chemical formula of the form $MF_e_2O_4$ where M is a bivalent metal ion (Co, Mg, Mn, Ni, etc.). These ferrites have anisotropy fields of the order of a few tens of Oersteds, which locate their gyromagnetic resonance in the vicinity of megahertz in the absence of applied magnetic field (natural gyromagnetic frequency). This type of ferrite is mainly used in the C, S and X frequency bands. Beyond X-band, the size of the permanent magnet needed to saturate the material, becomes too large to be integrated into the microwave devices.

The garnet type ferrites have a chemical composition of the $M_3Fe_3O_{12}$ form, M being one or more rare earth ions. The most common magnetic garnet is Yttrium-Iron (YIG) which has the chemical formula $Y_3Fe_5O_{12}$. These materials are widely used in microwave applications, despite their less saturation magnetization value because they exhibit very low losses.

The basic compounds of the hexaferrites are barium ferrite ($BaFe_{12}O_{19}$). Due to their crystallographic structure, these materials are characterized by their strong magnetic anisotropic field, which is 100 to 1000 times greater than that of garnet or spinel ferrites.

Hexaferrites possess saturation magnetization around 5000 Gauss. These ferrites find their applications particularly in the field of millimeter waves (30 GHz - 100 GHz), because of their high values of natural gyromagnetic resonance frequency. When pre-oriented during the fabrication process, with their high remanent magnetization, these materials can even avoid the use of an external DC biasing field. This results in a significant decrease in the physical volume of the devices.

1.2.1 Static properties

In the beginning of the twentieth century, Pierre Weiss put forward a theory on ferromagnetism. At microscopic level, magnetic moments are reorganized themselves and the magnetic material is spontaneously subdivided into domains (Figure I.2), in order to minimize the internal energy in the system. These domains are called Weiss domains. A homogeneous magnetization exists within each domain resulting in local saturation of the domain. Adjacent domains have different magnetization directions which results in the cancellation of moments and at the macroscopic level, there is no resultant moment, i.e. zero macroscopic magnetization.

These adjacent domains are separated by a transition zone called the Bloch wall, which correspond to a certain number of atomic planes whose moment orientation varies progressively from one domain to the other. In this zone, the magnetization changes its orientation gradually from one domain to another (Figure I.2).

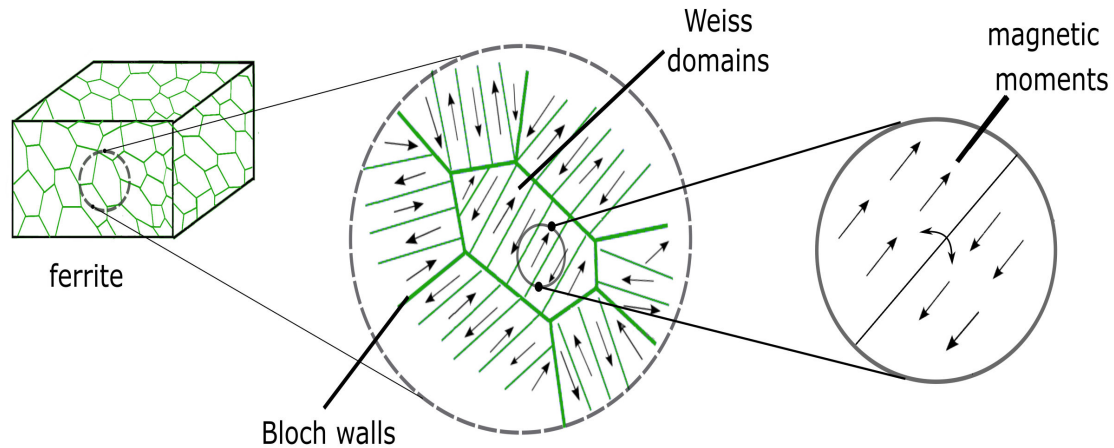


Figure I.2: Microscopic magnetic structure of ferrites.

Under the action of an external magnetic field H_{dc} , magnetic moments of the ferrites move away from their equilibrium positions in order to orient themselves in the direction of H_{dc} to minimize their potential energy. This results in the displacement of Bloch walls causing

energetically favorable domain creation and gradual disappearance of the others.

The domains whose orientation is close to the applied field direction will grow in size and the others which are oriented away from the field direction diminish in size. Consequently, a non-zero resultant magnetization M appears inside the ferrites. This behavior is characterized by the first magnetization curve and the hysteresis loop. The magnetization process in each grain in a polycrystalline material is similar to that of mono crystalline material. However net magnetization of the material becomes complicated due to the magneto-static processes and the magnetostriction between adjacent grains.

Hysteresis loop

During the first magnetization of ferrimagnetic material, the material is in demagnetized state with domains whose spontaneous magnetizations are oriented in different directions. In the low magnetic fields, a slight movement of the Bloch wall favors magnetization, resulting in a modification of the magnetic moment arrangement. The displacements of walls in this zone are reversible.

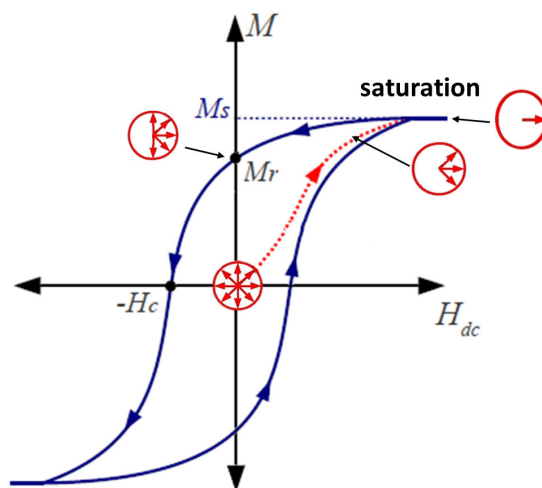


Figure I.3: Hysteresis loop.

Magnetization increases with increase in the static magnetic field strength, H_{dc} . During a medium magnetic field, magnetization M increases rapidly as a function of the applied field H_{dc} . The rotation of the magnetic moments becomes important and resulting in the switching of domains, a sudden change in direction of spontaneous magnetization in a domain. The switching of the domains and the displacements of walls in this zone are irreversible processes. This continues until the disappearance of Bloch walls and almost all the magnetic moments are aligned in the direction of the applied field. The magnetization M reaches a maximum value M_s (saturation magnetization), which is the sum of the contributions from all magnetic moments oriented in the same direction.

If the intensity of the static magnetic field is then decreased, we see that the variation of M is no longer the same. When the field becomes zero, there remains a certain magnetization, called *remanent magnetization* (M_r). To cancel this magnetization, it is necessary to apply a magnetic field of opposite direction with amplitude H_c . This field H_c is called *coercive field*. In general, the magnetization M as a function of the applied field is described by a closed loop, known as the hysteresis loop (Figure I.3) where all the phenomena mentioned above contribute to the static response of the material [4].

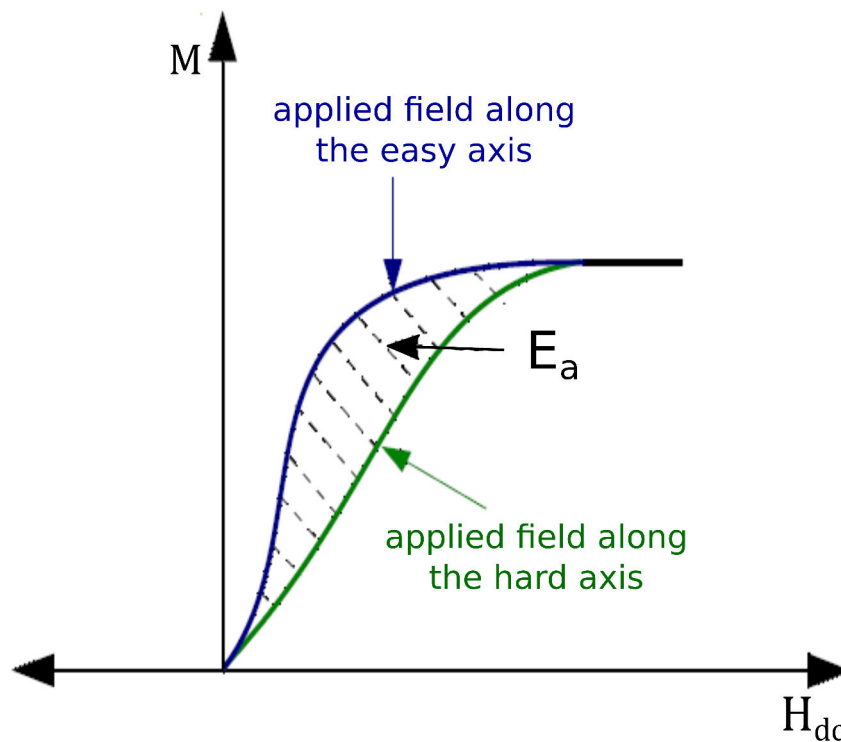


Figure I.4: Initial magnetization for easy and hard axis.

If we consider the domain configuration in the single crystal of a ferrite, we observe that the spontaneous magnetizations align in well-defined directions. Saturation of the material is reached more easily according to certain orientations of the static field. This leads to the definition of easy axes of magnetization (easy axes) where the magnetic field necessary to saturate the material is minimal and hard axes where the magnetic field necessary to saturate the material is maximal. Figure I.4 shows the first magnetization curves along the axes of easy and hard magnetization.

Depending on the magnetization direction relative to the easy axis of the crystal, anisotropy energy may be present in the crystal. The energy difference found between the two cases gives the energy of the magneto crystalline anisotropy E_a . This energy is associated with

the intrinsic anisotropy field H_a of the ferrite. Anisotropy field H_a characterizes the rigidity with which the magnetization is maintained in preferred directions of the crystal (easy axis). The smaller the anisotropy field, the more easily the magnetization moves under the action of an external magnetic field.

Magnetic materials can be classified into soft and hard magnetic materials according to their coercive field values. Generally soft materials have high value of permeability. The hysteresis loop covers only a small area, so only a small amount of energy is lost during magnetization of material. Reversal of the magnetization direction can be obtained with very small magnetic field strength. Soft magnetic materials are widely used for applications like transformer cores. Hard magnetic materials have high coercive fields and it is difficult to demagnetize them. They have high remanent magnetization and often used as permanent magnets. Hysteresis loop of these materials encloses a large area. Usually H_c of soft materials is less than 10 Oe whereas hard magnetic material have H_c values in the range of several hundred Oersteds.

Demagnetizing fields

Another static property of the finite ferrite sample is the demagnetizing field which is related to the shape of the sample. Due to the magnetization discontinuities at the boundaries, there exists a demagnetizing field (H_d) inside the sample, opposite in direction to applied static magnetic field.

The internal static field seen by the magnetic moments in the sample is decreased by the demagnetizing fields as given by:

$$\vec{H}_d = -\hat{N}\vec{M}. \quad (\text{I.1})$$

In this equation, \hat{N} is a tensor variable known as the demagnetizing factor, which depends only on the shape of the sample. This tensor becomes diagonal for ellipsoidal materials, where one of the axes is directed along the axis of revolution of the ellipsoid under consideration.

$$\hat{N} = \begin{bmatrix} N_x & 0 & 0 \\ 0 & N_y & 0 \\ 0 & 0 & N_z \end{bmatrix}$$

For the Cartesian coordinate system, we identify the diagonal coefficients N_x , N_y and N_z which are linked together by the relationship,

$$N_x + N_y + N_z = 1. \quad (\text{I.2})$$

In conclusion, the magnetic field internal to the ferrite can be expressed by the superposition of the different static magnetic fields in the form:

$$\begin{aligned}\vec{H}_{int} &= \vec{H}_{dc} + \vec{H}_a + \vec{H}_d \\ &= \vec{H}_{dc} + \vec{H}_a - \hat{N}\vec{M}\end{aligned}\tag{I.3}$$

For a uniformly magnetized elongated ellipsoid of diameter d , length L ($L/d \gg 1$) and axis of revolution z , the demagnetizing coefficient is zero in the axis of revolution, $N_z = 0$ and for a flattened ellipsoid ($L/d \ll 1$) $N_z = 1$.

For spherical sample, $N_x = N_y = N_z = 1/3$ [1, 5, 6]. Exact calculation of N factor is only possible in the case of ellipsoidal forms and uniform magnetization.

In the case of non-ellipsoidal samples, the use and calculation of the coefficients N_x , N_y and N_z is only by an approximation allowing the determination of the internal field using simple analytical relationships [7].

Several studies have proposed formulations to calculate the demagnetization coefficient of non-ellipsoidal shapes like hollow cylinder (thick ring) [8, 9].

For a longitudinally magnetized hollow ferrite cylinder of length L , outer diameter D , and inner diameter d , Sandomirskii et al [9] gives the following interpolating formulas for calculation of demagnetizing factor N ,

$$\lambda = \frac{L}{D}, \quad h = \frac{2.H}{D}, \quad H = \frac{D-d}{2}$$

$$E(\lambda) = \begin{cases} \frac{1}{1-\lambda^2} \left[1 - \frac{\lambda}{\sqrt{1-\lambda^2}} \arccos \lambda \right], & \text{for } 0 \leq \lambda < 1 \\ \frac{1}{\lambda^2-1} \left[\frac{\lambda}{\sqrt{\lambda^2-1}} \ln(\lambda + \sqrt{\lambda^2-1}) - 1 \right], & \text{for } \lambda > 1 \end{cases}\tag{I.4}$$

$$K(\lambda) = \frac{1 + 2.35 \ln(1 + 0.137\lambda)}{1 + 2.28 \ln(1 + 0.248\lambda)},\tag{I.5}$$

$$\epsilon = 0.3075 \left[1 + \frac{1}{\frac{1.41}{h(2-h)} - 1} \right], \quad \beta = 5^\epsilon \left[\frac{1.41}{h(2-h)} - 1 \right]\tag{I.6}$$

$$N \approx \begin{cases} h \cdot (2 - h) * E(\lambda) \cdot K(\lambda), & \text{for } 0.2 < \lambda < \infty, 0 \leq h \leq 1 \\ \frac{1}{1 + \beta \cdot \lambda^\epsilon}, & \text{for } \lambda \leq 0.2 \end{cases} \quad (\text{I.7})$$

These theoretical formulations (Eq. I.7) can be used to calculate the demagnetizing factor of hollow ferromagnetic cylinders when they are magnetized in the longitudinal direction.

I.2.2 Dynamic properties

It is well known that in a magnetized ferrite, magnetic moments within the grains and domains tend to align themselves in the direction of applied magnetic field to minimize their potential energy in the sample. This alignment is progressive and damped over time, reflecting the dissipative effects of ferrite materials.

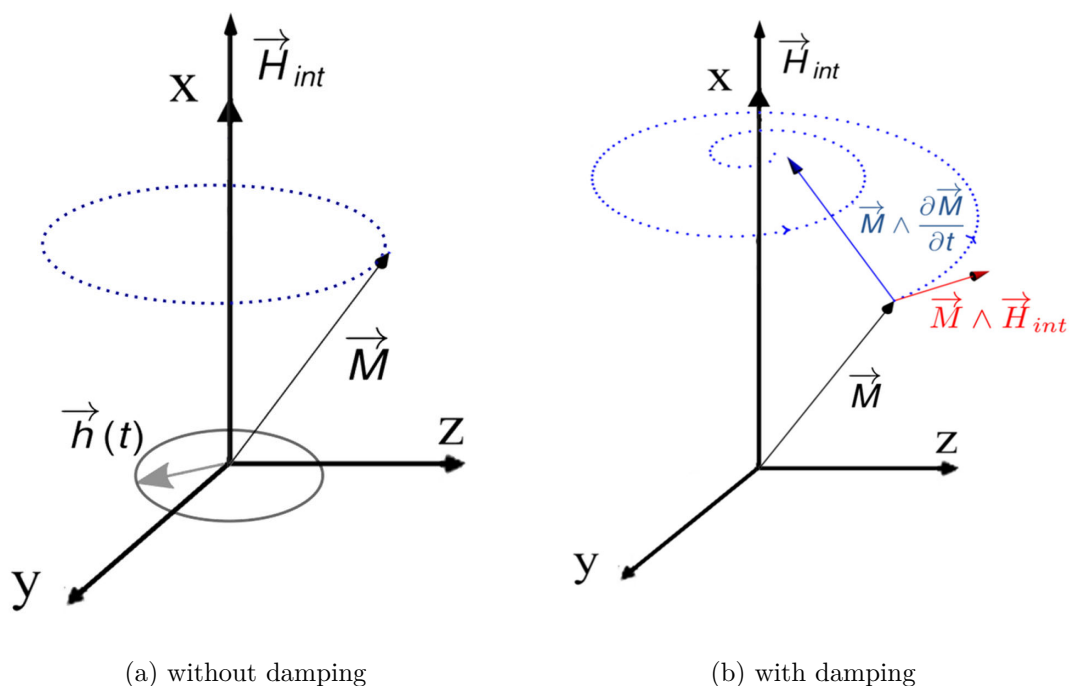


Figure I.5: Precession of magnetic moment.

In order to describe this behavior, Landau and Lifshitz [10] proposed the equation for the evolution of magnetic moment which was reformulated by Gilbert [11, 12].

The Landau- Lifshitz- Gilbert (LLG) equation can be written as,

$$\frac{\partial \vec{M}}{\partial t} = \gamma \cdot (\vec{M} \wedge \vec{H}_{int}) - \frac{\alpha}{|\vec{M}|} \left(\vec{M} \wedge \frac{\partial \vec{M}}{\partial t} \right), \quad (\text{I.8})$$

In this equation, γ is the gyromagnetic ratio (2.8 MHz/Oe), α is the damping factor related to material losses, M is the magnetization vector, and H_{int} is the local field seen by the individual moment.

The LLG equation (Eq. I.8) shows that the magnetic moment behaves like a gyroscope performing a damped precession movement around H_{int} (Figure I.5b). The first term represents the precession of the magnetization around its equilibrium position, under the action of a dynamic field perpendicular to the static field.

The second term represents the damping force which exerts a return torque and which leads the magnetic moment back to its equilibrium position.

This precession has an angular velocity called the Larmor frequency,

$$\omega_0 = \gamma H_{int} \quad (\text{I.9})$$

When the driving frequency is equal to the natural precession frequency of the moments, and the magnetic field rotates in the same direction as that of the magnetic moments, the energy from the microwave field is transferred most efficiently to the system. The permeability tensor shows a singularity at this frequency, which is known as the ferromagnetic resonance [13, 14].

When the ferrite is in the demagnetized state ($H_{dc} = 0$), the internal field (H_{int}) is equal to the anisotropy field (H_a) and the precession frequency is given by:

$$\omega_a = \gamma H_a \quad (\text{I.10})$$

This shows that resonance can be observed in ferrites even without an external magnetic field.

Polder-Smit effect

Polder and Smit have shown that the precession of the magnetization vectors can induce the presence of magnetic charges of opposite signs at the Bloch walls [15]. This leads to the appearance of dynamic demagnetizing fields inside the domains.

The magnetization vectors of the neighboring domains can then be considered as systems coupled by these dynamic demagnetizing fields. Domains with different sizes and orientation would induce a full distribution of local demagnetizing fields between zero and $4\pi M_s$.

This effect associated with a dispersion of the shape of the domains, and in the case of polycrystalline ferrites, an isotropic distribution of their orientation (relative to the field \vec{h}), leads to a spreading of the gyromagnetic resonance frequency relative to different domains present in the material.

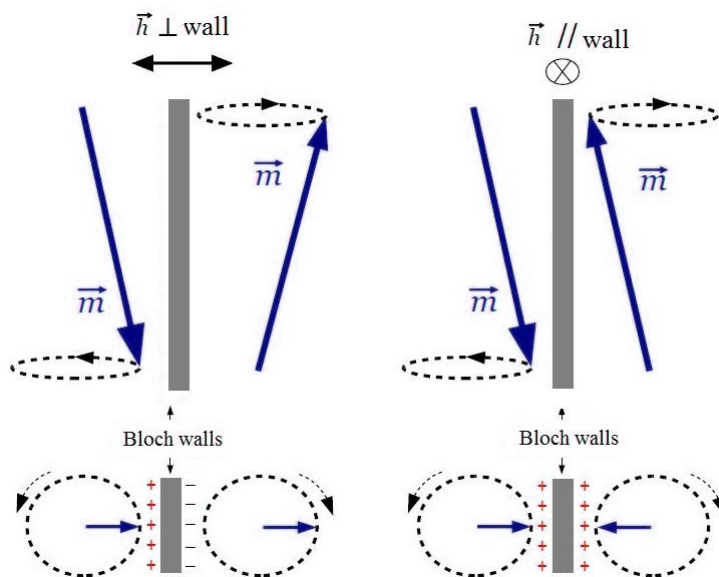


Figure I.6: Polder-Smit effect.

The gyromagnetic resonance phenomenon does not occur at a single frequency, but depending on the zone considered in the material will be spread between the two limit values: $\omega_1 = \gamma H_a$ and $\omega_2 = \gamma(H_a + 4\pi M_s)$.

Ferromagnetic losses

Ferrite materials in general, exhibit a power loss or absorption which is a function of an applied DC magnetic field [16] at microwave frequencies.

These losses are due to the damping forces which oppose the precessional motion. These forces exert a return torque which relaxes magnetic moments back to its equilibrium position.

Dynamic losses can be represented by the variation of imaginary part of susceptibility or permeability, as a function of applied magnetic field. This variation is usually non-Lorentzian in nature. To account these losses, a dimensionless damping coefficient α is introduced in Gilbert's equation (Eq. I.8). For ferrite materials showing this behavior, it is useful to characterize the absorption by means of an effective gyromagnetic ratio and a resonance linewidth.

In practice two different resonance linewidth parameters ΔH and ΔH_{eff} are used to represent these losses, which are extracted from the relation between imaginary part of measured permeability, μ'' and the applied field H_{dc} at a given frequency.

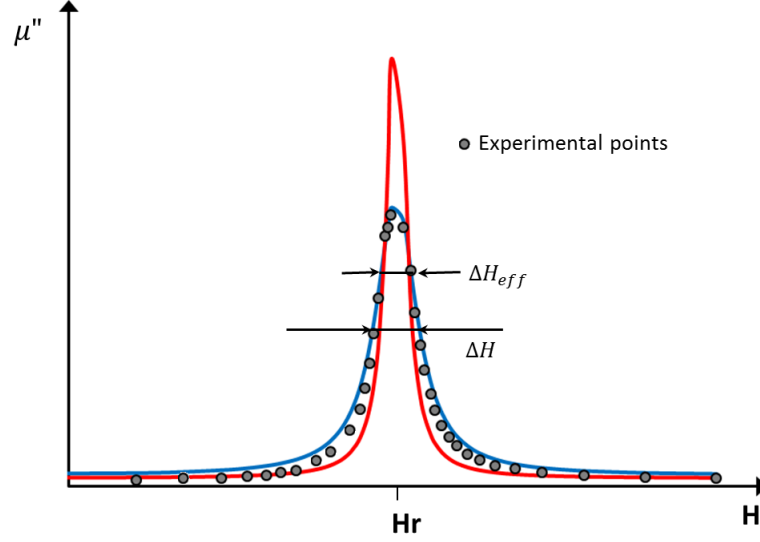


Figure I.7: Resonance linewidth.

- ΔH is the linewidth of the Lorentzian curve along the experimental μ'' points near the resonance ($H_{dc} \approx H_r$).

- ΔH_{eff} is the linewidth of the Lorentzian curve along the experimental μ'' points outside the vicinity of the resonance ($H_{dc} \neq H_r$), where

$$H_r = \frac{f_r}{\gamma} \quad (I.11)$$

f_r = gyromagnetic resonant frequency, γ = gyromagnetic ratio.

For a given microwave application, the choice between ΔH and ΔH_{eff} depends strictly on the magnetic field value H_{dc} .

At saturation, damping coefficient α is related to ΔH by the relation [14],

$$\alpha \simeq \frac{\gamma \Delta H}{2\omega} \quad , \quad (I.12)$$

where ω is the frequency at which linewidth is measured.

The resonant frequency in a real sample can be influenced by other losses due to demagnetization, magnetic anisotropy, porosity of the material, and crystalline imperfections. In many ferrites, this dependence is of a simple form, having a single maximum at some value of the magnetic field, which depends on the microwave frequency and on the specimen shape.

Standard method for resonance linewidth ΔH measurement of ferrites is by using a resonant cavity. This method is usually very accurate, but it is a mono-frequency method.

The measurements are done usually around 9.4 GHz using spherically shaped samples. The effective linewidth is calculated from the Q factor and resonance frequency measurements in a resonance cavity [16].

I.2.3 Microwave behavior of ferrites

The small signal approximation of the precession of the magnetic moments (Eq. I.8), subjected to a static magnetic field H_{dc} and a microwave magnetic field $\vec{h}(t)$, leads to the tensor relationship between the magnetic flux density \vec{b} and the field \vec{h} .

$$\vec{b} = \mu_0 \hat{\mu} \vec{h} \quad , \quad (\text{I.13})$$

where μ_0 is the permeability of vacuum ($4\pi * 10^{-7}$ H/m), and $\hat{\mu}$ is the tensor permeability. If the magnetic field is applied along the z axis of the Cartesian coordinate system, the tensor permeability is given by [14] :

$$\hat{\mu} = \begin{bmatrix} \mu & -j\kappa & 0 \\ j\kappa & \mu & 0 \\ 0 & 0 & \mu_z \end{bmatrix} \quad (\text{I.14})$$

When a ferrite material is placed in a static magnetic field H_{dc} , its EM properties vary according to the direction of wave propagation. Under the action of an external magnetic field, the extra diagonal term κ becomes non-zero and material becomes anisotropic in nature. This induced anisotropy is the reason for the nonreciprocal behavior of ferrites. On the other hand, for a demagnetized ferrite $\kappa = 0$, and the permeability tensor becomes diagonal. In this case the ferrite is considered as an isotropic material [2]. Ferrites are widely used in microwave devices due to this nonreciprocal behavior towards EM wave propagation.

In the field of microwave electronics, ferrites are widely used in many signal processing and telecommunication applications. Devices like circulators/isolators are based on the non-reciprocal behavior of EM wave propagation in magnetized ferrites. Devices like tunable filters, delay lines, phase shifters and variable attenuators etc. exploit the non linearity of the EM behavior of ferrites with respect to a static magnetic field. Ferrites are also used for miniaturization of antennas and realization of absorbers in UHF band. These devices exploit the high permeability exhibited by the ferrite materials in the demagnetized state.

The flexibility of the magnetic properties of the ferrite is obtained by controlling its magnetization state using the static magnetic field, H_{dc} . This static field determines the location of the magnetization of the ferrite in the hysteresis loop.

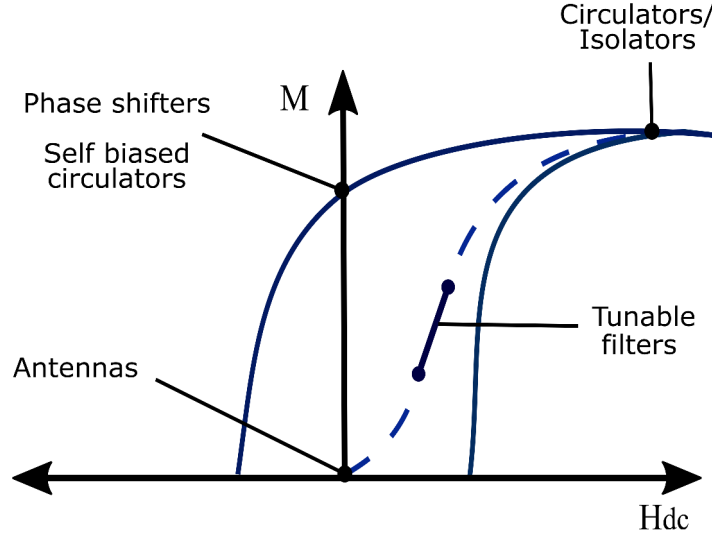


Figure I.8: Microwave devices based on ferrites.

Figure I.8 shows the state of magnetization of the various microwave applications based on ferrites. We find phase-shifters in the remanent state, circulators and isolators at saturation, tunable filters at partially magnetized states, and antennas in the demagnetized state.

In practice, anisotropy of the ferrites and the frequency tunability of the devices are achieved by the application of a static magnetic field [17]. Finally, ferrite in the state of remanence offers a fast and stable switching, which is very useful for phase shifters and makes it possible to avoid the use of permanent magnets in microwave devices

For majority of applications of reciprocal devices, there are one or more semiconductor-based devices that meet the same specifications. This is not the case for nonreciprocal devices. Semiconductor-based alternatives often have limitations in power, mechanical stress, and non-linearity. So, undoubtedly microwave devices based on magnetic materials play a very important role in microwave technology, especially in nonreciprocal devices.

Precise control of the performance of these devices requires prior knowledge of the dynamic behavior of ferrite materials. Dynamic behavior of the ferrites is first modeled by the susceptibility tensor, which defines the relation between the microwave magnetization \vec{m} and the microwave excitation \vec{h} in the form:

$$\vec{m} = \mu_0 \chi \vec{h} \quad (\text{I.15})$$

However, this behavior is usually represented by the permeability tensor, which connects the microwave magnetic induction \vec{b} and the microwave excitation \vec{h} , (Eq. I.13).

The elements of $\hat{\mu}$ tensor have a dual dependency on the frequency and the magnetic field. In practice, the static magnetic field H_{dc} determines the state of magnetization of the ferrite, that is to say its operating point, which thus influences the dynamic behavior of the ferrite.

$$\hat{\mu} = \begin{pmatrix} \mu(f, \vec{H}_{dc}) & -j\kappa(f, \vec{H}_{dc}) & 0 \\ j\kappa(f, \vec{H}_{dc}) & \mu(f, \vec{H}_{dc}) & 0 \\ 0 & 0 & \mu(f, \vec{H}_{dc}) \end{pmatrix} \quad (\text{I.16})$$

To fully describe the dynamic response of magnetic materials, including losses, complex components of the permeability tensor: $\mu = \mu' - j\mu''$, $\kappa = \kappa' - j\kappa''$ must be taken into account when applying in the Maxwell's equations.

The intrinsic gyromagnetic effects of the ferrites give a frequency resonant characteristic to the components of the tensor. The knowledge of permeability tensor (Eq: I.16) makes it possible to describe the dynamic EM behavior of the ferrites.

I.3 EM characterization of ferrite materials

Characterization of materials is an important and necessary step, even before the design and realization of microwave devices. There are different methods for characterizing the properties of materials. These methods vary according to their specifications such as the range of operating frequencies, the isotropic or anisotropic nature of the material, the shape of the sample and its dielectric or magnetic character.

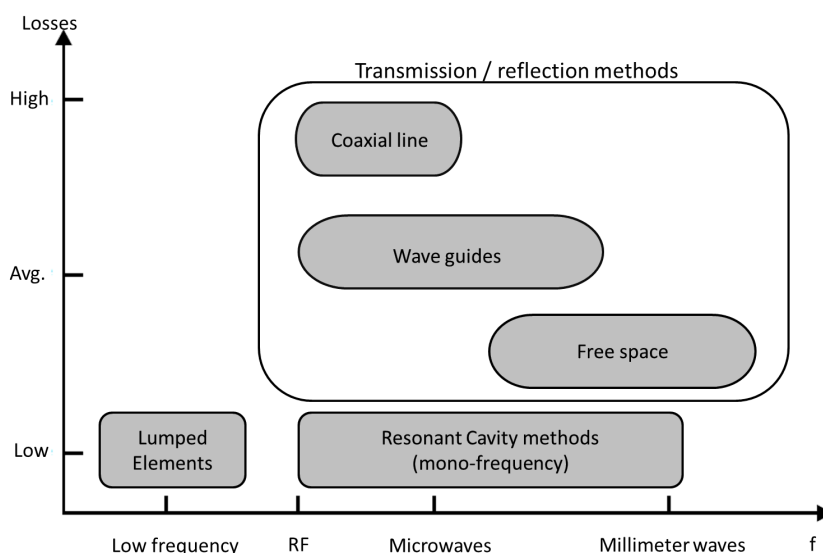


Figure I.9: EM characterization techniques.

This section gives a brief overview on the state of the art of the microwave theory and techniques for the characterization of magnetic materials. Figure I.9 illustrates qualitatively the techniques used to characterize the EM properties of materials as a function of frequency.

The resonant cavity methods make it possible to precisely determine the permittivity or the permeability of the magnetic material for a fixed frequency value. These methods are usually very accurate but they are mono-frequency techniques. There are constraints regarding the size and shape of the cavity and the sample to be measured. In order to obtain parameters at different frequencies, we have to use different cavities of different sizes. The frequency dependent properties of the material cannot be obtained with these methods. In addition, they are only suitable for low-loss materials. High magnetic losses will reduce the quality factor of the cavity, as well as the sensitivity of the measurement.

On the other hand with transmission/reflection techniques, it is possible to determine constituent parameters of the materials over a broad frequency band from the transmission and reflection coefficients. For the characterization of the constituent parameters of the material, it is necessary that the number of independent parameters measured, is greater than or equal to the number of constituent parameters to be determined. That is to say, to determine ϵ and μ of an isotropic material such as a demagnetized ferrite, it is necessary to measure at least two distinct parameters (S_{11} or S_{22} and S_{12} or S_{21}).

In the case of an anisotropic material, such as a magnetized ferrite where the permeability is a tensor quantity, it is necessary to measure three distinct S-parameters (S_{11} , S_{12} and S_{21}) in order to find μ , κ and ϵ in their complex form. Thus we have to make sure that the measurement cell is nonreciprocal in nature ($S_{21} \neq S_{12}$). Although the transmission/reflection techniques are very practical, S-parameter measurement in a wide frequency band leads to a reduction in the accuracy with respect to single-frequency resonant methods, in particular for low loss materials.

Experimentally, EM characterization of ferrites is commonly carried out in demagnetized or saturated states. For example the transmission/reflection technique in a coaxial line [18, 19] is used to extract the scalar permittivity and scalar permeability of isotropic ferrites in the demagnetized state. In saturation, a resonant cavity is used for the linewidth measurements (ΔH and ΔH_{eff}). This quantity, which represents the magnetic losses of the material, is an input parameter of the Polder model. The characterization of ferrites in partial magnetization states is less easy. For partially magnetized states which are found in practice in self-biased circulators/ isolators, phase shifters and tunable antennas or filters, different characterization techniques have been developed in the laboratory, Lab-STICC, using micro strip line [20], rectangular waveguides [21] and strip lines [22, 23]. The main advantage of these techniques is directly related to the fact that they provide access to the constituent material parameters, scalar permittivity and permeability tensor components.

We will discuss in detail about some of the resonant cavity methods and transmission-reflection measurement methods in the following.

I.3.1 Demagnetized state - Coaxial line method

The coaxial line characterization method was developed by Weir [18] using the work of Nicolson and Ross [19] and is called Nicholson-Ross-Weir (NRW) method. This method became the reference method for the permittivity and permeability measurements of isotropic materials in the demagnetized state. Main advantage of this method is the simplicity in the analysis and calculations using the classical transmission line theory. It is possible to calculate the magnetic permeability and the electrical permittivity from the measured S-parameters simultaneously with this approach.

The sample is toroidal in shape and inserted in between the inner and outer conductors of the coaxial line. The fundamental mode of propagation in a coaxial line is the TEM mode.

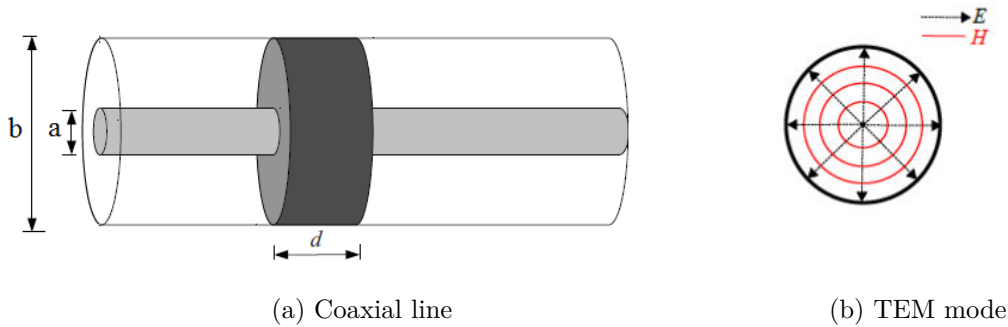


Figure I.10: Coaxial line method.

The validity of the method is related to the frequency (f_c) of the occurrence of the first higher order mode. The appearance of higher order modes in a coaxial line depends on the dimensions of the line and the EM properties of the propagation medium (permeability and permittivity).

$$f_c = \frac{2c}{\pi(a+b)\sqrt{\epsilon_r\mu_r}}, \quad (\text{I.17})$$

where a and b are the inner and outer diameters of the coaxial line respectively.

For APC7 coaxial line standard, cut off frequency, is equal to 19 GHz. Using the transmission line theory, it is possible to connect the S-parameters to the scalar permittivity and scalar permeability of the material.

Nicolson, Ross, and Weir have formulated relations between the scattering parameters of the line and the permeability and permittivity of the material,

$$\varepsilon = \sqrt{c_1 c_2} \quad \text{and} \quad \mu = \sqrt{\frac{c_1}{c_2}}, \quad \text{where} \quad (\text{I.18})$$

$$c_1 = - \left(\frac{c}{\omega d} \ln \left(\frac{1}{T} \right) \right)^2,$$

$$c_2 = \left(\frac{1 + \Gamma}{1 - \Gamma} \right)^2$$

$$\Gamma = \chi \pm \sqrt{\chi^2 - 1}$$

$$T = \frac{S_{11} + S_{21} - \Gamma}{1 - (S_{11} + S_{21})\Gamma}$$

$$\chi = \frac{S_{11}^2 - S_{21}^2 + 1}{2S_{11}}.$$

Given the symmetrical character ($S_{11} = S_{22}$) and the reciprocal nature ($S_{21} = S_{12}$) of the coaxial line, this method cannot be used to characterize ferrite materials in the magnetized state.

For a plane wave propagating through ferrite material with a biasing field applied in the propagation direction, there are two modes of propagation due to the Faraday effect [14]. The propagated wave can be considered as a combination of a right hand circularly polarized wave (RHCP) with a propagation constant γ^+ and a left hand circularly polarized wave (LHCP) with a propagation constant γ^- .

$$\gamma^+ = \frac{\omega}{c} \sqrt{\varepsilon} \sqrt{\mu + \kappa} \quad (\text{I.19})$$

$$\gamma^- = \frac{\omega}{c} \sqrt{\varepsilon} \sqrt{\mu - \kappa}$$

In this expression, μ and κ are the diagonal and extra-diagonal terms of the permeability tensor.

For RHCP wave, ferrite material can be represented with a medium of effective permeability $\mu + \kappa$ and where as for LHCP wave, the effective permeability is $\mu - \kappa$. In other words,

the propagated wave finds the same effective medium in the two directions of propagation, i.e the measurement cell is reciprocal in nature.

This effective medium has an effective permeability which depends on the intrinsic parameters of the material through the expression:

$$\gamma = \frac{\omega}{c} \sqrt{\epsilon} \sqrt{\mu_{eff}} \quad (I.20)$$

$$\mu_{eff} = \left[\frac{\sqrt{\mu + \kappa} + \sqrt{\mu - \kappa}}{2} \right]^2, \quad (I.21)$$

It is not possible to determine the permeability tensor components μ and κ with this method. As the cell is reciprocal in nature, the inverse problem gives the effective permeability μ_{eff} . Accuracy of this measurement method is limited by the errors due to the air gaps between the sample and the conductors. When the sample length is the multiple of half wavelength in the material, there may be undesirable ripples and accuracy is limited.

In conclusion, the coaxial line method is widely used for the broadband measurement of EM parameters of demagnetized ferrites, but it is not well suited for the permeability tensor measurement of saturated or partially magnetized media.

I.3.2 Saturated state - Resonant cavity methods

Resonant cavity methods are widely used for measuring the dielectric or magnetic properties of the materials due to their sensitivity and high accuracy [4, 16]. The general principle of resonant cavity perturbation methods consists of measuring the shift in the resonance frequency (F_r) and quality factor (Q) of the loaded cavity with respect to that of an empty cavity. The resonance frequency and quality factor of the cavity is determined with and without the sample. From these values, the permittivity and permeability are then extracted using theoretical relations.

The sample must be very small compared with the size of the cavity so that there is only a small shift in frequency when the sample is inserted. The sample length must be less than $\lambda/4$ of the cavity to avoid dimensional resonances. These are mono-frequency methods based on the perturbation theory. To measure the dielectric properties of the material, sample should be placed in a cavity where the electric field is at maximum and magnetic field is at minimum. When the sample is placed at a position where magnetic field is at maximum, magnetic properties of the material can be characterized.

I.3.2.1 Permeability measurement

For permeability measurements, the sample is placed in the cavity where electric field is zero or permittivity is equal to that of vacuum ϵ_0 . The shift in the resonance frequency when the sample is inserted with respect to the empty cavity is given by the relation,

$$\frac{f_{Loaded} - f_{empty}}{f_{empty}} = A(\mu'_r - 1) \frac{V_s}{V_c} , \quad (I.22a)$$

$$\frac{1}{Q_{empty}} - \frac{1}{Q_{Loaded}} = B\mu''_r \frac{V_s}{V_c} , \quad (I.22b)$$

where V_s and V_c , are the respective volumes of the sample and the cavity. The quantities A and B depend on the propagation modes used for the study and the shape and position of the sample. These parameters are usually determined using a calibration measurement with a sample of known parameters.

In literature there are different types of resonant cavities used for the characterization of magnetic materials [4, 16]. A cylindrical cavity is the most commonly used geometry. The ferrite sample is placed at the center of the cavity cross section, where the magnetic field is at maximum. By solving the wave equations for the propagated modes, the real and imaginary parts of the permeability μ are obtained from analytical relations. Generally, in this case the exploited modes are TM_{010} and TM_{020} . Spherical and disk shaped samples are the mostly used forms for cavity measurement due to the fact that they have less demagnetizing field effects and their demagnetizing coefficients are well known.

I.3.2.2 Resonance linewidth measurements

At microwave frequencies, ferrite materials, in general, exhibit a power loss or absorption as a function of an applied DC magnetic field [16]. For ferrite materials showing this behavior, it is useful to characterize the absorption by means of an effective gyromagnetic ratio, γ and a resonance linewidth. In practice two different resonance linewidth parameters ΔH and ΔH_{eff} , are used to represent these losses. Conventionally, these linewidth parameters are extracted from the relation between imaginary part of measured susceptibility χ and the applied field H_{dc} at a given frequency using the resonant cavity method.

(a) Gyromagnetic resonance linewidth, (ΔH)

Gyromagnetic resonance linewidth is a fundamental property used to describe the dynamic losses in the ferrite material. Resonance linewidth ΔH is defined as the difference between the applied field values at which absorption is half of the maximum value. Standard method for measuring the resonance linewidth, ΔH of ferrites is by using resonant cavities as described in IEC standard [16].

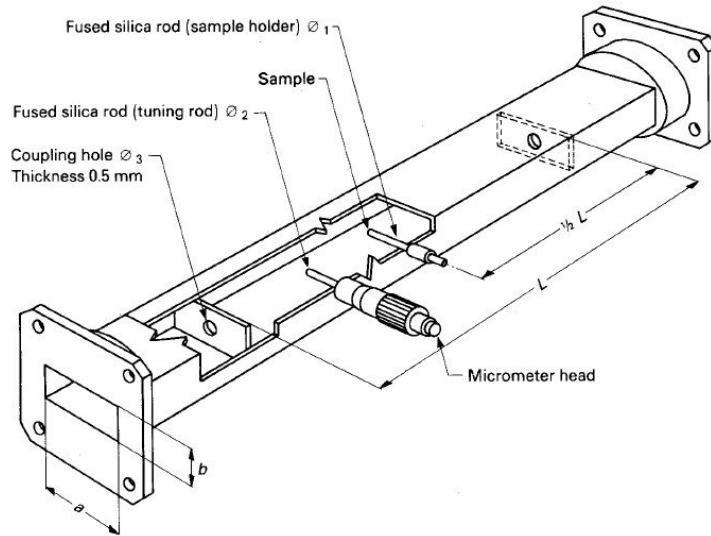


Figure I.11: Cavity for ΔH measurement (IEC std.2006 [16]).

This method is based on the cavity perturbation theory which requires that the sample dimension should be small compared to one quarter of the wavelength of the microwave radiation in the sample. This method is limited to a single frequency, corresponds to the resonant frequency of the measurement cavity (generally operating around 9.4 GHz). This method is applicable to saturated ferrites with uniform precession resonance (Kittel's mode). Ambiguities due to other magneto static modes are ignored.

A typical measurement cell is a transmission type cavity resonates between 9 and 10 GHz with a loaded Q greater than 2000. The sample is in the form of a small polycrystalline sphere. The sample is positioned away from the cavity walls mounted on a fused silica or other dielectric rod at a point of minimum microwave electric field and maximum microwave magnetic field. The hole for inserting the specimen into the cavity is located in the narrow cavity wall and is no larger than 1.90 mm in diameter for the X-band cavity. It is necessary that the microwave frequency should be adjusted to cavity resonance for all the measurements.

The absorption in the sample is measured by determining the change of incident power on the cavity, required to keep the output power at a fixed reference level when the sample is loaded. Reference level is set when transmission is at maximum in the empty cavity. Sample insertion should have negligible effect on the output level. Magnetic field is adjusted to get maximum absorption, i.e. minimum transmission.

To maintain a reference output level, attenuator is inserted between the source and the cavity. The variation in inserted attenuation is taken as the variation in input power. The new attenuator value α_R is determined at which the reference output level is restored.

The attenuation required to obtain the reference output level at half-power points of absorption is then calculated from the expression,

$$\alpha_{1/2} = \alpha_0 + 20 \log 2 - 20 \log \left(10^{\frac{(\alpha_0 - \alpha_R)}{20}} + 1 \right) , \quad (I.23)$$

where α_0 is the reference attenuator value measured, when the cavity is empty.

The precision attenuator is now set to this calculated value, $\alpha_{1/2}$. The magnetic field is then varied and the two field values at which the output reaches the reference output level are measured.

The difference between these magnetic fields will give the ferromagnetic resonance linewidth (ΔH).

$$\Delta H = |H_1 - H_2| . \quad (I.24)$$

(b) Effective linewidth, (ΔH_{eff})

For the devices that work outside the gyromagnetic resonance region, calculation of permeability tensor using the gyromagnetic resonance linewidth ΔH value will result in an error. In order to take into account losses in off resonance region and the deviations from the classical Lorentzian behavior, an effective linewidth parameter ΔH_{eff} is introduced (see Figure I.7).

This effective linewidth is defined as the linewidth of the Lorentzian curve along the experimental μ'' curve outside the vicinity of the gyromagnetic resonance. Standard method for measuring effective linewidth parameter is by using the resonant cavity [16].

This method is valid for saturated ferrite materials working at low power, outside the vicinity of the gyromagnetic resonance region. This method includes the measurement of permeability tensor components in a resonant cavity at a single frequency and effective linewidth is deduced from cavity Q factor and gyromagnetic resonance frequency.

For an isotropic magnetic material, magnetic flux density B is related to H by the relation,

$$B = \mu_0 \mu H = \mu_0 (1 + \chi) H \quad (I.25)$$

Effective linewidth ΔH_{eff} is related to imaginary part of effective susceptibility, χ_e , by the relation,

$$\Delta H_{eff} = 2M_s \cdot \text{Im} \left(\frac{1}{\chi_e} \right) \quad (I.26)$$

The basic measurement setup consists of a cylindrical TM_{110} , high Q cavity and a rod-shaped sample. The sample is inserted through holes in the cavity wall and a uniform axial magnetic field is applied.

For an applied field of H_0 and a microwave magnetic field with circular polarization in the clock wise direction, the resonant frequency and the cavity Q factor are measured with and without sample. The permittivity values are measured separately (IEC std-Clause.9).

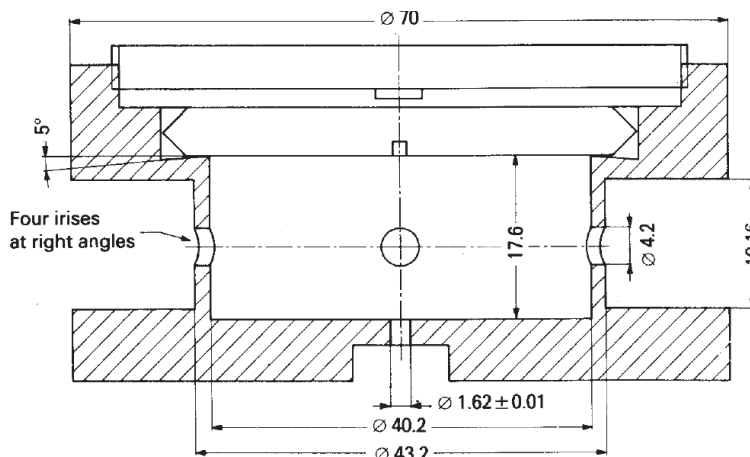


Figure I.12: Cavity for ΔH_{eff} measurement at 9.1 GHz (IEC std.2006 [16]).

By knowing the cavity dimensions, the real and imaginary parts of effective susceptibility can be calculated using the relations given by [16].

The effective resonance linewidth ΔH_{eff} is then measured from the susceptibility values by using the relation given above (Eq. I.26).

Although these resonant methods give precise and reliable values of the constitutive parameters of the ferrites, they are very limited in frequency since the working frequency is related to the dimensions of the cavity.

There are constraints due to the shape and size of the sample. The development of a method to lower frequency would require large measurement cavities. Moreover, these methods remain limited to a saturated state.

I.3.3 Partially magnetized state

For partially magnetized ferrites, different characterization techniques have been developed in Lab-STICC using micro strip line [20], rectangular waveguides [21] and strip line [22, 23]. These methods make use of the nonreciprocal nature of the respective measurement cells to characterize the permeability tensor of anisotropic ferrites.

I.3.3.1 Nonreciprocal microstrip line – Quasi-TEM method

In order to characterize the anisotropic properties of the magnetized materials, it is necessary to ensure the nonreciprocal character of the measuring cell $S_{12} \neq S_{21}$. A nonreciprocal microstrip line characterization method based on quasi-TEM analysis was previously developed [22] within Lab-STICC. This method makes it possible to measure the permeability tensor $\hat{\mu}$ and permittivity ϵ of magnetized ferrites in a wide frequency band.

The measurement cell is a microstrip transmission line partially filled with the sample to be characterized. The cross-section of this line is asymmetrically loaded with two dielectric materials of different permittivities (Figure I.13b).

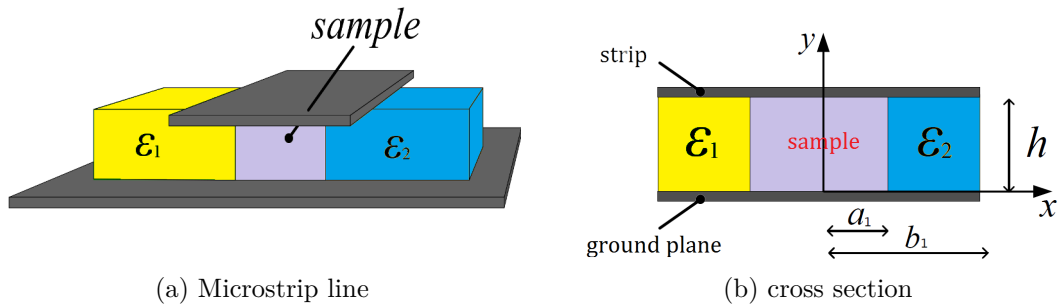


Figure I.13: Measurement cell

To increase cell sensitivity, the center conductor is made wide compared with the thickness of the ferrite so that most of the microwave energy is concentrated in the rectangular section containing the test sample.

The arrangement of the dielectrics and the field displacement phenomenon in gyromagnetic propagation structures, result in a nonreciprocal behavior ($S_{21} \neq S_{12}$) of the measurement cell. This condition is necessary to solve a system of equations that has three complex unknowns: permittivity, diagonal and extra-diagonal elements of the permeability tensor. This method allows characterization of a material in any state of magnetization.

In this method, the EM analysis is based on a quasi-static approach, where the fundamental mode considered is a quasi-TEM mode. The existence of a pure TEM fundamental mode in a microstrip line is impossible because the continuity of the EM fields is disturbed by

the appearance of the longitudinal components. The quasi-static approximation is valid at low frequency as long as the amplitudes of the longitudinal components remain negligible with respect to the transverse components. Thus the EM analysis of the quasi-static mode remains limited to frequencies lower than the first higher order mode.

Method can be divided into two stages: the direct problem and the inverse problem.

Direct problem:

The EM modeling of this measurement cell is done with the classical theory of transmission lines adapted to a nonreciprocal line. In this approach, a new parameter, called the memductance, M is introduced to take into account the anisotropic properties of the magnetized materials and to model the nonreciprocal effect.

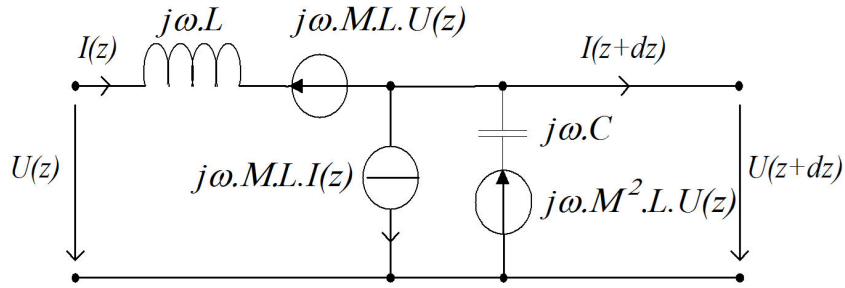


Figure I.14: Equivalent electrical circuit model of loaded section

An equivalent electrical circuit model of a short portion of the loaded line is shown in Figure I.14. By solving the Telegrapher's equations with the new parameter, M , two different solutions are obtained for the propagation constants γ^+ and γ^- , depending on the direction of propagation.

$$\gamma^+ = \omega \left(\sqrt{M^2 L^2 + LC} + ML \right) \quad (\text{I.27})$$

$$\gamma^- = \omega \left(\sqrt{M^2 L^2 + LC} - ML \right) \quad , \quad (\text{I.28})$$

where ω is the angular frequency of the signal. The quantities L , C and M are the inductance, capacitance and memductance parameters per unit length respectively.

The propagation constants γ^+ and γ^- correspond to the forward and backward propagation waves.

These parameters are directly related to the dimensions of the line (a_1, b_1) , properties of the dielectrics (ϵ_1, ϵ_2) , and properties of the magnetic material $(\epsilon_f, \mu, \kappa)$. In the quasi TEM approximation, the μ_y component of the tensor is not excited by any component of the magnetic field, so it disappears from the dispersion relations.

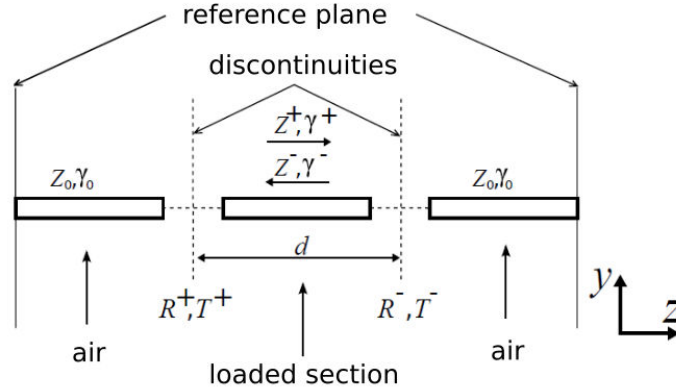


Figure I.15: Equivalent model of the measurement cell loaded with sample

In the loaded section of the cell, the wave is characterized by the propagation constant γ^+ in the forward direction and by γ^- in the backward direction over a distance d , which corresponds to the length of the magnetic material. The global transfer matrix $[T]$ is calculated by taking into account the wave propagation in the loaded section of the line and the impedance discontinuities between the empty and loaded sections of the transmission line in the propagation direction of the wave (Figure I.15).

The discontinuities are characterized by the reflection and transmission coefficients. Finally, the scattering parameters of the measurement cell are calculated by using the relations between the transfer matrix $[T]$ and scattering matrix $[S]$. A comparison between the analytical S-parameters and the measured results makes it possible to validate the Quasi-TEM assumption up to 6 GHz [22].

Inverse problem

In order to find the permeability tensor components μ and κ , the inverse problem relies on the EM analysis described previously. From this analysis, explicit analytic expressions of $\mu(\omega)$ and $\kappa(\omega)$ are obtained as a function of the measured S parameters.

This procedure is carried out in two steps. The first step consists of calculating the propagation constants γ^+ and γ^- , as a function of the measured S-parameters.

The expressions obtained are:

$$\gamma^+ = \frac{j}{d} \ln \left(\frac{S_{21}}{1 - R^+ S_{11}} \right) \quad \text{and} \quad \gamma^- = \frac{j}{d} \ln \left(\frac{S_{12}}{1 - R^+ S_{22}} \right), \quad (\text{I.29})$$

where d is the length of the sample. This length must be sufficiently short to avoid the appearance of dimensional resonances in the working frequency band.

Then in the second step, the diagonal component μ and the extra-diagonal component κ are obtained from the expressions proposed by P. Queffelec and S. Malléol in [22]:

$$\mu(\omega) = \frac{2a - 1 \cdot \gamma^+ \gamma^-}{\mu_0 \varepsilon_0 \omega^2 [(b_1 - a_1) \cdot (\varepsilon_1 + \varepsilon_2) + 2a_1 \varepsilon_f] - 2(b_1 - a_1) \cdot \gamma^+ \gamma^-} \quad (\text{I.30a})$$

$$\kappa(\omega) = \frac{[(b_1 - a_1) \cdot \mu(\omega) + a_1] \cdot (\gamma^+ \gamma^-)}{\mu_0 \varepsilon_0 \omega^2 (\varepsilon_1 + \varepsilon_2) \cdot (b_1 - a_1)} . \quad (\text{I.30b})$$

These explicit expressions for the components of the permeability tensor allow us to solve the inverse problem while avoiding the use of a numerical optimization procedure which often requires long calculation times. The expressions Eq. I.30 are valid for the case of saturated or partially magnetized ferrites in the frequency band where the quasi-TEM approximation is verified.

In conclusion, the main advantage of this method is that it gives analytical expressions for the permeability and allows us to find the permeability tensor components at different states of magnetization. Finally, the explicit analytical expressions make it possible to avoid the use of a numerical optimization procedure, this will reduce the calculation time.

I.3.3.2 Partially filled waveguide method

A characterization method based on full wave EM analysis [21, 24] to measure the complex permeability tensor components, and complex permittivity of magnetized ferrites was previously developed in our laboratory. This method uses a rectangular waveguide partially filled with a magnetic sample and a dielectric material [24] (Figure I.16) as the measurement cell.

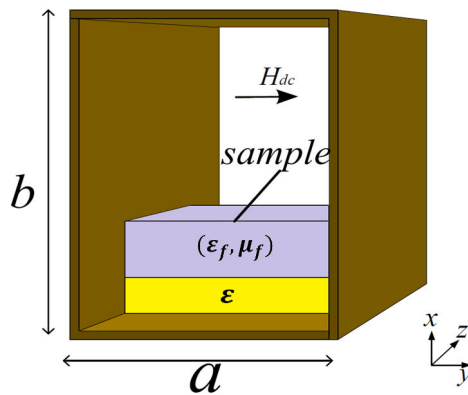


Figure I.16: Rectangular waveguide measurement cell

The principle behind this method is the use of the magnetic anisotropy of the material to achieve non-reciprocity for the measurement cell in order to have the same number of measurable parameters (S-parameters) as the number of parameters to be determined. The measurement configuration is similar to the one used for the nonreciprocal waveguide devices, except that there is no absorbing material. The waveguide is placed between the poles of an electromagnet.

Application of a static magnetic field H_{dc} , along the short side of this wave guide (y-axis) causes field displacement effect along the large side of the guide (x-axis). This effect associated with the arrangement of the materials in the guide (Figure I.16), ensures the nonreciprocal nature of the device ($S_{21} \neq S_{12}$). The sample has different effects on the forward directed modes (wave propagated in the positive direction) and the reverse modes (wave propagated in the negative direction), so transmission coefficients of the measurement cell (S_{21}, S_{12}) will be different.

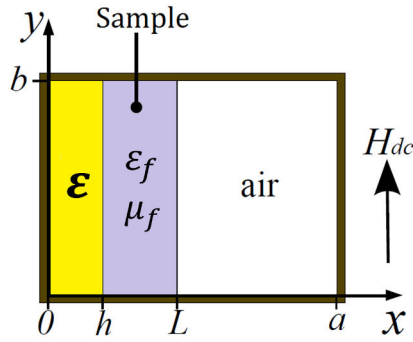


Figure I.17: Cross section of the rectangular waveguide-based measurement cell

The determination of material properties includes two different calculation procedures: direct problem and inverse problem.

The direct problem calculates the scattering parameters as functions of the scalar permittivity, tensor permeability, and dimensions of the ferrite through a rigorous EM model analysis (mode matching method). In this analysis, propagation constant of each mode inside the guide is determined (propagation constant and associated field pattern). Then, the continuity of the transverse components of the fields associated with these modes is checked at the discontinuities between empty and loaded section of the waveguide.

From this theoretical analysis, S-parameters of the waveguide are calculated. The final part is a numerical optimization procedure, which permits the determination of the scalar permittivity, (ϵ_f) and permeability (μ, κ) of the sample material by matching the theoretical S-parameters with the measured results.

Direct problem

The propagation constants of all the modes in each section of the guide (empty and loaded) must be determined by a modal analysis. In the empty sections, waveguide EM theory gives a complete analytical description of the modes [14]. On the other hand, in the loaded section, a more rigorous analysis must be carried out.

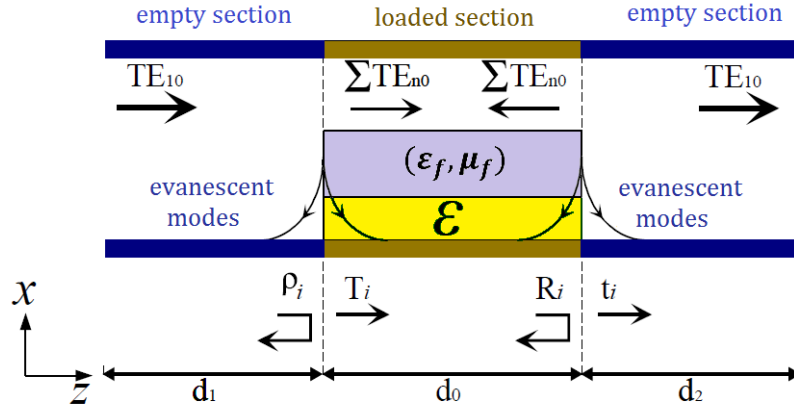


Figure I.18: Modal analysis of the measurement cell.

The loaded section is composed of three different materials: ferrite, dielectric, and air (Figure I.17). Electromagnetic fields in each of these materials are determined by solving Maxwell's equations. Then the boundary conditions are established for these fields at the boundaries between the material ($x = h$ and $x = L$), thus making it possible to determine the dispersion equation of the loaded section. The solutions to this equation are the propagation coefficients of the modes in the forward direction (γ_i^+) and in the reverse direction (γ_i^-) of the wave guide.

Once the propagation constants of these modes are determined, a mode matching technique is applied at the wave guide discontinuities between the empty sections and the loaded section (Figure I.18) and reflection coefficients (ρ_i and R_i) and transmission coefficients (T_i and t_i) are determined.

The theoretical S-parameters (S_{11} and S_{21}) can be obtained from the coupling coefficients of the dominant mode in the empty transmission line ρ_1 and t_1 , which is given by:

$$S_{11} = \rho_1 e^{-2\gamma_0 d_1} \quad (\text{I.31a})$$

$$S_{21} = t_1 e^{-\gamma_0(d_1+d_2)} \quad (\text{I.31b})$$

In these expressions, γ_0 is the propagation constant of the dominant mode in the empty sections of the guide.

To determine the parameters S_{22} and S_{12} , the same procedure is performed but considering that the fundamental mode TE_{10} propagates in the backward direction. The number of modes taken into account by this dynamic analysis is truncated to a value n which ensures the convergence of the calculated S-parameters.

Inverse problem

Dynamic methods are based on the rigorous resolution of Maxwell's equations which take into account many EM phenomena, such as the appearance of higher order modes (propagated or evanescent), radiation phenomenon in open structures, metal losses, etc. Although dynamic EM analysis requires far more complex calculations than a quasi-static analysis, it ensures high levels of accuracy. In general, the complexity of the equations to be solved does not allow the determination of explicit solutions. This fact leads to the use of numerical optimization procedures for the determination of μ and κ .

The optimization procedure involves matching the theoretical and measured parameters by minimizing an error function of several variables. Theoretical S-parameters as a function of the scalar permittivity and permeability tensor components are calculated using the previously described EM analysis.

The objective function can be defined as a sum of squared functions as,

$$E(\epsilon_f, \mu, \kappa) = \sum_{i=1}^2 \sum_{j=1}^2 \left| S_{ij}^{theo}(\epsilon_f, \mu, \kappa) - S_{ij}^{meas} \right|^2, \quad (I.32)$$

where the quantities ϵ_f , μ and κ are the optimization variables.

At a given frequency, the optimization procedure consists of adjusting the complex values of ϵ_f , μ and κ in successive iterations in order to ensure a convergence between the theoretical S-parameters (S_{ij}^{theo}) and the measured S-parameters (S_{ij}^{meas}). The optimization function which permits fast location of the global minimum by avoiding the local minima, is chosen. The procedure used is the sequential quadratic type, in order to impose limits on the optimization variables and thus to avoid non-physical solutions [25].

The dynamic analysis of the method assumes that only the fundamental mode TE_{10} is propagated in the empty section of the guide. Therefore, the operating band of this method remains limited to the single-mode band of the waveguide (8-12 GHz for an X-band guide).

This method can be applied to several guide sizes to cover varying operating frequency bands. On the other hand, any change in cross-section of the rectangular guide results in a change of sample, thus additional steps of machining and measurement.

I.3.3.3 Nonreciprocal strip line method

Another broadband transmission/reflection method was developed in the Lab-STICC based on the work of J. Lezaca [23, 26]. This method is intended to measure the properties of isotropic and anisotropic materials. The measurement using a strip line is advantageous compared to other type of transmission lines (waveguide, microstrip etc.), because the fundamental propagation mode is TEM while in others the fundamental mode is quasi-TEM.

This topology allows "in-situ" measurements, i.e. with a sample shape very close to that met in practice, for example in circulators realized using the microstrip technology.

The validity of this method extends from 100 MHz to 10 GHz [26]. The measurement cell consists of an asymmetric strip line partially filled with the material to be characterized. It is shown in Figure I.19a. Two identical samples are placed above and below the metal strip. The width of the strip is greater than the height between the strip and the ground planes, to avoid the fringing field effects.

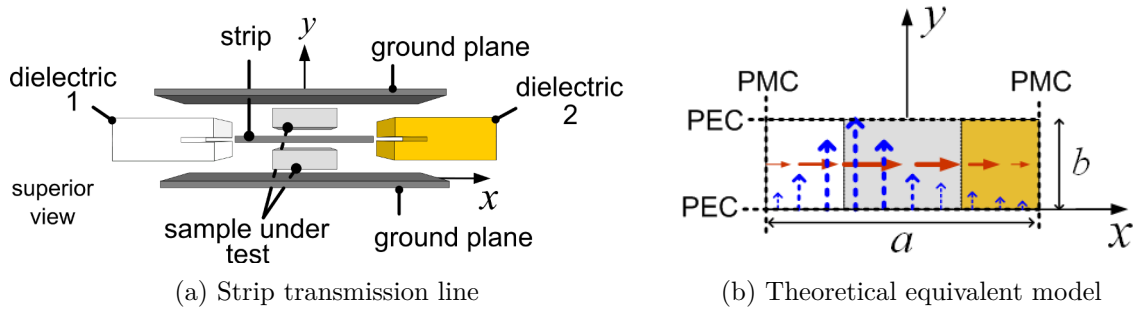


Figure I.19: Asymmetrically loaded strip line

Two dielectrics with different permittivity values (ϵ_1, ϵ_2) are placed on each side of the strip line to ensure the nonreciprocal behavior of the structure ($S_{12} \neq S_{21}$), when the magnetic sample is magnetized. In the forward direction of EM wave propagation, there is a strong wave-material interaction with the dielectric 1.

In the backward direction, the EM wave interacts with the dielectric 2 under the displacement effect of the field. This nonreciprocal nature of the measurement cell makes it possible to determine the extra-diagonal component κ of the permeability tensor.

Direct problem

This corresponds to the dynamic EM analysis of the measurement cell loaded by the material to be characterized. This procedure makes it possible to retrieve the S parameters theoretically from the constituent parameters of the material.

This problem can be described in two steps. First part is the full wave analysis of the loaded section of strip line and the calculation of dispersion diagram of the first N modes.

In the second part, a mode matching technique is employed at the impedance discontinuities to find out the theoretical S-parameters.

Material parameters are defined by analytical models, which describe the frequency dependent behavior of the parameters $\epsilon(\omega)$, $\mu(\omega)$ and $\kappa(\omega)$ from the measurable physical quantities of the materials. In the case of ferrites, the Generalized Permeability Tensor (GPT) model [27] is used to represent the tensor permeability $\hat{\mu}$ and the Debye model [4] to represent the permittivity.

The loaded section can be represented by a theoretical equivalent structure as shown in Figure I.19b. In this structure perfect electric conductors (PEC) replace the strip and the ground conductors, and perfect magnetic conductors (PMC) are used to enclose the energy inside. The equivalent structure represents one half of the measurement cell. In the other half the fields are mirror quantities and therefore do not interfere with the energy repartition inside the cell [26].

In the full wave analysis, fields inside each material are calculated, by taking into account the boundary conditions defined in the theoretical model. Applying boundary conditions at the dielectric-ferrite discontinuities leads to a system of equations.

By annulling the determinant of coefficient matrix, the dispersion equation can be obtained as follows,

$$F(\gamma, \omega, \mu, \kappa, \epsilon) = 0 \quad (\text{I.33})$$

This dispersion equation depends on the frequency, propagation constant and the EM properties of the material. The values of γ for which Eq. I.33 is satisfied, will give the propagation constants of the different modes inside the line. Once the propagation constants of all the modes (forward and reverse) in the loaded and air sections of the transmission line are known, S-parameters can be obtained by using a mode matching technique in the Oz direction.

Inverse problem

In order to measure the permeability and the permittivity of the material, an optimization procedure is defined to match theoretical S-parameters with the measured values by minimizing a broad band error function.

The optimization variables are the input parameters of the analytical models used to define frequency dependent parameters $\epsilon(\omega)$, $\mu(\omega)$, and $\kappa(\omega)$ in the direct problem.

The broadband error function is defined as,

$$E [\epsilon(\omega), \mu(\omega), \kappa(\omega)] = \sum_{f=f_{min}}^{f_{max}} \left[\sum_{i=1}^2 \sum_{j=1}^2 \left(|S_{ij}^f|_{theory} - |S_{ij}^f|_{meas} \right)^2 \right], \quad (\text{I.34})$$

This corresponds to the error value between the magnitudes of the theoretical and the measured S-parameters for each frequency value over the entire working band. The optimization procedure is done by the MATLAB subroutine *lsqnonlin*.

Only the magnitudes of the S-parameters are used in the error function to avoid phase related errors which are very important at frequencies corresponding to dimensional resonances (related to the thickness of the sample under test).

When the theoretical S-parameters are converged to the measured S-parameters, the analytical functions $\epsilon(\omega)$, $\mu(\omega)$, and $\kappa(\omega)$ represent the constituent parameters of the sample.

It should be noted that this procedure allows the characterization of samples of significant lengths because the method exploits only the magnitudes of the S-parameters. Thus the uncertainties on the phases measurements related to the appearance of dimensional resonances do not hinder the optimization procedure. On the contrary, these resonances are used to match the S-parameters more rapidly.

With strip line method we push the limits of nonreciprocal measurement methods by incorporating a non-50 Ω measurement cell, a de-embedding procedure, a general model for permeability tensor and a full wave analysis. This method has shown its ability to characterize magnetic materials for different magnetization states [23, 26, 28].

I.4 Motivation and Objectives

Microwave ferrite circulators/isolators are essential components for telecommunication applications because of their low insertion losses and high isolation properties. The operation of microwave circulators/isolators is based on the non-reciprocal effect of magnetically saturated ferrites. Precise control over the performance of these components requires prior knowledge of the dynamic behavior of ferrite materials. To fully describe the dynamic response of magnetic materials, including losses, complex quantities of the permeability tensor components $\mu = \mu' - j\mu''$, $\kappa = \kappa' - j\kappa''$, and the complex permittivity $\epsilon = \epsilon' - j\epsilon''$ have to be taken into consideration when applying in the Maxwell's equations.

Experimentally, the EM characterization of ferrites is commonly carried out in demagnetized or saturated states. For partially magnetized states different characterization techniques have been developed in the laboratory using microstrip line [20], rectangular waveguides [21] and strip line [22, 23]. The main advantage of these techniques is that they provide access to the constituent material parameters, scalar permittivity and permeability tensor.

One of the characteristics of the magnetic materials is the dependence of their dynamic response to the shape of the sample. In addition, for non-ellipsoidal magnetic material which is the case most commonly encountered in ferrite devices, the internal static biasing field is not uniform. In a previous study, it is seen that in the most common microwave applications, unsaturated regions in ferrimagnetic materials still exist, even when strong fields are applied [29]. This is due to the inhomogeneous nature of the demagnetizing fields within non-ellipsoidal samples.

Under these conditions, characterization of material from an actual or average permeability does not constitute the most accurate solution to help the designer with ferrite devices.

Commercial simulation softwares use different theoretical models to describe the permeability tensor, $\hat{\mu}$ according to the state of magnetization. These models use a number of physical parameters like saturation magnetization, anisotropy field, resonance linewidth, etc., as input parameters to describe the tensor permeability. With this procedure, one can describe the behavior of the ferrites only in the saturated state in a very satisfactory manner.

However, most of the EM simulators remain limited to certain states of magnetization, due to the simplified assumptions on which their permeability models are based upon. This limitation makes the design of devices laborious when the ferrite is neither in the saturated nor demagnetized state.

Designers often use two linewidth parameters, the resonance linewidth ΔH and the effective

linewidth ΔH_{eff} to represent the ferromagnetic losses. These quantities are not physical parameters in the strict sense of the term, which appear in Maxwell's or LLG equations like the damping factor. These quantities are directly related to damping factor by Polder's formulations, which is only valid in the saturated state. Resonant cavity methods make it possible to measure ΔH and ΔH_{eff} at a given frequency (mono-frequency method). Measuring these parameters in a wide band of frequencies would involve too many cavities and sample sizes. Moreover, the representation of the magnetic losses by two values, one near the vicinity of the gyromagnetic resonance (ΔH) and the other outside this resonance (ΔH_{eff}), reduces the predictive character of the permeability model.

Design of the new classes of ferrite devices has to be based on the combination of experimental methods and theoretical tools capable of describing the dynamic EM behavior of the ferrites. We need experimental methods to find the physical parameters of the ferrites and theoretical models which will use these parameters to describe the dynamic behavior of ferrites in all magnetization states. In this context, the general objective of our research work is to improve the EM modeling of anisotropic ferrites in order to make the design procedure more predictive and accurate for any state of magnetization.

In this line of research our objective is to develop a predictive theoretical EM simulation tool for accurate modeling of ferrite based devices by integrating the magneto-static analysis and generalized permeability tensor model with a commercial EM simulation software. A dynamic EM analysis of the structure, considering inhomogeneity of the internal fields and a generalized permeability tensor model would enable us to understand the inhomogeneous internal field distribution and the demagnetizing field effects on the performances of ferrite devices.

Most of the input parameters of generalized permeability model are the static properties of the ferrite, except the damping factor used to represent the dynamic losses. The damping factor α is a more realistic representation of the microwave losses of ferrites than the parameters currently used: ΔH and ΔH_{eff} . Static input parameters like saturation magnetization M_s , anisotropy field H_a , etc. can be measured using standard measurement methods. But the damping factor, α cannot be directly characterized with the standard measurement methods (VSM-vibrating sample magnetometer). Determination of α will allow us to describe the dynamic EM behavior of anisotropic ferrites accurately at all magnetization states.

Our first objective is to develop a simple and generalized broadband measurement method for the characterization of damping factor of polycrystalline ferrites by overcoming the constraints of the standard linewidth measurements. This parameter being the only dynamic input parameter of the theoretical model will be very useful for the designers of the microwave devices. It will allow us to predict the dynamic behavior of the ferrites more

accurately at any magnetization state and thus to optimize the design procedures.

The demagnetizing field effects due to the size and shape of the sample are prominent in non-ellipsoidal samples and accurate calculation of internal DC fields and understanding of the demagnetizing field effects are necessary to get better results with EM simulations. This brings us to our second objective, which is to improve the EM modeling of ferrite devices by integrating the magneto-static analysis and generalized permeability tensor model with a commercial simulation software like Ansys HFSS. By taking into account the variation in direction and magnitude of the demagnetizing tensor, \hat{N} , a rigorous theoretical tool will be able to predict EM properties of the ferrites more accurately and will help the designers with the design of the ferrite based devices like Circulators/Isolators, tunable filters, phase shifters, etc.

Chapitre 1. Résumé

Les matériaux ferrites sont largement utilisés dans l'électronique hyperfréquence pour de nombreuses applications de télécommunication en raison de leur forte résistivité électrique et de leur aimantation spontanée élevée. Les dispositifs comme les circulateurs/Isolateurs sont basés sur le comportement non réciproque de la propagation électromagnétique (EM) dans les ferrites aimantés. Les dispositifs tels que les filtres accordables, les lignes à retard, les déphaseurs et les atténuateurs variables, etc., exploitent la non-linéarité du comportement EM des ferrites par rapport à un champ magnétique statique. Les ferrites sont également utilisées pour la miniaturisation des antennes et la réalisation d'absorbants dans la bande UHF. Ces dispositifs exploitent la perméabilité et la permittivité élevées qui caractérisent les ferrites à l'état désaimanté.

Un contrôle précis des performances de ces composants nécessite une connaissance préalable du comportement dynamique des matériaux de ferrite. Le comportement dynamique des ferrites est représenté par la perméabilité, qui est une grandeur tensorielle $\hat{\mu}$ lorsque le milieu est aimanté. Chaque composant du tenseur a une double dépendance par rapport à la fréquence et au champ magnétique statique H_{dc} . Par conséquent, la conception et l'optimisation des dispositifs micro-ondes utilisant des ferrites nécessitent une connaissance réaliste de leur réponse dynamique, à savoir la perméabilité qui est un tenseur d'ordre 3 lorsque le matériau est aimanté (anisotropie induite par un champ magnétique statique de polarisation). statique.

Ce premier chapitre est consacré à la présentation de l'état de l'art des méthodes de caractérisation des matériaux en hyperfréquences et au contexte général de nos travaux de recherche. Ce chapitre décrit les propriétés intrinsèques des ferrites ainsi que leur réponse dynamique dans le domaine des hyperfréquences. Les problèmes qui se posent dans le domaine de la caractérisation micro-ondes des ferrites sont mis en évidence pour définir les objectifs de notre travail.

La caractérisation des matériaux est une étape importante et nécessaire, en amont de la conception et la réalisation des dispositifs hyperfréquences. Il existe différentes méthodes pour caractériser les propriétés EM des matériaux. Ces méthodes diffèrent selon différentes réalités expérimentales telles que la gamme de fréquences du matériau, sa nature isotrope ou anisotrope, la forme de l'échantillon et son caractère diélectrique ou magnétique. Ce

chapitre dresse une synthèse de l'état de l'art des techniques de caractérisation EM des matériaux magnétiques.

Expérimentalement, la caractérisation EM de ferrites est généralement réalisée dans des états désaimanté ou saturé. Par exemple, la technique en transmission / réflexion basée sur l'utilisation d'une ligne coaxiale est utilisée pour extraire la permittivité et la perméabilité scalaires des ferrites polycristallines à l'état désaimanté qui sont pas nature isotropes. A l'état saturé, une cavité résonante est utilisée pour déterminer les largeurs de raies d'absorption à mi-hauteur (ΔH et ΔH_{eff}). Ces grandeurs, qui représentent les pertes magnétiques du matériau, constituent un paramètre d'entrée du modèle de Polder, dont les formulations analytiques ne sont valables pour des milieux totalement saturés. La caractérisation des ferrites dans ses états de partielle aimantation est moins facile. Pour les états partiellement aimantés qui se retrouvent en pratique dans des circulateurs/ Isolateurs auto-polarisés, des déphaseurs et des antennes ou des filtres accordables, différentes techniques de caractérisation ont été développées dans notre laboratoire. Ces techniques utilisent des lignes microruban, des guides d'ondes rectangulaires et des lignes triplaques. Le principal avantage de ces techniques est lié au fait qu'elles permettent de remonter directement aux éléments complexes du tenseur de perméabilité, quel que soit l'état d'aimantation du ferrite, ainsi qu'à sa permittivité scalaire.

L'une des spécificités des matériaux magnétiques est la dépendance de leur réponse dynamique vis-à-vis de la forme de l'échantillon. La perméabilité d'un échantillon torique n'est pas la même que celle d'une plaquette. En outre, pour un matériau magnétique de forme non ellipsoïdale, ce qui est le cas le plus couramment rencontré dans les dispositifs à ferrite, le champ de polarisation statique interne n'est pas uniforme. Dans ces conditions, la caractérisation du matériau via une perméabilité effective ne constitue pas la solution la plus précise pour aider le concepteur de dispositifs à ferrite.

Les ferrites polycristallins présentent dans le domaine des hyperfréquences des effets dissipatifs qui dépendent du champ magnétique statique de polarisation appliqué. Ces pertes peuvent être représentées par une force d'amortissement qui contrecarre le mouvement de précession des moments magnétiques de spin. Les pertes dynamiques peuvent être représentées par la variation de la partie imaginaire de la susceptibilité ou de la perméabilité, en fonction du champ magnétique appliqué. Cette variation est habituellement de nature non-Lorentzienne. Pour tenir compte de ces pertes, un coefficient d'amortissement α est introduit dans l'équation de la cinétique d'un moment magnétique de spin, appelé équation de Landau-Lifshitz-Gilbert (LLG). En pratique, les concepteurs utilisent deux paramètres différents de largeur raie d'absorption ΔH et ΔH_{eff} qui représentent les pertes magnétiques dynamiques respectivement au voisinage de la résonance gyromagnétique et en dehors de la résonance gyromagnétique. Ces paramètres de largeur de raie à mi-hauteur sont extraits

des points expérimentaux qui donnent l'évolution de la partie imaginaire de la perméabilité mesurée μ'' en fonction du champ statique appliqué H_{dc} à une fréquence donnée. Ces quantités ne sont pas des paramètres physiques au sens strict du terme, qui apparaissent dans les équations de Maxwell ou l'équation LLG, comme peut l'être le facteur d'amortissement. Ces quantités sont directement liées au facteur d'amortissement par les formulations de Polder, qui, rappelons-le, ne sont valables qu'à l'état saturé.

Les méthodes basées sur l'utilisation de cavités résonantes permettent de mesurer ΔH et ΔH_{eff} à une fréquence donnée (méthodes mono-fréquence). La mesure de ces paramètres dans une large bande de fréquences impliquerait trop de cavités et de tailles différentes d'échantillons. En outre, la représentation des pertes magnétiques par deux valeurs, l'une au voisinage de la résonance gyromagnétique (ΔH) et l'autre en dehors de cette résonance (ΔH_{eff}), réduit le caractère prédictif du modèle de perméabilité.

La conception des nouvelles classes de dispositifs de ferrite doit être basée sur la combinaison de méthodes expérimentales et d'outils théoriques capables de décrire le comportement EM dynamique des ferrites. Nous avons besoin de méthodes expérimentales pour déterminer les paramètres physiques des ferrites, notamment leurs caractéristiques statiques (aimantation à saturation, champ d'anisotropie) et dynamiques (facteur d'amortissement) et des modèles théoriques qui utiliseront ces paramètres pour décrire le comportement dynamique des ferrites quel que soit leur état d'aimantation. Dans ce contexte, l'objectif général de notre travail de recherche est, d'une part le développement d'une technique de mesure du facteur d'amortissement et, d'autre part, d'améliorer la modélisation électromagnétique des ferrites afin de rendre la procédure de conception plus réaliste, prédictive et précise pour tout état d'aimantation.

In fine, notre objectif est de développer un outil de simulation EM prédictif pour la modélisation précise des dispositifs à base de ferrite. Préalablement, nous avons besoin d'une méthode de mesure large bande et simple d'utilisation pour la détermination du facteur d'amortissement des ferrites polycristallines de manière à contourner les contraintes des mesures de largeur de raie d'absorption standard de nature mono-fréquence. Ce paramètre, qui est le seul paramètre d'entrée dynamique du modèle de perméabilité théorique, sera très utile pour les concepteurs des dispositifs hyperfréquences à ferrite. Cela nous permettra de prédire le comportement dynamique des ferrites plus précisément et ce quel que soit leur état d'aimantation. Au final cela permettra d'optimiser les procédures de conception.

La modélisation électromagnétique des ferrites peut être améliorée en intégrant l'analyse magnétostatique et le modèle de tenseur de perméabilité généralisé avec dans un logiciel de simulation commercial comme HFSSTM d'Ansys, compte tenu de l'inhomogénéité des champs de polarisation interne. En tenant compte de la variation de direction et de la grandeur valeur des éléments du tenseur de démagnétisation désaimantation \hat{N} , un outil

théorique rigoureux pourra prédire plus précisément les propriétés EM des ferrites et aidera les concepteurs à concevoir des dispositifs à base de ferrite comme les circulateurs / isolateurs, des filtres accordables, des déphaseurs, etc. Une analyse électromagnétique dynamique de la structure, compte tenu de l'inhomogénéité des champs internes et d'un modèle de tenseur de perméabilité généralisé, nous permettrait de comprendre la distribution inhomogène du champ interne et les effets du champ de démagnétisation/démagnétisants sur les performances de ces dispositifs.

Chapter II

A Coaxial Line Method For Damping Factor Measurement

Contents

II.1 Introduction	58
II.2 Permeability tensor models	58
II.2.1 Saturated state - Polder model	58
II.2.2 Demagnetized state - Schloemann model	60
II.2.3 Partially magnetized state	62
II.2.4 Any magnetization state: Generalized permeability tensor model (GPT)	65
II.3 Measurement cell	70
II.4 General description of the method	72
II.5 Direct problem	73
II.5.1 Analytical functions for constituent parameters	74
II.5.2 EM analysis of the measurement cell	76
II.5.3 Direct problem - Results	83
II.6 Validation of the direct problem	85
II.6.1 Dielectric material	86
II.6.2 Magnetic material	87
II.7 Conclusion	90

II.1 Introduction

The purpose of this chapter is to present a simple and generalized measurement method for the determination of damping factor α , a unique quantity representing the dynamic losses in ferrite material. This unique dynamic property combined with the static characteristics (saturation magnetization, anisotropy field, etc.) would be the input parameters of theoretical tool describing the dynamic properties of the ferrite material. First, we will present theoretical models of permeability existing in the literature for different states of magnetization. Secondly a general principle of the proposed coaxial line method will be presented. Finally a description of quasi-TEM analysis of measurement cell will be presented and the EM analysis will be validated in the limit cases.

II.2 Permeability tensor models

When a static magnetic field is applied on a ferrite material, its intrinsic characteristics change. It exhibits a magnetic anisotropy and tensor permeability, $\hat{\mu}$, is then used to describe the dynamic behavior of the material. Determination of the dynamic behavior of ferrites has been the subject of numerous studies leading to different expressions for the permeability tensor components, Schloemann [30] for demagnetized ferrites, Rado [31], Green and Sandy [32], and Igarashi and Naito [33, 34] for partially magnetized ferrites, and Polder [35] for saturated media.

Within the Lab-STICC, Gelin and Queffelec have developed a model to determine the permeability tensor components in any state of magnetization, taking into account the hysteresis phenomenon and the Polder-Smit effect [27, 36].

In this section we will discuss the most remarkable models proposed in the literature to determine the permeability tensor, $\hat{\mu}$ identifying their main characteristics and limitations. We classified the models into four different cases: models working in saturated state, partially magnetized state, demagnetized state and model working at all magnetization states.

II.2.1 Saturated state - Polder model

The permeability of a ferrite material is directly related to its internal structure, and in particular to the existence of domains and domain wall formations. It is well known that magnetic moments tend to align themselves in the direction of applied magnetic field. At saturation, the intensity of the applied static field H_{dc} is strong enough to overcome the internal constraints, leading to a disappearance of domains and Bloch walls. All the moments are then aligned in the direction of the static field. Thus, it is possible to consider, for this state, a single moment of magnetization M_s , called saturation magnetization.

The small signal approximation of the equation of evolution of the magnetic moments, subjected to a static magnetic field, H_{dc} and perpendicular microwave magnetic field \vec{h} , leads to the tensor relationship between the magnetic flux density \vec{b} and the field $\vec{h}(t)$.

$$\vec{b} = \mu_0 \hat{\mu} \vec{h}.$$

$$\vec{b} = \mu_0 \begin{bmatrix} \mu & -j\kappa & 0 \\ j\kappa & \mu & 0 \\ 0 & 0 & \mu_z \end{bmatrix} \vec{h} \quad (\text{II.1})$$

$$\mu = 1 + \frac{\omega_m(\omega_0 + j\alpha\omega)}{(\omega_0 + j\alpha\omega)^2 - \omega^2} \quad (\text{II.2a})$$

$$\kappa = \frac{\omega_m\omega}{(\omega_0 + j\alpha\omega)^2 - \omega^2}, \quad (\text{II.2b})$$

where α is the damping factor that describes the dissipative effects in the material, ω_0 is the gyromagnetic resonance frequency (Larmor frequency) and ω_m is the frequency proportional to the saturation magnetization M_s of the material.

$$\omega_0 = \gamma H_{int}$$

$$\omega_m = \gamma M_s,$$

where γ is the gyromagnetic ratio (2.8 MHz/Oe).

The tensor $\hat{\mu}$ is called the Polder tensor [35]. The extra-diagonal terms denoted by $\pm j\kappa$ represent the induced anisotropy of the medium under the external magnetic field and results in the nonreciprocal nature of the EM wave propagation in a ferrite material.

The spectra of tensor components μ and κ are presented in Figure II.1. These components exhibit resonant behavior and the resonance peak occurs at the gyromagnetic resonance frequency of the ferrite material. The expressions of μ and κ (Eq. II.2a and Eq. II.2b) are valid only for uniform precession of the magnetic moments of a supposedly infinite medium and in a completely saturated state of magnetization.

In order to make the model more realistic, Kittel [37] proposes an expression for the local effective field H_{int} , which takes into account the demagnetizing fields related to the finite dimensions of the ferrite.

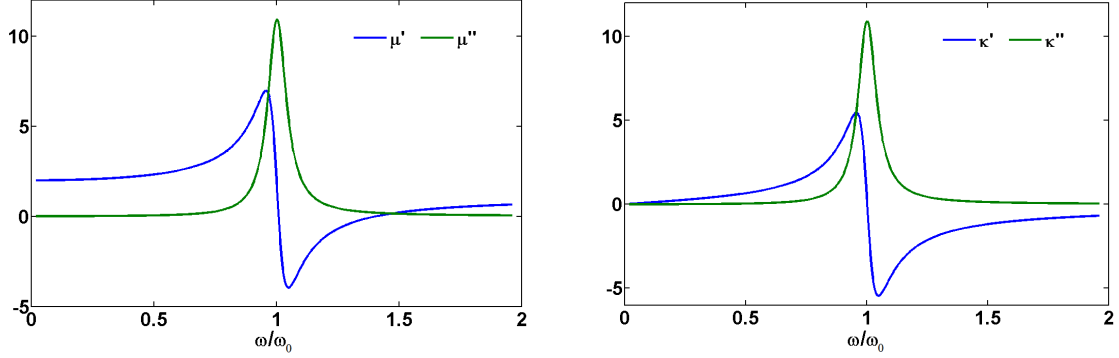


Figure II.1: Spectra of the real and imaginary parts of the diagonal μ and off-diagonal κ components of the Polder tensor.

When the applied field H_{dc} is along the z-direction, the local effective field H_{int} in a ellipsoidal sample is given by the expression [37],

$$H_{int} = \sqrt{(H_{dc} + (N_y - N_z)M_s)(H_{dc} + (N_x - N_z)M_s)}. \quad (\text{II.3})$$

The demagnetization components N_x , N_y , and N_z are directly related to the shape of the sample, and results in the displacement of gyromagnetic resonance frequency.

II.2.2 Demagnetized state - Schloemann model

In 1970 Schloemann characterized the dynamic behavior of ferrites in the demagnetized state based on the magneto-static approximations, by defining an effective permeability tensor [30]. The model is based on cylindrically symmetric domain configuration and contains only two types of domains:- ‘up’, u and ‘down’, d. These domains are magnetized to saturation and have a local permeability tensor comparable to that of Polder model, because within each domain, all the moments are parallel to each other.

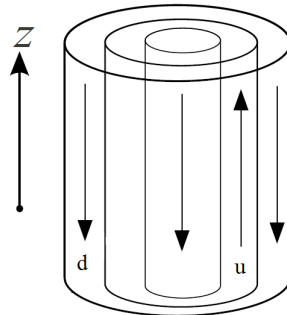


Figure II.2: Schloemann model

Thus the permeability tensors of these two domains are given by:

$$\hat{\mu}_u = \begin{bmatrix} \mu & -j\kappa & 0 \\ j\kappa & \mu & 0 \\ 0 & 0 & 1 \end{bmatrix} \quad \text{and} \quad \hat{\mu}_d = \begin{bmatrix} \mu & j\kappa & 0 \\ -j\kappa & \mu & 0 \\ 0 & 0 & 1 \end{bmatrix} \quad (\text{II.4})$$

The application of effective medium approximation (mean field theory) allows expressing the components of an effective permeability from the elements of the Polder tensor (Eq. II.4).

$$\hat{\mu}_e = \begin{bmatrix} \mu_e & -j\kappa_e & 0 \\ j\kappa_e & \mu_e & 0 \\ 0 & 0 & 1 \end{bmatrix} \quad (\text{II.5})$$

The extra-diagonal components of the effective tensor permeability disappear in the demagnetized ferrite. This effective tensor can now be represented by a diagonal tensor,

$$\hat{\mu}_e = \begin{bmatrix} \mu_e & 0 & 0 \\ 0 & \mu_e & 0 \\ 0 & 0 & 1 \end{bmatrix}, \quad (\text{II.6})$$

The components of the effective permeability (Eq. II.6) are then expressed as a function of the elements of the Polder tensor as follows:

$$\mu_e^2 = \mu^2 - \kappa^2 \quad (\text{II.7})$$

Taking into account the randomness of the magnetization direction of the domains and by making the spatial average of the three diagonal elements of the local permeability tensor, Schloemann proposed an expression for the scalar permeability of the demagnetized state :

$$\mu_{demag} = \frac{1 + 2\mu_e}{3}$$

$$\mu_{demag} = \frac{1}{3} + \frac{2}{3} \sqrt{\frac{\omega^2 - (\omega_0 + \omega_m)^2}{\omega^2 - \omega_0^2}}, \quad (\text{II.8})$$

where ω is the microwave signal frequency, ω_m is the frequency proportional to the saturation magnetization ($\omega_m = \gamma M_s$), and ω_0 is the gyromagnetic resonance frequency.

The equation Eq. II.8 is initially established for the lossless case. This can be generalized by taking the damping factor into account by replacing ω_0 by $(\omega_0 + j\alpha\omega)$. Although the Schloemann model correctly describes the microwave response of ferrites, in particular the real part of the permeability spectrum, the model remains valid only for the demagnetized case.

II.2.3 Partially magnetized state

When a ferrite is partially magnetized, existence of Weiss domains and Block walls are inevitable. Dynamic properties of the ferrite can no longer be studied using the approximation of a single magnetic moment precessing around the magnetic field. In this case, the component of the permeability tensor in the applied field direction is no longer equal to one.

Generally at any magnetization state if the applied field is along z direction, permeability tensor can be defined as:

$$\hat{\mu} = \begin{bmatrix} \mu & -j\kappa & 0 \\ j\kappa & \mu & 0 \\ 0 & 0 & \mu_z \end{bmatrix} ,$$

where, μ_z is the component of the permeability in the direction of the applied magnetic field. Polder formulations are not applicable in this state. We will now describe models that give expressions for the different components of the permeability tensor in the partial magnetization states.

II.2.3.1 Permeability model by Rado

In 1953, Rado published a theory based on the microscopic phenomena of magnetization which allowed him to deduce the expressions of the permeability tensor components [31] in partially magnetized state. By making a statistical average over all the directions of easy magnetization of the domains, this theory takes the heterogeneous factor of the media into account. In his model, Rado considers an isotropic and random distribution of magnetic moments around the direction of the static magnetic field.

By performing a spatial average, the following expressions are obtained for permeability tensor components:

$$\begin{aligned} \mu &= \mu_z = 1 \quad , \\ \kappa &= \frac{-M \omega_m}{M_s \omega} \end{aligned} \tag{II.9}$$

For frequencies above the gyromagnetic resonance ($\omega_a = \gamma H_a$), this model gives relatively accurate expressions for the extra diagonal term κ , but gives inaccurate values for the diagonal ones. The diagonal components ($\mu=\mu_z=1$) are far from reality.

In conclusion, this theory presents serious limitations for the permeability modeling of unsaturated media.

II.2.3.2 Green and Sandy model

Based on the analysis of the experimental results, Green and Sandy proposed an empirical model for the components of the permeability tensor, $\hat{\mu}$ [32].

They developed a method for the direct measurement of the permeability as a function of magnetization state of the material. These measurements are done with a cylindrical cavity TM_{110} in which ferrite rods are introduced. The permeability is then calculated as a function of the change in the resonance frequency and the quality factor, Q of the cavity. The ferrite rod is magnetized by using an electromagnet. The poles of the electromagnet are in contact with the ends of the ferrite rod to close the magnetic flux, thus ensuring the uniformity of the magnetization. Parallel permeability components μ'_z and μ''_z were measured by using spherical samples with rectangular TE_{102} reflection cavity.

From the experimental results, Green and Sandy proposed the following empirical expressions for the diagonal terms of permeability tensor:

$$\mu = \mu_{(H=0)} + \left(1 - \mu_{(H=0)}\right) \left(\frac{M}{M_s}\right)^{\frac{3}{2}} \quad (\text{II.10})$$

$$\mu_z = \mu_{(H=0)} \left(1 - \frac{M}{M_s}\right)^{\frac{5}{2}} \quad (\text{II.11})$$

$$\mu_{(H=0)} = \frac{2}{3} \left[1 - \left(\frac{\gamma 4\pi M_s}{\omega}\right)^2\right]^{\frac{1}{2}} + \frac{1}{3} \quad (\text{II.12})$$

In these expressions, M_s is the saturation magnetization of the sample, and the ratio, M/M_s represents the reduced magnetization of the sample.

The expression for diagonal terms obtained by Green and Sandy for $\mu_{(H=0)}$ is similar to that proposed by Schloemann in the demagnetized case (Eq. II.8). But in magnetized states, this model is not very accurate. Moreover, it does not give access to the magnetic losses of the material.

II.2.3.3 Igarashi and Naito

In their papers [33, 34] Igarashi and Naito presented two models with semi empirical formulations for the permeability tensor components. In their first paper [33], the authors propose expressions for the diagonal components of the tensor. In their subsequent paper [34], they gave an expression for the extra diagonal terms.

These formulations are made using spatial averages and adjustment parameters set using

the experimental results. They describe the medium through a random distribution of domains with different magnetizations, positive and negative, without imposing a particular shape on them.

For partially magnetized ferrites with random domain orientation, they give an expression for the diagonal component of the effective tensor permeability,

$$\langle \mu \rangle = \frac{2}{3} \left\{ \sqrt{\mu^2 - \kappa^2} (1 - \langle \alpha_3 \rangle^2) + \mu \langle \alpha_3 \rangle^2 \right\} + \frac{1}{3} . \quad (\text{II.13})$$

Compared to the other models, the main difference is the introduction of the quantity $\langle \alpha_3 \rangle$ in the tensor calculations. Igarashi and Naito have proposed an empirical formulation for the variable $\langle \alpha_3 \rangle$ of the form:

$$\langle \alpha_3 \rangle = \sin(bH_N) , \quad (\text{II.14})$$

$$H_N = \frac{H}{N_z M_s / \mu_0} \quad (\text{II.15})$$

where N_z corresponds to the demagnetizing coefficient in the direction of magnetization, H is the static field applied and the coefficient b is an adjustable coefficient.

In the particular case of the demagnetized state ($\langle \alpha_3 \rangle = 0$), the results correspond well to the theory proposed by other models such as Schloemann's. Similarly when the material is saturated ($\langle \alpha_3 \rangle = 1$), this model coincides with the expression of the diagonal components of Polder model.

In their second model [34], authors deduce expressions for the diagonal component μ_z and the off-diagonal component κ of the permeability tensor. The expression obtained for the off-diagonal component κ is the same as that proposed by Rado. For the μ_z component, the authors proposed the following expression:

$$\langle \mu_z \rangle = 1 + \chi (1 - \langle \alpha_3 \rangle^2) = 1 + \frac{\omega_m (\omega_e + j\alpha\omega)}{(\omega_e + j\alpha\omega)^2 - \omega^2} [1 - \langle \alpha_3 \rangle^2] \quad (\text{II.16})$$

In this expression, when the magnetization is close to saturation, $\langle \alpha_3 \rangle$ approaches unity, and the real part of μ_z tends to 1 while the imaginary part tends to zero.

In the partially magnetized case, the parameter ω_e in the expressions of the tensor components has to be adjusted experimentally. Since the values of b and H are determined experimentally, this model cannot be considered as a predictive model. Moreover, this model does not take into account the hysteresis phenomenon. Finally, the expression cannot predict the displacement of the gyromagnetic resonance frequency with the magnitude of the field H .

II.2.4 Any magnetization state: Generalized permeability tensor model (GPT)

The models described above are not suitable for rigorously describing the dynamic behavior of the components of the permeability tensor, $\hat{\mu}$ at all the magnetization states. In general, these models do not take into account all the static and dynamic phenomena influencing the dynamic behavior of the ferrites. For example, none of the models predicts the actual value of the static magnetic field within domains. For the most part, these models use the ratio M/M_s to represent the magnetization state of the ferrite.

However, this is not sufficient to describe the static properties of ferrites (direction and configuration of magnetic moments, local internal field to the domains, hysteresis phenomenon, etc.). Consequently, it is necessary to have a better approach at the static level, for example, with a magnetization law connected to the internal structure which makes it possible to calculate the local fields in the domains. In the previous models, dynamic interactions between magnetic domains are not taken into account, with the exception of the Schloemann model. These interactions essentially influence the dynamic behavior of the magnetized media and depend considerably on the shape of the magnetic domains, defects or porosity [15].

Under these conditions, Gelin and Queffelec [27, 36] proposed a generalized model for the permeability tensor components known as the "Generalized Permeability Tensor Model" (GPT). This model predictively describes the dynamics of the permeability tensor components of polycrystalline ferrites using a more realistic approach than previously proposed models. This approach takes into account the inherent physical phenomena in polycrystalline ferrites such as the Polder-Smit effect, the hysteresis phenomenon and statistical distribution on the shape of grains and domains.

GPT model framework

The GPT model considers ferrite as an agglomeration of grains, which are themselves divided into magnetic domains. The model approach is divided into two problems, as shown in Figure II.3.

First the static quantities are determined within each domain. This includes the calculation of the magnitude and direction of the internal magnetic field H_{int} and the associated magnetization vector \vec{M} as a function of the static field applied by taking into account the hysteresis phenomena, the demagnetizing fields and the anisotropy field. This procedure is called the static problem.

The second step is called the dynamic problem, consists of taking into account the interactions between adjacent domains and grains which depend on their respective shapes (Polder-Smit effect [15]). This is done by solving the equation of evolution of the magnetic

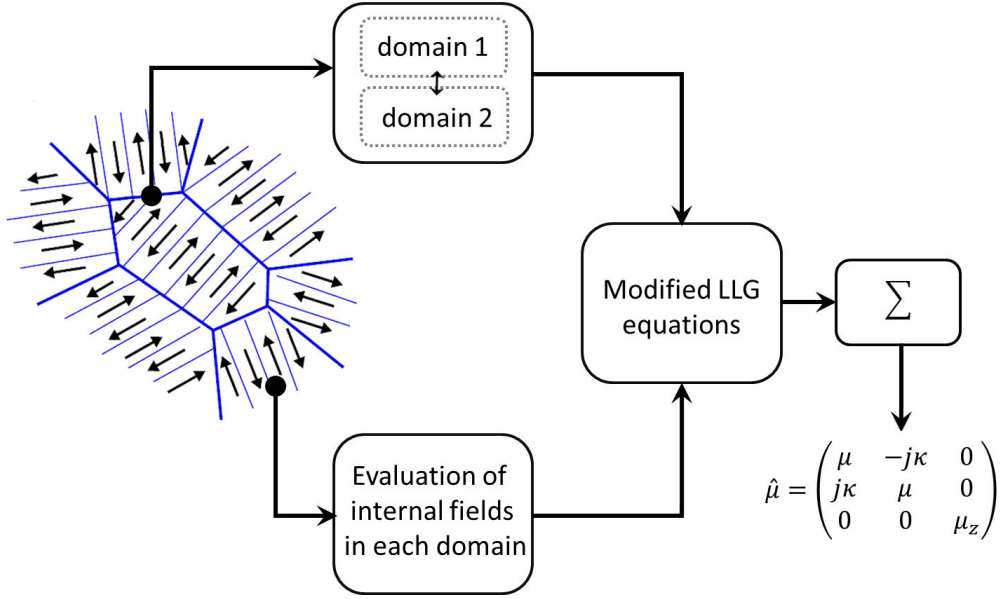


Figure II.3: GPTmodel- Principle.

moments (Eq. II.21) in each domain. Once these two problems are solved, a statistical summation of the set of dynamic magnetization vectors \vec{m}_i is carried out in space to obtain the permeability tensor $\hat{\mu}$ of the ferrite. The limits of this statistical summation vary according to the state of magnetization of the material.

As this model plays an important part of our research work, we will make a more detailed description in the following.

Static problem

In the demagnetized state, grains in polycrystalline ferrite are divided into domains as in Figure II.4. The grains are considered as mono crystals with easy axis described by the angles (ϑ, φ) (see Figure II.4a). Within each grain, adjacent domains are aligned either parallel or antiparallel to the easy axis direction.

Consequently magnetization vector \vec{M}_1 in domain 1 will have a direction \vec{u}_1 and \vec{M}_2 in domain 2 will have a direction \vec{u}_2 . Thus, for two adjacent domains the effective magneto static fields will be $\vec{H}_1 = H_a \vec{u}_1$ and $\vec{H}_2 = H_a \vec{u}_2$, where H_a corresponds to the anisotropy field.

When the ferrite is in a partially magnetized state (Figure II.4b), the magnitudes of magnetizations (\vec{M}_1, \vec{M}_2) and their equilibrium positions (\vec{u}_1, \vec{u}_2) change with respect to their initial values (see Figure II.4b). This change depends on the magnitude of the static field H_{dc} , the anisotropy field H_a , and also on the previous state of magnetization (hysteresis phenomenon). In order to find the new effective local magnetic field and its associated

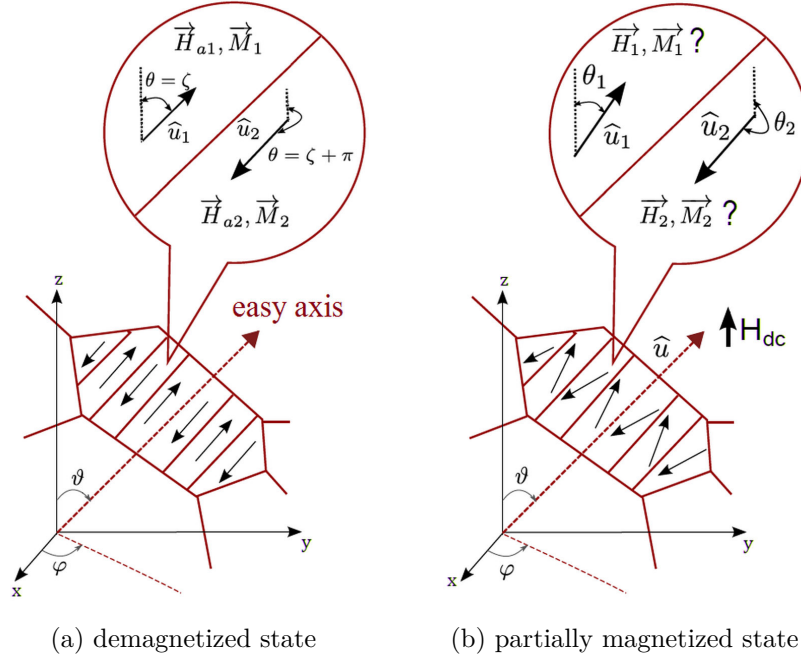


Figure II.4: Moment directions in polycrystalline ferrites.

equilibrium direction, a hysteresis model based on the work of Stoner and Wohlfarth [38] is used.

The model of Stoner and Wohlfarth (1948) is an energy model that links the behavior of the magnetization M to the applied field H_{dc} . This model assumes that the domains are isolated from each other and considers only the hysteresis phenomenon by rotation and tilting of the magnetic moments. The value of the equilibrium direction \vec{u}_i is obtained by minimizing the total energy W_i of a domain i (Figure II.5).

This energy W_i is the sum of the magneto-crystalline energy and the magneto static energy. The new equilibrium direction ζ is thus determined by the equation,

$$K_1 \sin 2(\vartheta - \zeta) = M_s H_0 \sin \zeta, \quad (\text{II.17})$$

K_1 is related to anisotropy field H_a ,

$$H_a = \frac{2K_1}{M_s}. \quad (\text{II.18})$$

It is important to note that the position ζ is independent of the angle φ (Figure II.5). The magnetic field within the domain H_i corresponds to the second order derivative of the

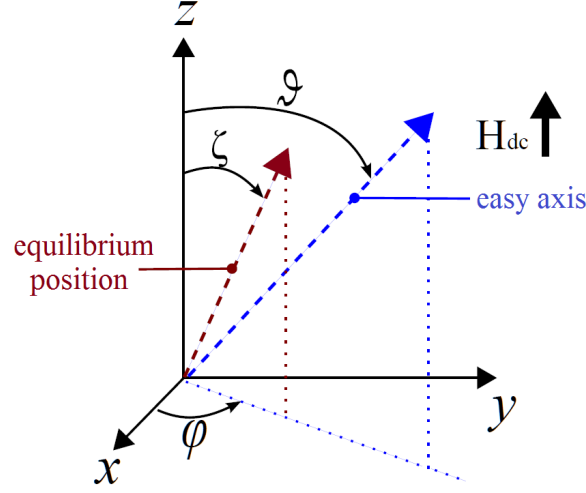


Figure II.5: Magnetized equilibrium direction of the domains

energy W_i and is given by,

$$H_i(H_0, \vartheta) = H_a \cos(2\vartheta - 2\zeta) + H_0 \cos \zeta. \quad (\text{II.19})$$

For the demagnetized state, where $H_0 = 0$ and $\zeta = \vartheta$, internal field H_i is equal to anisotropy field H_a . Finally, the GPT model takes into account macroscopic demagnetizing fields related to the shape of the ferrite sample. The internal static field is then corrected according to the relation:

$$\vec{H}_0 = \vec{H}_{dc} - N\vec{M} \quad (\text{II.20})$$

The demagnetizing coefficient N in the direction of the static field depends only on the geometrical dimensions of the ferrite sample.

Dynamic problem

The GPT model uses the Landau-Lifshitz-Gilbert equation to describe the evolution of magnetic moments under the effect of the microwave field $\vec{h}(t)$ taking into account the inter-domain coupling [10].

$$\frac{\partial \vec{M}_i(t)}{\partial t} = \gamma \vec{M}_i \times (\vec{H}_i + \vec{h}_i(t)) - \frac{\alpha}{M_s} \vec{M}_i(t) \times \frac{\partial \vec{M}_i(t)}{\partial t}, \quad (\text{II.21})$$

$$\vec{M}_i = M_s \hat{u}_i + \vec{m}_i(t) ,$$

$$\vec{H}_i = H_i \hat{u}_i, \quad \text{where } i = 1, 2 .$$

In the equation Eq. II.21, \vec{m}_i is the dynamic magnetization in the domain 'i', α is the damping coefficient, $\vec{h}_i(t)$ is the local variable magnetic field, γ is the gyromagnetic ratio and M_s is the saturation magnetization.

The equation Eq. II.21 is then applied to all the adjacent domains of the grain and thus forming a system of coupled equations Eq. II.22. These adjacent domains have their internal fields defined respectively by \vec{H}_1 and \vec{H}_2 with their associated directions \hat{u}_1 and \hat{u}_2 .

$$\frac{\partial \vec{M}_1(t)}{\partial t} = \gamma \vec{M}_1 \times (\vec{H}_1 + \vec{h} - \vec{h}_d - \vec{h}_g) + \frac{\alpha}{M_s} \vec{M}_1 \times \frac{\partial \vec{M}_1(t)}{\partial t} \quad (\text{II.22a})$$

$$\frac{\partial \vec{M}_2(t)}{\partial t} = \gamma \vec{M}_2 \times (\vec{H}_2 + \vec{h} - \vec{h}_d - \vec{h}_g) + \frac{\alpha}{M_s} \vec{M}_2 \times \frac{\partial \vec{M}_2(t)}{\partial t} , \quad (\text{II.22b})$$

The field \vec{h}_d corresponds to the dynamic demagnetizing field bounded to the shape of the domain and n_d is the demagnetizing coefficient in the direction of the dynamic magnetization (Eq. II.23). This term allows to take into account Polder-Smit effect [15], that is to say the dynamic coupling between magnetic moments of adjacent domains.

$$\vec{h}_d = -n_d (\vec{m}_1 - \vec{m}_2) , \quad (\text{II.23})$$

$$\vec{h}_g = -n_g \left(\frac{\vec{m}_1 + \vec{m}_2}{2} - \frac{M}{M_s} \langle \vec{m} \rangle \right) \quad (\text{II.24})$$

It should be noted that \vec{h}_d is maximal when \vec{m}_1 and \vec{m}_2 are opposite in phase and minimal when they are in phase. Similarly, the field \vec{h}_g represents the dynamic demagnetizing field linked to the shape of the grain and n_g is the demagnetizing coefficient in the direction of the dynamic magnetization (Eq. II.24). This grain is surrounded by an effective medium with an effective magnetization $\langle \vec{m} \rangle$.

Permeability tensor

Once all the static parameters are determined, the system of coupled equations of the dynamic problem (Eq. II.22) can be solved and the dynamic magnetization vector \vec{m}_i is calculated as a function of microwave field \vec{h}_i , the applied magnetic field (H_{dc}, ϑ) and the demagnetizing coefficients of the grain (n_g) and the domain (n_d).

$$\vec{m}_i = (H_{dc}, \vartheta, \vec{h}_i, n_g, n_d) . \quad (\text{II.25})$$

In order to calculate the permeability tensor $\hat{\mu}$ of a bulk sample, a statistical summation of the local dynamic magnetizations is performed. This summation takes into account the possible directions of the vector \vec{m}_i described by the angles ϑ and φ and the possible grain

and domain shapes (Eq. II.26).

$$\langle \vec{m}_i(\vec{h}, H_{dc}) \rangle = \int_{\varphi} \int_{\vartheta} \int_{n_g} \int_{n_d} P_1 \cdot P_2 \cdot P_3 \vec{m}_i \, dn_d dn_g d\vartheta d\varphi, \quad (\text{II.26})$$

$$P_1 = P_1(\varphi, \vartheta), \quad P_2 = P_2(n_g), \quad P_3 = P_3(n_d) \quad .$$

The functions P_1 , P_2 and P_3 are the distribution functions chosen as a function of the easy axes orientation, and the grain and domain shapes. Finally permeability tensor is obtained using the relation,

$$\vec{b} = \mu_0 \left(\vec{h} + \langle \vec{m}(\vec{h}, H_{dc}) \rangle \right) = \mu_0 \hat{\mu}_{gpt} \vec{h} \quad (\text{II.27})$$

From a self-consistent theoretical approach, this model provides the tensor permeability $\hat{\mu}_{gpt}$, whatever the frequency range and the state of magnetization are, from the demagnetized state to the saturation. This model takes into account the demagnetizing field effects in the grains and domains and the dynamic interactions between domains and grains and ensures causality of the tensor components.

II.3 Measurement cell

Broadband measurement techniques allow characterization of materials in a very broad frequency band. Among the broadband techniques, there are basically three types: free space, guided structures and radiating probes (for example coaxial probe). Radiating probes are limited to the characterization of dielectric materials because only one parameter is measured, i.e. the reflection coefficient, giving access to one constitutive parameter of the material to be characterized. Then, the case of magnetic materials can not be treated by this approach because two constitutive parameters, the permittivity and the permeability of the materials are unknown.

Free space techniques offer some freedom in choosing the shape of the sample. But there are some errors related to the edge effects. These methods are more suitable for the millimeter wave range with typical surface area of the sample around $10 \times 10 \text{ cm}^2$. On the other hand in guided structures, the sample under test is placed inside a waveguide or a transmission line where it can fill all or part of its cross-section. For these structures, the size of the sample under test is generally smaller than the one required with the free space method. The operating frequency band of these techniques is determined by the cut off frequency of the first higher order mode. In the case of waveguides, operating band remains relatively narrow, ranging from the frequency of appearance of the fundamental mode to the frequency

of occurrence of the first higher order mode. These two frequencies are closely related to the dimensions of the waveguide.

In the case of transmission lines, the fundamental mode is the TEM (or quasi-TEM for planar structures : microstrip and coplanar) mode and the occurrence of first higher order mode can easily be chosen above 10 GHz. The shielding provided by the outer conductor of the coaxial line or the two ground planes of the strip line avoid radiation losses. The fundamental mode in these transmission lines is the TEM mode. On the other hand, in the case of the microstrip and coplanar transmission lines, fundamental mode is quasi-TEM. TEM mode can be easily described by the classical transmission-line theory and its inclusion in a dynamic EM analysis is simple and straightforward. Under these conditions, a transmission/reflection technique is the most adapted method for the problem posed.

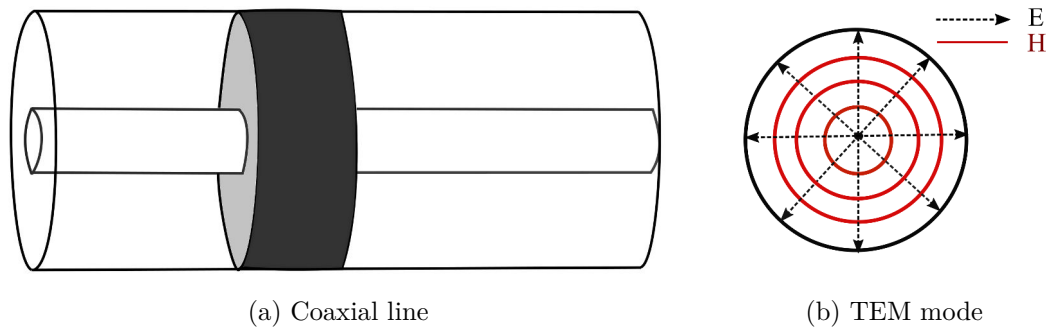


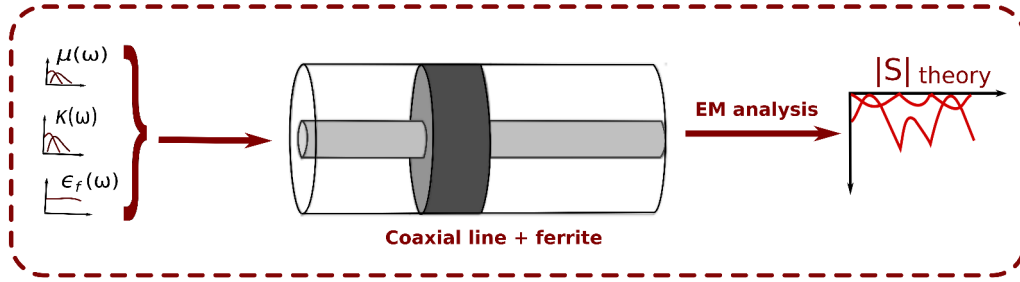
Figure II.6: Coaxial line-based measurement cell and field pattern for the TEM dominant mode.

Material characterization techniques previously developed in Lab-STICC [20–23] make use of the non-reciprocity of the measurement cell to directly access the constituent material parameters, scalar permittivity and tensor permeability components. Our objective is to develop a method to determine the damping factor which will be then used as an input parameter for theoretical tools to describe the dynamic behavior of anisotropic ferrites. Since the only parameter to be determined is the damping factor, nonreciprocal behavior of the measurement cell is not a requirement any more.

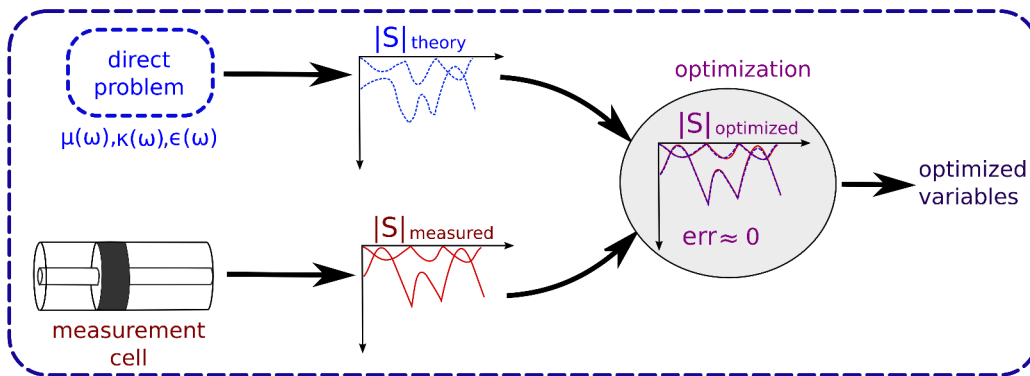
Considering all this factors, a coaxial line is chosen as the measurement cell for the proposed method. The coaxial measurement cell is of APC7 standard with an outer diameter of 7 mm and an inner diameter of 3.04 mm. The fundamental mode of propagation in the empty section of coaxial line is pure TEM mode. The sample is square toroidal in shape. The ferrite sample is inserted between the inner and the outer conductors of the coaxial line. The coaxial line partially filled with sample to be characterized is placed in between the poles of an electromagnet and the sample is magnetized in the longitudinal direction (propagation direction). Under the action of an applied static magnetic field, sample becomes anisotropic in nature.

II.4 General description of the method

The proposed measurement method can be divided into two parts: the direct problem (EM analysis) and the inverse problem (optimization procedure) as shown in Figure II.7.



(a) direct problem



(b) inverse problem

Figure II.7: General description of the method.

The direct problem corresponds to the dynamic EM analysis of the measurement cell containing the sample to be characterized. This dynamic analysis takes into account the contributions from the fundamental quasi-TEM and higher symmetrical modes in the wave propagation inside the sample. The propagation constant of the symmetric modes (quasi-TEM) in the ferrite sample are calculated by solving boundary value problems, when the fields in the ferrite are made to satisfy the boundary conditions at the inner and outer conductor surfaces.

The S-parameters of the loaded section of the coaxial cell are determined theoretically from this EM analysis. In these calculations, the constitutive parameters of the sample ϵ_f , μ , and κ are represented by the analytical functions which reproduce dispersive and resonant behavior of the materials.

Generalized permeability model is used to describe the permeability tensor components and Cole-Cole model [39] is used to represent the dispersive nature of permittivity. The input parameters of these analytical functions are the static and dynamic properties of the material. In summary, the direct problem provides a relation between constituent parameters of the material and the theoretical S-parameters of the measurement cell.

The inverse problem consists of a broadband optimization procedure for finding the damping factor of the sample to be characterized. The optimization procedure ensures the convergence of theoretical S-parameters with the measured S-parameters over the entire frequency band, by minimizing a broadband error function. This numerical procedure uses the damping factor and applied field as optimization variables.

This broadband characterization method can be used from DC to millimeter wave frequencies since the dominant mode propagated in the empty coaxial line is TEM mode which has no cut-off frequency. Only the magnitudes of the S-parameters are taken into account in the optimization procedure to avoid phase related errors associated with the dimensional resonances. The frequency of occurrence of these resonances is strictly related to the length of measured sample. Thus by avoiding the use of the phase in the optimization procedure, these dimensional resonances do not affect the accuracy of the method. On the contrary, the inverse problem use these dimension resonances to converge S-parameters more rapidly and more precisely.

II.5 Direct problem

In our case, direct problem consists of the calculation of theoretical S-parameters of the measurement cell from constitutive parameters (ϵ, μ, κ) of the material. It is based on the rigorous description of the EM behavior of the coaxial transmission line loaded by the material to be characterized by using a quasi-TEM approximation.

Direct problem takes place in two steps:

- Definition of the analytic functions representing the frequency dependent parameters $\epsilon(\omega)$, $\mu(\omega)$, and $\kappa(\omega)$ of the material.
- An EM analysis to compute theoretical S-parameters.

Once the analytical functions $\epsilon_f(\omega)$, $\mu(\omega)$, and $\kappa(\omega)$ are defined, an EM analysis is carried out at the discontinuities between the empty section and ferrite loaded section of the coaxial line. A complex root searching procedure is used to calculate the theoretical propagation constants of the electromagnetic wave propagating inside the loaded section of the measurement cell. Theoretical S-parameters are then determined using classical transmission line theory.

II.5.1 Analytical functions for constituent parameters

The direct problem requires prior knowledge of the constituent parameters ϵ , μ , κ of the material present in the cell. These parameters will be represented by analytical functions which reflect the physical properties of material. The resonant character of permeability, and slightly dispersive or relaxation behavior of permittivity can be represented either by existing theoretical models of permeability [33, 35, 36] and permittivity [39] or simply by using general polynomial functions.

Cole-Cole model [39] can be used to represent the dispersion of permittivity of dielectrics and those of ferrites. A general Cole-Cole formulation is given by,

$$\epsilon_f(\omega) = \epsilon_\infty + \frac{\epsilon_s - \epsilon_\infty}{(1 + j\omega\tau)^{1-\psi}} \quad (\text{II.28})$$

This function depends on four variables: the static permittivity ϵ_s , ‘infinite frequency’ permittivity ϵ_∞ , the relaxation time τ , and an experimental correction factor ψ ($1 < \psi < 0$). Note that when $\psi=0$, the Cole-Cole function becomes a Debye-type relaxation function [39]. The Cole-Cole function makes it possible to represent the majority of the cases encountered in our study: materials with constant permittivity (when τ is zero), low dispersive materials (when τ is low) and materials with relaxation behavior.

Several theoretical models have already been proposed in the literature to describe the permeability tensor components [27, 30–36].

Table II.1 summarizes the main features of the permeability tensor models presented in (Section II.2).

	Model	Properties	Limitations
1	Polder	<ul style="list-style-type: none"> ◇ LLG equation ◇ Linewidth parameters, ΔH and ΔH_{eff} 	<ul style="list-style-type: none"> ◇ Saturated state
5	Schloemann	<ul style="list-style-type: none"> ◇ Predictive model, in particular for $\text{Re}\{\mu\}$ ◇ interactions between domains ◇ Simple domain structure 	<ul style="list-style-type: none"> ◇ Demagnetized state ◇ Does not follow Polder model

2	Rado	<ul style="list-style-type: none"> ◇ Spatial average of different orientations of the domains 	<ul style="list-style-type: none"> ◇ Partially magnetized state ◇ Non-predictive for diagonal elements of the μ tensor ◇ Interactions between domains are neglected
3	Green and Sandy	<ul style="list-style-type: none"> ◇ M/M_s ratio to define magnetization state ◇ Consistent with Schloemann's model 	<ul style="list-style-type: none"> ◇ Does not take into account the hysteresis effect ◇ Limited to low magnetic losses
4	Igarashi and Naito	<ul style="list-style-type: none"> ◇ Magnetization law ◇ Consistent with Schloemann and Polder models ◇ Spatial average of evolution of magnetic moments 	<ul style="list-style-type: none"> ◇ Non-predictive ◇ Semi empirical model ◇ Does not take into account the hysteresis effect
6	Generalized Permeability Tensor	<ul style="list-style-type: none"> ◇ Calculation of internal field as a function of external field ◇ Hysteresis phenomenon ◇ Taking into account the interaction between domains ◇ LLG equation ◇ Taking into account demagnetizing fields ◇ Good agreement with measurements 	<ul style="list-style-type: none"> ◇ The choice of probability distribution functions on grain and domain shapes is difficult.

Table II.1: Comparison between the permeability tensor models.

Most of these models remain limited to a single state of magnetization. With the exception of the GPT model, no model is able to predict the evolution of the permeability tensor, starting from demagnetized state to remanent state passing through saturation.

Designers often use Polder model due to the fact that it describes dynamic behavior of ferrite materials in a very satisfactory manner in the saturated state. The losses are determined from two linewidth quantities ΔH and ΔH_{eff} , one deducted from the magnetic susceptibility measurements in the vicinity of the gyromagnetic resonance (ΔH), the other

determined from experimental data obtained outside the resonance region (ΔH_{eff}). Damping factor α is calculated from the linewidth parameters using Polder theory. As a result, device designers often perform interpolations to calculate losses at different frequencies. In addition, Polder model assumes a uniform magnetization in the material with ellipsoidal sample shapes, which is not always true in practice. Non-ellipsoidal sample forms used in practice lead to non-homogeneity of the demagnetizing fields.

On the other hand, Generalized Permeability Tensor (GPT) model developed in our laboratory obtained satisfactory results in the description of permeability tensor components of the polycrystalline ferrites for any state of magnetization. GPT model can describe a more realistic and predictive frequency behavior of ferrites from known intrinsic quantities. The input parameters are static properties like saturation magnetization $4\pi M_s$, anisotropy field H_a , and the damping factor α used to represent the ferromagnetic losses in the ferrite material.

Damping factor being the single dynamic input parameter of GPT model, helps us to describe a relation between the intrinsic losses in ferrites with its high frequency behavior. Thanks to its predictive nature, GPT model can be used for confrontation of theory with measurement for different magnetization states. Since our objective is to find a unique value for damping factor, we chose GPT model to compute the permeability tensor components of anisotropic ferrites.

II.5.2 EM analysis of the measurement cell

The theoretical solutions for cylindrical waveguide filled with ferrite medium magnetized in the longitudinal direction, are well known in literature [40, 41]. The case of ferrite filled coaxial wave guide magnetized in the longitudinal direction is implied by Kales [40]. Epstein [41] presented explicit theoretical solutions for fields inside a coaxial wave guide filled with ferrite medium.

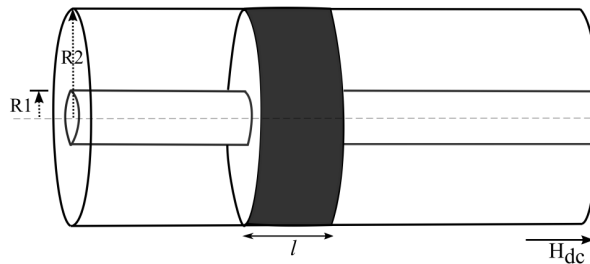


Figure II.8: Axially magnetized coaxial cell filled with ferrite sample.

When a coaxial line containing ferrite medium is magnetized in the longitudinal direction, ferrite medium become anisotropic in nature. This leads to a tensor relationship between the magnetic induction B and applied field H ,

$$B = \hat{\mu}H \quad , \quad (\text{II.29})$$

Here $\hat{\mu}$ denotes the tensor permeability.

$$\hat{\mu} = \begin{bmatrix} \mu & -j\kappa & 0 \\ j\kappa & \mu & 0 \\ 0 & 0 & \mu_z \end{bmatrix} \quad , \quad (\text{II.30})$$

For a time dependence $e^{j\omega t}$ and z-dependence $e^{-\gamma z}$, Kales defined a pair of wave equation of the form [40],

$$\Delta_t^2 u_1 + S_1^2 u_1 = 0 \quad (\text{II.31})$$

$$\Delta_t^2 u_2 + S_2^2 u_2 = 0$$

The functions u_1 and u_2 are defined as the solutions to the wave equation (Eq. II.31).

The parameters S_1 and S_2 are called the separation constants. They are defined as the square root of Kale's separation constants [40] for convenience.

$$S_i^2 = \frac{1}{2} \left[a + c \pm \sqrt{(a - c)^2 + 4bd} \right] \quad , \quad (\text{II.32})$$

where

$$a = \omega^2 \epsilon \mu_0 \frac{\mu^2 - \kappa^2}{\mu} - \gamma^2$$

$$b = j\omega \gamma \mu_0 \frac{\kappa}{\mu}$$

$$c = \frac{1}{\mu} (\omega^2 \epsilon \mu_0 \mu - \gamma^2)$$

$$d = -j\omega \gamma \epsilon \frac{\kappa}{\mu}.$$

In these relations $\gamma = \alpha + j\beta$ is the propagation constant and ω is the angular frequency.

If r is the radial variable and an angular field dependence of $e^{jn\phi}$ is assumed, Eq. II.31 becomes Bessel's equation of order n with solution,

$$u_i = [A_i J_n(S_i r) + B_i N_n(S_i r)] e^{jn\phi} , \quad (\text{II.33})$$

where A_i, B_i are unknown field magnitudes, the functions J_n and N_n are the Bessel functions of first and second kinds respectively.

The general field equations can be written as,

$$E_z = \sum_{i=1}^2 S_i^2 [A_i J_n(S_i r) + B_i N_n(S_i r)] e^{\pm jn\phi} \quad (\text{II.34a})$$

$$H_z = \sum_{i=1}^2 \frac{(S_i^2 - a)}{b} S_i^2 [A_i J_n(S_i r) + B_i N_n(S_i r)] e^{\pm jn\phi} \quad (\text{II.34b})$$

$$E_r = \sum_{i=1}^2 \left\{ \frac{S_i^2 - a}{b} \frac{\mu n}{j\gamma\kappa} [A_i J_n(S_i r) + B_i N_n(S_i r)] - j\gamma S_i [A_i J'_n(S_i r) + B_i N'_n(S_i r)] \right\} e^{\pm jn\phi} \quad (\text{II.34c})$$

$$E_\phi = \sum_{i=1}^2 \left\{ \frac{\gamma n}{r} [A_i J_n(S_i r) + B_i N_n(S_i r)] + \frac{\mu(S_i^2 - a)}{\gamma\kappa} S_i [A_i J'_n(S_i r) + B_i N'_n(S_i r)] \right\} e^{\pm jn\phi} \quad (\text{II.34d})$$

$$H_r = \sum_{i=1}^2 \left\{ -n\omega\epsilon [A_i J_n(S_i r) + B_i N_n(S_i r)] + (\omega^2\mu\epsilon - \gamma^2 - S_i^2) \frac{S_i}{\omega\kappa} [A_i J'_n(S_i r) + B_i N'_n(S_i r)] \right\} e^{\pm jn\phi} \quad (\text{II.34e})$$

$$H_\phi = \sum_{i=1}^2 \left\{ (\omega^2\mu\epsilon - \gamma^2 - S_i^2) \frac{jn}{\omega\kappa r} [A_i J_n(S_i r) + B_i N_n(S_i r)] + j\omega\epsilon S_i [A_i J'_n(S_i r) + B_i N'_n(S_i r)] \right\} e^{\pm jn\phi} \quad (\text{II.34f})$$

II.5.2.1 Theoretical solutions for propagation constant

In the general field equations, setting $n = 0$ yields the expressions for the quasi-TEM and all higher symmetrical modes. The technique for obtaining the propagation constant inside a ferrite filled coaxial line has been reported [42–44] in literature. The propagation constant of the quasi-TEM mode is obtained by solving the boundary value problems when the fields in the ferrite are made to satisfy the boundary conditions at the inner and outer conductor surfaces of the coaxial line.

The tangential electric fields of the quasi-TEM mode and higher symmetrical modes in the ferrite filled section are given by,

$$E_z = \sum_{i=1}^2 S_i^2 [A_i J_0(S_i r) + B_i N_0(S_i r)] \quad (\text{II.35})$$

$$E_\phi = \sum_{i=1}^2 \frac{\mu(S_i^2 - a)}{\beta\kappa} S_i [A_i J_0'(S_i r) + B_i N_0'(S_i r)] \quad (\text{II.36})$$

Applying boundary conditions, tangential components of the electric field vanishes at the inner ($r = R_1$) and outer ($r = R_2$) conductor surfaces of the coaxial line. This boundary conditions yield four linear, homogeneous equations with unknown coefficients of A_i and B_i .

For nontrivial solutions of these system of equations, the determinant of the coefficient matrix must be equal to zero.

The characteristic determinant equation is given by,

$$\begin{bmatrix} (S_1^2 - a)S_1 J_1(S_1 R_1) & (S_2^2 - a)S_2 J_1(S_2 R_1) & (S_1^2 - a)S_1 N_1(S_1 R_1) & (S_2^2 - a)S_2 N_1(S_2 R_1) \\ (S_1^2 - a)S_1 J_1(S_1 R_2) & (S_2^2 - a)S_2 J_1(S_2 R_2) & (S_1^2 - a)S_1 N_1(S_1 R_2) & (S_2^2 - a)S_2 N_1(S_2 R_2) \\ S_1^2 J_0(S_1 R_1) & S_2^2 J_0(S_2 R_1) & S_1^2 N_0(S_1 R_1) & S_2^2 N_0(S_2 R_1) \\ S_1^2 J_0(S_1 R_2) & S_2^2 J_0(S_2 R_2) & S_1^2 N_0(S_1 R_2) & S_2^2 N_0(S_2 R_2) \end{bmatrix} = 0 \quad (\text{II.37})$$

Eq. II.37 is a transcendental equation in the propagation constant since the separation constants S_1 and S_2 are functions of propagation constant and material parameters. The zeros of the determinant equation will correspond to the propagation constants of the symmetrical modes. The separation constants S_1 and S_2 are either pure real or pure imaginary in the lossless case. When the losses are included, the separation constants become complex.

Propagation constant inside the loaded section of coaxial line

The zeros of the characteristic determinant equation (Eq II.37) occur at the propagation constants of the symmetrical modes. A complex root searching procedure based on Muller's method is implemented to calculate propagation constant inside the loaded section of the measurement cell. Muller's method is based on secant method, but considers three consecutive points. For each iteration Muller's method constructs a parabola through these three points, and takes x-intercept as the next approximation. In the following, we present propagation constant of wave propagating inside the loaded section of the coaxial line calculated for different scenarios.

(a) Dielectric material

In order to validate the results obtained using the complex root searching procedure, we calculated propagation constant in a coaxial line containing dielectric materials and compared with propagation constant obtained directly using transmission line theory [14].

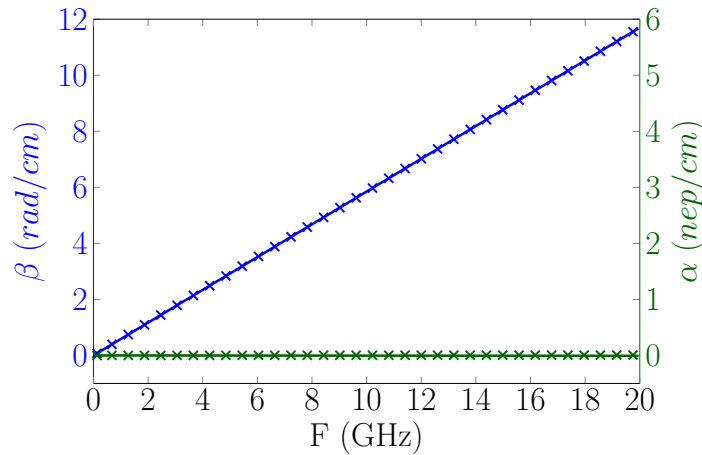


Figure II.9: Propagation constant

For a material with permittivity $\epsilon = 7.8 - j0.01$ and thickness 2.9 mm, propagation constant is calculated using both the methods and the results obtained are shown in Figure II.9. The solid lines in the figure correspond to the results from our numerical root searching procedure, and 'x' corresponds to the results obtained using transmission line theory [14].

We observe a perfect agreement between the phase and attenuation constants calculated using transmission line theory and those computed with our root search method. We emphasize that in the absence of magnetic material, the fundamental mode in the loaded region remains as pure TEM mode (fundamental mode in the empty coaxial line).

(b) Magnetic material

In the case of magnetic material, we need a theoretical model to describe the permeability tensor components in different magnetization states.

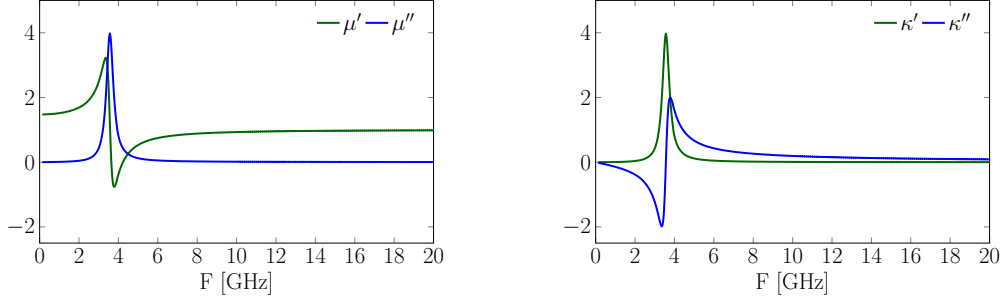


Figure II.10: Permeability tensor components.

Permeability tensor components are defined using Generalized Permeability Tensor model [36]. The spectra of the permeability tensor components (μ and κ) obtained with the GPT model are shown in Figure II.10.

The sample is a ferrite with a relative permittivity $\epsilon_f = 7.8 - j0.01$, saturation magnetization $4\pi M_s = 600$ G, magneto-crystalline anisotropy field $H_a = 81$ Oe, damping factor $\alpha = 0.06$, and thickness $l = 2.9$ mm. The ferrite is magnetized with a static magnetic field of $H_{dc} = 1600$ Oe.

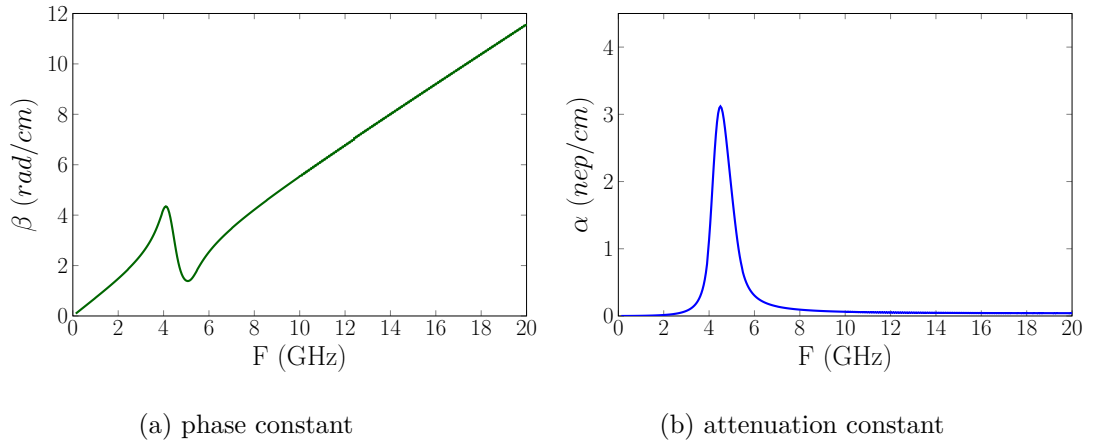


Figure II.11: Propagation constant inside the ferrite material.

The real and imaginary parts of propagation constant is shown in Figure II.11. In an empty coaxial line, the fundamental mode is TEM mode. In the ferrite loaded section of the coaxial line fundamental mode is quasi-TEM mode.

II.5.2.2 Theoretical solutions for scattering parameters

An equivalent model of the coaxial line partially filled with the ferrite sample is shown in Figure II.12. In the loaded section, the wave is characterized by a propagation constant γ .

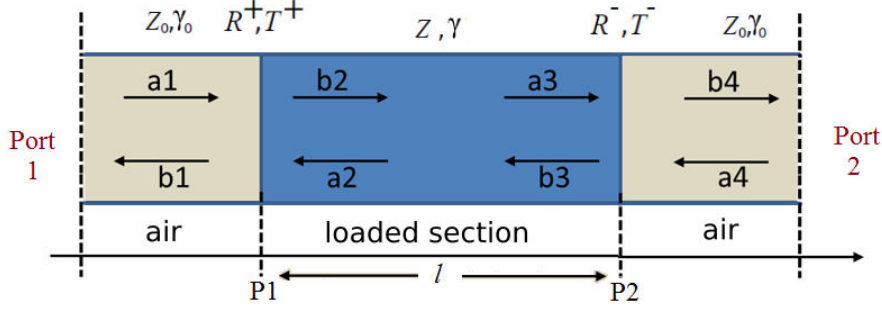


Figure II.12: Measurement cell - discontinuities.

The discontinuities are characterized by the reflection and transmission coefficients. In [42], Brodwin and Miller described a relation between the propagation constant in the ferrite and an approximation to the TEM mode reflection coefficient (R) at the ferrite-air interface.

$$R = \frac{1 - \frac{\omega\epsilon}{\gamma} \sqrt{\frac{\mu_0}{\epsilon_0}}}{1 + \frac{\omega\epsilon}{\gamma} \sqrt{\frac{\mu_0}{\epsilon_0}}} \quad (\text{II.38})$$

Applying the transmission line theory, a transmission matrix of the ferrite sample is calculated from the propagation constant in the ferrite and the reflection coefficients at the air-ferrite-air interfaces.

The wave matrices at the ferrite-air and the air-ferrite interfaces are,

$$\begin{bmatrix} a_3 \\ b_3 \end{bmatrix} = \frac{1}{1 - R} \begin{bmatrix} 1 & -R \\ -R & 1 \end{bmatrix} \begin{bmatrix} b_4 \\ a_4 \end{bmatrix} \quad (\text{II.39})$$

$$\begin{bmatrix} a_1 \\ b_1 \end{bmatrix} = \frac{1}{1 + R} \begin{bmatrix} 1 & R \\ R & 1 \end{bmatrix} \begin{bmatrix} b_2 \\ a_2 \end{bmatrix} \quad (\text{II.40})$$

The global transfer matrix $[T]$ is calculated by taking into account the wave propagation in the loaded section of the line and the impedance discontinuities between the empty and

loaded sections of the transmission line in the propagation direction of the wave.

$$\begin{bmatrix} T_{11} & T_{12} \\ T_{21} & T_{22} \end{bmatrix} = \frac{1}{1-R^2} \begin{bmatrix} 1 & R \\ R & 1 \end{bmatrix} \begin{bmatrix} e^{j\gamma l} & 0 \\ 0 & e^{-j\gamma l} \end{bmatrix} \begin{bmatrix} 1 & -R \\ -R & 1 \end{bmatrix} \quad (\text{II.41})$$

Finally, the scattering parameters are calculated by using the relations between the transfer matrix $[T]$ and scattering matrix $[S]$ as given by,

$$\begin{aligned} T_{11} &= \frac{1}{S_{11}} \quad , \quad T_{12} = -\frac{S_{22}}{S_{11}} \\ T_{21} &= \frac{S_{11}}{S_{21}} \quad , \quad T_{22} = S_{12} - \frac{S_{11}S_{22}}{S_{21}} \end{aligned} \quad (\text{II.42})$$

S-matrix can be represented as,

$$[S] = \begin{bmatrix} S_{11} & S_{12} \\ S_{21} & S_{22} \end{bmatrix} = \begin{bmatrix} \frac{R(1-T^2)}{1-R^2T^2} & \frac{T(1-R^2)}{1-R^2T^2} \\ \frac{T(1-R^2)}{1-R^2T^2} & \frac{R(1-T^2)}{1-R^2T^2} \end{bmatrix} \quad (\text{II.43})$$

II.5.3 Direct problem - Results

Complex permittivity and tensor permeability of the material are defined by analytical functions where the input parameters are the static and dynamic properties of the material. Once the analytical functions $\epsilon_f(\omega)$, $\mu(\omega)$, and $\kappa(\omega)$ are defined, an EM analysis is carried out at the discontinuities between the empty and ferrite loaded section of the coaxial line.

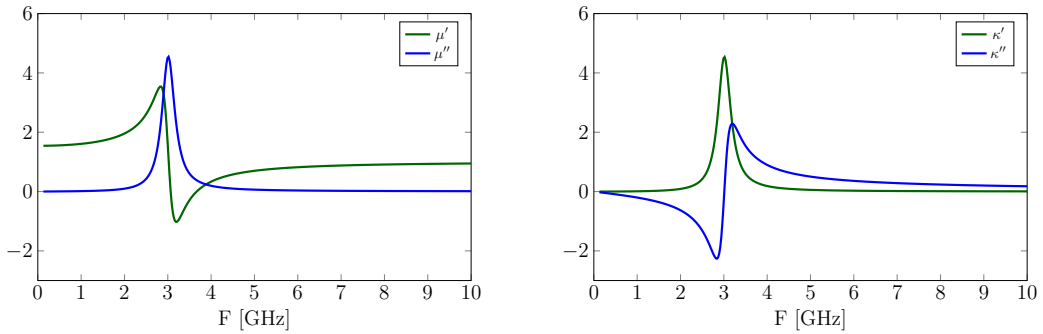


Figure II.13: Spectra of real and imaginary parts of the diagonal and off-diagonal components of permeability tensor computed using GPT model. Sample properties: $\epsilon_f = 7.8 - j0.01$, $4\pi M_s = 580$ G, $H_a = 54$ Oe, $\alpha = 0.06$, and thickness = 2.9 mm. $H_{dc} = 1400$ Oe.

Applying boundary conditions, we get a determinant equation, zeros of which correspond to the propagation constant of the wave propagating inside the material. A complex root searching procedure is used to calculate the theoretical propagation constant inside the loaded section of the measurement cell by solving the characteristic determinant equation.

Once the propagation constant is calculated, reflection coefficient at the air-ferrite interface is calculated from the propagation constant and material parameters using the relation described by Eq. II.38. Then theoretical S-parameters are determined at the reference planes P1 and P2 using the transmission line theory.

We study the configuration where a ferrite material is inserted between the inner and outer conductors of the coaxial line. The sample is magnetized in the longitudinal direction by using an electromagnet.

The sample under test is a ferrite with a relative permittivity $\epsilon_f = 7.8 - j0.01$, saturation magnetization $4\pi M_s = 580 \text{ G}$, magneto-crystalline anisotropy field $H_a = 54 \text{ Oe}$, damping factor $\alpha = 0.06$, and thickness $l = 2.9 \text{ mm}$. The ferrite is magnetized with a static magnetic field of $H_{dc} = 1400 \text{ Oe}$. In our EM analysis, GPT model is used to calculate the diagonal and off-diagonal components of permeability tensor (Figure II.13).

From the calculated S-parameters (Figure II.14), we can easily determine the frequencies at which the magnetic effects are most important. A change can be observed in the frequency dependence of the S-parameters with respect to the conventional dielectric behavior due to the presence of gyromagnetic resonance.

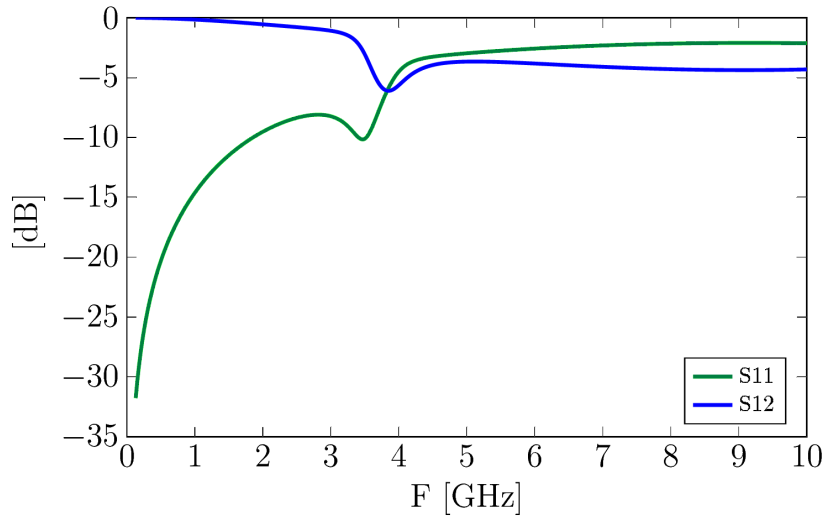


Figure II.14: Theoretical S-parameters.

Power absorption can be calculated from the scattering parameters using the relation,

$$P = 1 - |S_{11}|^2 - |S_{21}|^2 \quad (\text{II.44})$$

The losses in the system can be characterized by power absorption spectrum (Figure II.15). Maximum absorption of EM energy in the power absorption spectrum occurs at a frequency

slightly higher than the gyromagnetic resonance of the ferrite material.

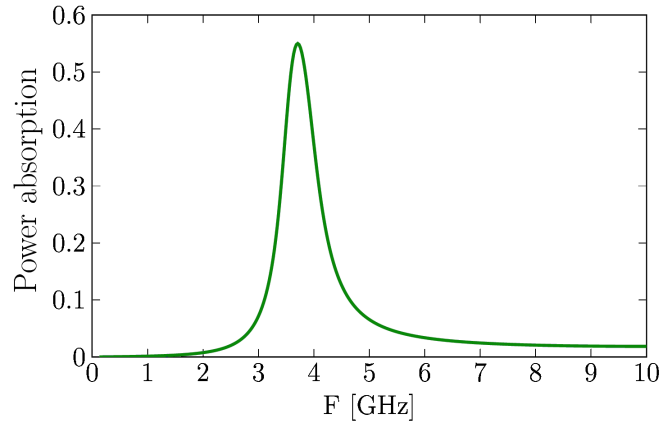


Figure II.15: Power absorption in the system.

EM analysis is independent of the analytic functions chosen for $\epsilon_f(\omega)$, $\mu(\omega)$, and $\kappa(\omega)$. This analysis constitutes the main part of the inverse problem in the proposed method. Therefore, we can conclude that in the direct problem we determine the relation between the permittivity and the permeability spectra of the sample, and theoretical S-parameters of the measurement cell. This analytic relation is not explicit, and is based on the resolution of Maxwell's equations.

II.6 Validation of the direct problem

In order to validate our direct problem, we consider three limit cases - dielectric material, demagnetized ferrites, and saturated ferrites. The measurement cell is loaded by standard samples and S-parameters are measured with vector network analyzer. Theoretical S-parameters are calculated with direct EM analysis. Direct problem results are then compared with measured S-parameters. It is very difficult to define a standard ferrite material. In the demagnetized state, Nicholson- Ross -Weir method [18, 19] allows us to determine the scalar permittivity and effective permeability of ferrite materials. For magnetized ferrites, currently standard measurement methods can not directly trace the permeability tensor components in a broad frequency range.

Commercial simulation software use theoretical model to describe the permeability tensor in different magnetization states. These theoretical models are often limited to a single magnetization state that depends on the assumptions on which they are based upon. Suppliers of ferrite materials give specifications like saturation magnetization (M_s) and resonance linewidth parameters (ΔH and ΔH_{eff}) at microwave frequency. They give no information

about the broadband behavior of their permeability tensor. Although we can use these static and microwave parameters in the theoretical permeability tensor models [30, 35], we cannot guarantee the predictive character of these parameters. Most of the commercial simulation software uses Polder model [35], which provides a satisfactory description of the microwave behavior of ferrites in the saturated states. So we chose to compare theoretical results with a commercial 3D simulation software (Ansys HFSS) in saturated states where the Polder model is applicable.

II.6.1 Dielectric material

First we consider the case where a standard dielectric material is inserted between inner and outer conductors of the coaxial line.

For a material with complex permittivity $7.8 - j0.01$ and thickness 2.9 mm, theoretical S-parameters of the coaxial line are calculated using our EM analysis and results are compared with simulation software Ansys HFSS.

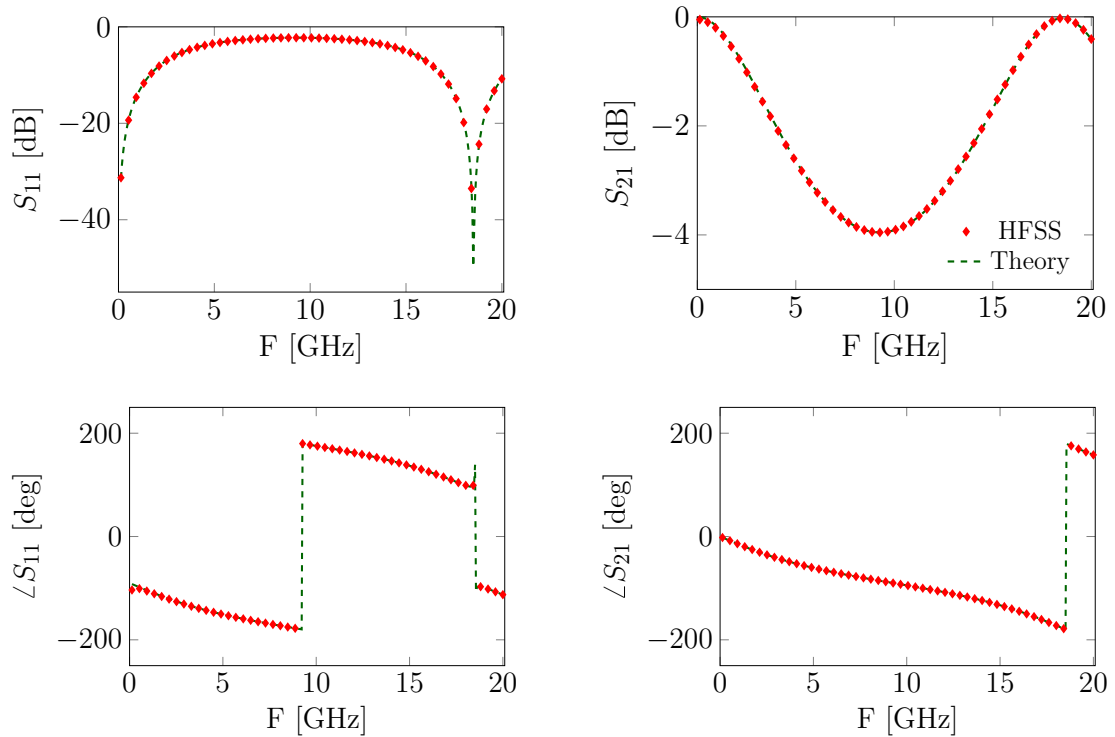


Figure II.16: S-parameters calculated using EM analysis and Ansys HFSS. Dielectric sample: $\epsilon = 7.8 - j0.01$, thickness = 2.9 mm.

Figure II.16 presents S-parameters calculated from the two theoretical approaches. A very

good agreement is found between the S-parameters obtained from these two methods. This result validate our EM analysis in the case of dielectric material.

II.6.2 Magnetic material

In order to validate EM analysis in the case of magnetic material, we study the configuration where a ferrite material is inserted between the inner and outer conductors of the coaxial line. For comparison we take two different case scenarios: demagnetized state and saturated state. The standard measurement methods can not trace the permeability tensor components in the magnetized state. So we compared direct problem results with a commercial simulation software Ansys HFSS when the material is in the saturated state.

II.6.2.1 Demagnetized ferrites

In the demagnetized state Nicholson-Ross-Weir (NRW) method allows us to characterize the ferrite materials from measured scattering parameters. By using this method we can calculate the scalar permittivity and permeability of the ferrite material from the measured reflection and transmission coefficients.

The sample under test is a Yttrium Iron Garnet (YIG) composite material (magnetic volume fraction 70%) of thickness, $l= 2.9 \text{ mm}$. The ferrite sample is inserted in a APC7 coaxial line and S-parameters are measured using a vector network analyzer (VNA). The measurement are done in the frequency range 130 MHz to 10 GHz.

The permittivity and permeability of the sample is calculated from measured S-parameters. The permittivity and permeability spectra obtained using NRW approach is shown in Figure II.17.

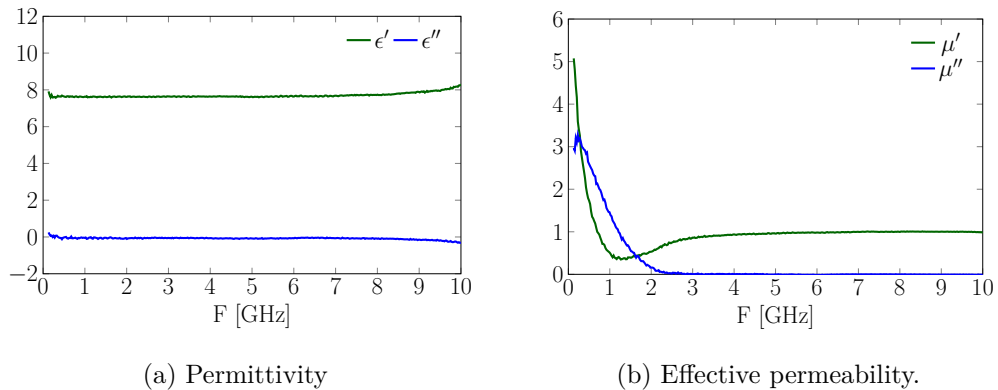


Figure II.17: Real and imaginary parts of scalar permittivity, and permeability spectra measured using NRW method. Sample: YIG composite material (magnetic volume fraction=70%), thickness $l =2.9 \text{ mm}$.

These effective values are then used to define the electrical and magnetic properties of the sample in the direct analysis. Off-diagonal terms of the permeability tensor are defined as zeros.

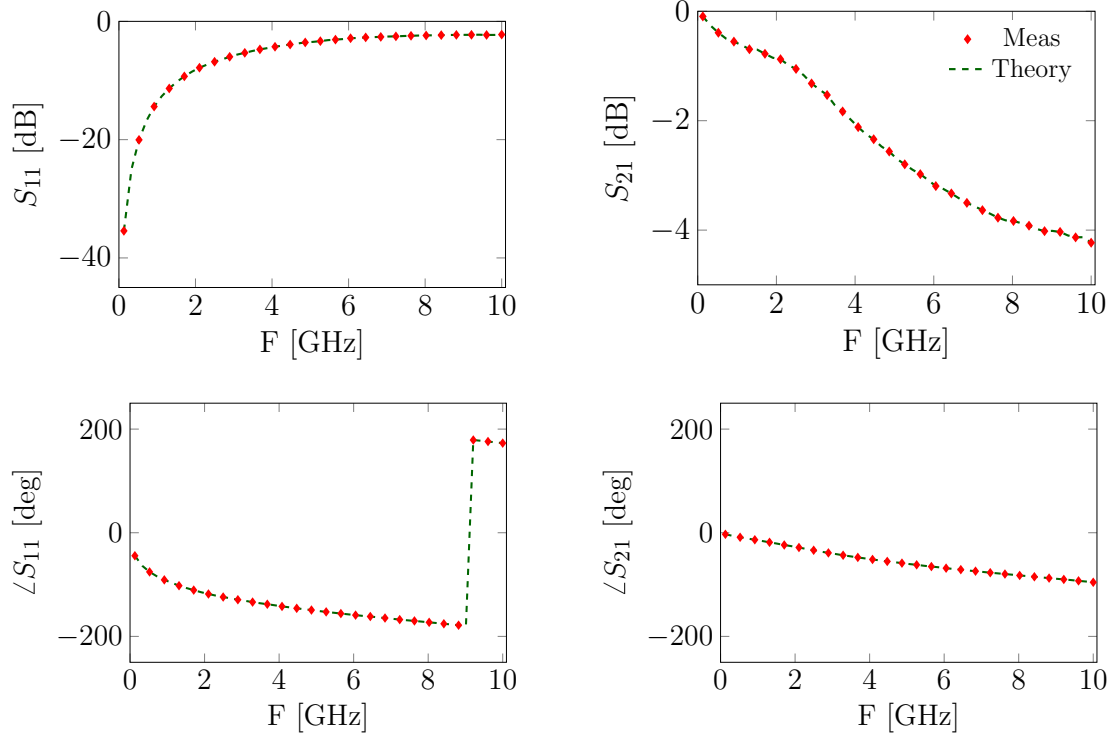


Figure II.18: Measured and simulated S-parameters of demagnetized ferrite material. Sample: YIG composite material (magnetic volume fraction=70%), thickness $l = 2.9 \text{ mm}$.

Theoretical scattering parameters are calculated using the direct EM analysis and compared with the measured S-parameters. The results obtained are presented in Figure II.18. A very good agreement is found between theoretical and measured S-parameters.

II.6.2.2 Saturated ferrites

In the saturated state, most of the commercial software use Polder tensor model [35] to describe the tensor permeability of ferrite materials. In order to validate the direct problem in saturated state, we compare theoretical S-parameters with the 3D simulation software, Ansys HFSS.

In order to take into account the macroscopic demagnetizing effects due to the shape of the magnetic sample, the internal field is calculated from the relation,

$$H_{int} = H_{dc} - N_z * 4\pi M_s. \quad (\text{II.45})$$

The sample under test is a ferrite with a relative permittivity $\epsilon_f = 7.8 - j0.01$, saturation magnetization $4\pi M_s = 580 \text{ G}$, resonance linewidth $\Delta H = 400 \text{ Oe}$, and thickness $l = 2.9 \text{ mm}$.

The ferrite is magnetized to saturation in the longitudinal direction with a static magnetic field of $H_{dc} = 1600 \text{ Oe}$. In our EM analysis, Polder model is used to calculate the diagonal and off-diagonal components of permeability tensor. The permeability spectra obtained using the Polder model is shown in Figure II.19.

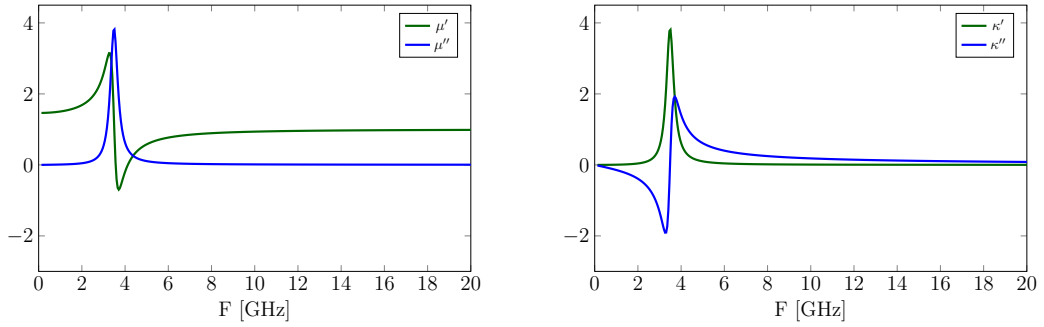


Figure II.19: Real and imaginary parts of diagonal and off-diagonal components of the permeability tensor (Polder model) in saturated state. Sample properties: $\epsilon_f = 7.8 - j0.01$, $4\pi M_s = 580 \text{ G}$, $\Delta H = 400 \text{ Oe}$, $l = 2.9 \text{ mm}$. $H_{dc} = 1600 \text{ Oe}$.

In the saturated state, HFSS uses Polder model to determine the permeability tensor components (μ and κ). The internal field value calculated from Eq. II.45 is used to define the uniform magnetic biasing field in HFSS.

S-parameters obtained using direct EM analysis and HFSS simulation software are shown in Figure II.20.

S-parameters obtained from the two simulations are in good agreement with each other. A slight difference near the resonance frequency is due to the fact that HFSS considers all the higher order modes in the full wave analysis where as our EM analysis is based on quasi-TEM approximation. These simulation results validate the direct problem in the saturated case.

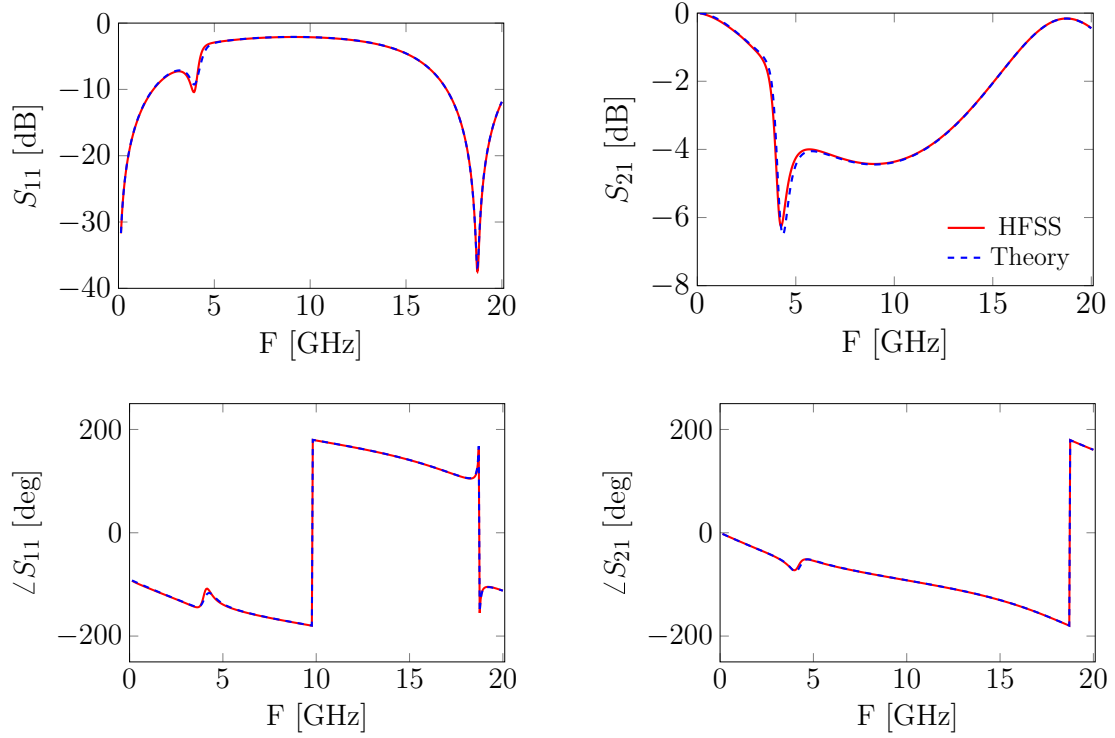


Figure II.20: S-parameters calculated using theoretical EM analysis, and Ansys HFSS for saturated ferrite material. Sample properties: $\epsilon_f = 7.8 - j0.01$, $4\pi M_s = 580 \text{ G}$, $\Delta H = 400 \text{ Oe}$. Sample thickness $l = 2.9 \text{ mm}$. Applied DC field $H_{dc} = 1600 \text{ Oe}$.

Direct problem is validated in the case of dielectric material, demagnetized ferrite and saturated ferrites. Considering these limit cases we can conclude that direct problem can be used for different magnetizations states.

II.7 Conclusion

In this chapter, we presented a new method for measuring the damping factor α , a physical quantity that represents the magnetic losses of polycrystalline ferrites which is the only dynamic input parameter of the generalized permeability tensor model. Validation of the direct problem in several limit cases are presented. This direct EM analysis plays an important part in the inverse problem developed to find the damping factor (α) from the S-parameters measured in the coaxial measurement cell. In the next chapter we will present the optimization procedure which will match theoretical S-parameters with measured S-parameters by minimizing a broadband error function.

Chapitre 2. Résumé

Le but de ce chapitre est de présenter une méthode de mesure simple permettant de déterminer la grandeur physique représentant les pertes magnétiques des ferrites, le facteur d'amortissement, de manière à remplacer la technique conventionnelle qui consiste à mesurer la largeur de raie d'absorption à mi-hauteur qui requiert l'usinage d'échantillon sphérique et qui donne accès à cette dernière grandeur qu'à une certaine valeur de fréquence (9,40 GHz pour la technique standard). Le facteur d'amortissement associé aux caractéristiques statiques (aimantation à saturation $4\pi M_s$, champ anisotropie H_a) constituent les paramètres d'entrée d'un modèle de perméabilité développé au laboratoire prédisant les propriétés dynamiques des ferrites polycristallins.

Lorsqu'une ferrite est soumise à un champ magnétique statique, ses caractéristiques intrinsèques changent et le tenseur de perméabilité $\hat{\mu}$ est ensuite utilisé pour décrire le comportement dynamique du matériau. La détermination du comportement dynamique des ferrites a fait l'objet de nombreuses études menant à différentes expressions pour les composants du tenseur de perméabilité, Schloemann pour les ferrites démagnétisées, ou Rado, Green et Sandy, et Igarashi et Naito pour les ferrites partiellement magnétisées. Au laboratoire, Gelin et Queffelec ont développé un modèle pour déterminer les composantes du tenseur de perméabilité dans n'importe quel état d'aimantation, compte tenu du phénomène d'hystérésis et de l'effet Polder-Smit. Nous avons discuté des modèles les plus courants proposés dans la littérature pour déterminer le tenseur de perméabilité, $\hat{\mu}$ en identifiant leurs principales caractéristiques et les limites de leur domaine de validité respectives. Nous avons classé les modèles en quatre catégories : les modèles décrivant l'état saturé, l'état partiellement aimanté, l'état totalement désaimanté et le modèle développé au laboratoire qui permet de calculer le tenseur de perméabilité quel que soit l'état d'aimantation du matériau.

Les techniques de caractérisation des matériaux développées précédemment au laboratoire utilisent la non-réciprocité de la cellule de mesure pour accéder directement aux éléments du tenseur de perméabilité et à la permittivité scalaire. Notre objectif est de développer une méthode pour déterminer le facteur d'amortissement α qui sera ensuite utilisé comme paramètre d'entrée pour la modélisation afin de décrire le comportement dynamique des ferrites anisotropes. Étant donné que le seul paramètre à déterminer expérimentalement est le facteur d'amortissement, le comportement non réciproque de la cellule de mesure n'est

plus une exigence.

Compte tenu de tous ces facteurs, une ligne coaxiale est choisie comme cellule de mesure pour la méthode proposée. La cellule de mesure coaxiale est de norme APC7. Le mode de propagation fondamental dans la section vide de la ligne coaxiale est le mode TEM. L'échantillon est de forme toroïdal section carrée. L'échantillon de ferrite est inséré entre les conducteurs intérieur et extérieur de la ligne coaxiale. La ligne coaxiale chargée par l'échantillon à caractériser est placée entre les pôles d'un électro-aimant et l'échantillon est aimanté dans la direction axiale. Dans un champ magnétique appliqué, l'échantillon devient anisotrope de par l'alignement des moments magnétiques dans la direction du champ statique de polarisation.

En général, le problème direct consiste à calculer les paramètres S théoriques de la cellule de mesure à partir des paramètres constitutifs du matériau (ε , μ , κ). Il est basé sur la description rigoureuse du comportement EM de la ligne de transmission coaxiale chargée par le matériau à caractériser en utilisant une approximation quasi-TEM.

Le problème direct se déroule en deux étapes:

- Définition des fonctions analytiques représentant les paramètres constitutifs du matériau qui dépendent de la fréquence ($\varepsilon(\omega)$, $\mu(\omega)$, $\kappa(\omega)$).
- Analyse EM pour trouver des paramètres S théoriques

Une fois que les fonctions analytiques $\varepsilon(\omega)$, $\mu(\omega)$, et $\kappa(\omega)$ sont définies, une analyse EM complète de la cellule de mesure est effectuée. Cette dernière est constituée de deux discontinuités qui séparent la section vide et la section chargée en ferrite de la ligne coaxiale. Une procédure de recherche des racines complexes d'une équation déterminante complexe est utilisée pour calculer les constantes de propagation théoriques de l'onde EM se propageant à l'intérieur de la section chargée de la cellule de mesure. Les paramètres S théoriques sont ensuite déterminés à l'aide de la théorie classique des lignes de transmission.

Afin de valider notre problème direct, nous considérons trois cas limites: matériau diélectrique, ferrites désaimantés et ferrites saturés. La cellule de mesure est chargée par un échantillon et les paramètres S sont mesurés avec un analyseur de réseau vectoriel. Les paramètres S théoriques sont calculés à partir de l'analyse EM (problème direct). Les résultats issus du problème direct sont ensuite comparés aux paramètres S mesurés.

À l'état désaimanté, la procédure de dépouillement des données intitulée méthode de Nicholson-Ross-Weir nous permet de déterminer la permittivité scalaire et la perméabilité effective des ferrites testés. Pour les ferrites aimantés, les méthodes de mesure conventionnelles ne peuvent pas remonter directement aux composantes du tenseur de perméabilité dans une large gamme de fréquences. Les logiciels de simulation commerciaux

utilisent un modèle théorique pour décrire le tenseur de perméabilité dans différents états d'aimantation. Ces modèles théoriques sont souvent limités à un seul état d'aimantation selon les hypothèses simplificatrices sur lesquelles ces modèles sont basés. Et il s'agit dans la majorité des cas de modèles empiriques, non prédictifs car ils font intervenir dans les formulations proposés la valeur de l'aimantation du matériau, grandeur que l'expérimentateur ou le concepteur de dispositif ne peut connaître. En effet, c'est le champ statique de polarisation que l'expérimentateur contrôle et non l'aimantation qui va dépendre de « l'histoire magnétique » qu'a suivi le milieu (phénomène d'hystérésis). C'est pour cette raison que ces modèles empiriques sont qualifiés de non prédictifs.

La plupart des logiciels de simulation commerciaux utilisent le modèle Polder, qui fournit une description satisfaisante du comportement hyperfréquence des ferrites à l'état saturé. Nous avons donc choisi de comparer les résultats théoriques avec le logiciel commercial de simulation EM 3D (Ansys HFSSTM) dans des états saturés pour lesquels le modèle de Polder est applicable et apportent des résultats satisfaisants.

Le problème direct est validé dans le cas d'un matériau diélectrique, d'un ferrite totalement désaimanté et de ferrites saturés. Dès lors que la comparaison théorie/expérience sera validée pour ces cas limites, nous pourrions conclure que le problème direct peut être utilisé pour différents états d'aimantation.

Dans ce chapitre, nous avons présenté une nouvelle méthode de mesure du facteur d'amortissement, grandeur physique qui représente les pertes magnétiques des ferrites polycristallins et qui constitue l'unique paramètre d'entrée dynamique des modèles du tenseur de perméabilité. La validation du problème direct dans plusieurs cas limites est présentée. Cette analyse EM directe joue un rôle primordial dans le problème inverse développé pour remonter au facteur d'amortissement (α) à partir des paramètres S mesurés sur la cellule de mesure coaxiale.

Chapter III

Inverse Problem- Experimental Results

Contents

III.1 Introduction	96
III.2 Inverse problem	96
III.2.1 Optimization procedure	97
III.2.2 Choice of the permittivity and permeability models	99
III.2.3 Optimization algorithm	100
III.3 Measurement setup	102
III.4 Measurement results	103
III.4.1 Composite ferrites	106
III.4.2 Bulk ferrites	110
III.4.3 Validation of results	116
III.5 Conclusion	118

III.1 Introduction

In this chapter, we present the inverse problem of the proposed coaxial line method and the experimental results in detail. The inverse problem will optimize the damping factor α by matching theoretical S-parameters with the measured S-parameters. Results will be validated by comparing with supplier data sheet.

III.2 Inverse problem

The main objective of the inverse problem is to extract damping factor, α by comparing theoretical S-parameters obtained from direct problem (electromagnetic analysis of the measurement cell) with the measured S-parameters.

The general scheme of the inverse problem is presented in Figure III.1.

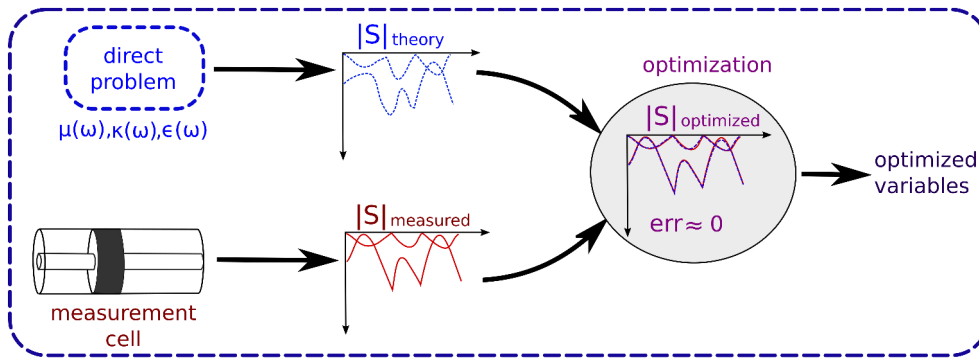


Figure III.1: Inverse problem - Description

Theoretical S-parameters are calculated using the direct EM analysis of the measurement cell. A numerical optimization procedure is defined to match the theoretical S-parameters with measured ones. In this optimization procedure, a broadband error function (Err) is minimized to match the theoretical S-parameters with measured S-parameters.

The optimization variables are the input parameters of the analytical functions chosen in the direct problem. The aim of the optimization procedure is to match theoretical S-parameters to the measured S-parameters by iteratively adjusting the input parameters of the analytical functions representing the properties of the material.

Once the error between the theoretical and measured S-parameters is minimized ($Err \approx 0$), the optimized functions represent the constituent parameters of the sample to be characterized. The optimization variable will then represent the values of parameter to be measured.

III.2.1 Optimization procedure

Generally inverse problems of this type are solved using a frequency-by-frequency applied optimization procedure. At each frequency value, a system of 6 equations (differences between the magnitudes and the phases of the S-parameters) is solved for unknown parameters. However, appearance of dimensional resonances in the operating band makes some uncertainties in the phase measurements of the reflection coefficients. Therefore, in order to ensure the accuracy of the results, these optimization procedures require a relatively short sample length to avoid the appearance of dimensional resonances in the operating frequency band.

In order to avoid these problems, we decided to use a broadband optimization procedure instead of frequency by frequency method considering only the magnitudes of the S-parameters. A set of error values measured over the entire frequency band is used to define the objective error function. Given the quantity of information acquired over the set of S-parameters, this comparison gives us an over sized system of equations, where the number of equations is greater than the number of unknowns. In this system the number of equations is given by the sampling number taken in practice for the S parameter measurements and the number of unknowns is given by the number of input variables of the analytical functions defined in the direct problem.

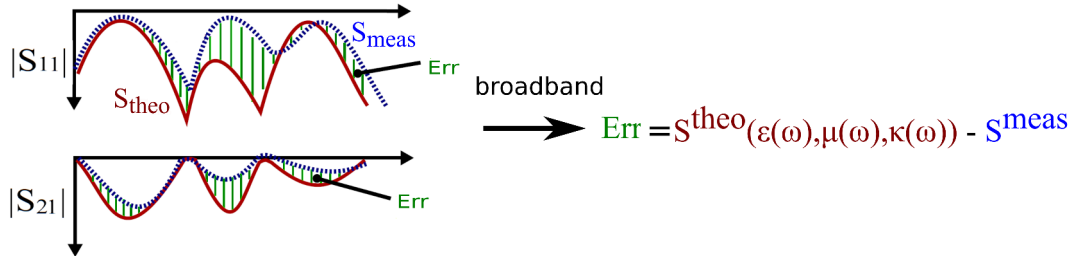


Figure III.2: Broadband optimization procedure

The number of adjustment parameters depends on the analytical functions chosen in the direct problem. Our inverse problem has only two optimization variables (H_{dc} and α). All other input parameters ($4\pi M_s$, H_a , etc.) are determined through standard static measurements. The optimization procedure determines the values for input parameters H_{dc} and α by matching theoretical S-parameters with those measured over a wide frequency band. By taking into account only the magnitudes of S-parameters, uncertainties due to the dimensional resonances are avoided in the inverse problem. On the contrary, our inverse problem exploits these resonances to converge S-parameters more rapidly and more precisely.

Resolution of the system of equation

We solve our system of equations using the curve fitting techniques. The scientific computing software MATLAB has a library of subroutines dedicated to numerical optimization:- Optimization toolbox.

We use *lsqnonlin* (non-linear least square fitting) subroutine from optimization tool box to solve our system of equations.

The subroutine *lsqnonlin* is designed to minimize the modulus of an error vector denoted *Err* in the least squared direction. This vector *Err* is obtained by calculating the difference between the fixed data curve and the variable curve. The variable curve must be a function of the coefficient vector (*X*) which contains the parameters to be optimized.

$$Err(X) = f_{var}(X) - f_{data}, \quad (III.1)$$

where *Err*, *f_{var}* and *f_{data}* are vectors of size η (number of frequency points) and *X* is a vector of size *v* (number of optimization parameters). The subroutine *lsqnonlin* will solve the system for *v* parameters of the vector *X*.

$$\sum_{i=1}^{\eta} Err_i(X)^2 = \min \left(Err_1(X)^2 + Err_2(X)^2 + Err_3(X)^2 + \dots + Err_{\eta}(X)^2 \right). \quad (III.2)$$

Moreover *lsqnonlin* subroutine gives the possibility to define lower limits L_i and higher limit U_i for the optimization variables of the vector *X*.

$$L_i < X_i < U_i$$

In summary, Eq. III.2 represents the objective error function of the system. The values of L_i and U_i are the bound constraints of the system. This *lsqnonlin* subroutine is based on Trust region reflective method [45]. For each iteration cycle this subroutine determines an approximate solution to the objective function with conjugate gradient method.

A major disadvantage of curve fitting routines is the non-uniqueness of the solution. An overabundant system does not necessarily have a unique solution. To find the correct solution of our system of equations, we must ensure that the *lsqnonlin* subroutine can only work with physical (realistic) solutions.

To do this we must guarantee two conditions:- the determination of an initial point (for optimization variables) which is not very far from the physical solution, and the definition of values L_i and U_i which limits the variables of optimization within physical reality. It is possible to achieve these conditions by choosing realistic models of permittivity and permeability based on physical parameters.

III.2.2 Choice of the permittivity and permeability models

Generally dielectric materials exhibit low dispersion in the microwave region. In order to take into account the dispersive nature of permittivity, Cole-Cole model [39] is used to represent the ferrite permittivity in the direct problem. The high frequency behavior of the permittivity can be described by the Cole-Cole model as shown in Figure III.3.

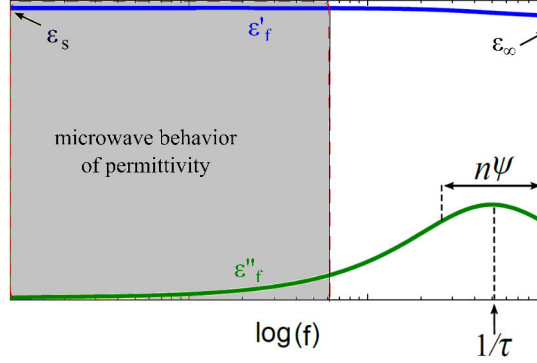


Figure III.3: Microwave behavior of permittivity- Cole-Cole model

A general Cole-Cole formulation is given by,

$$\epsilon_f(\omega) = \epsilon_\infty + \frac{\epsilon_s - \epsilon_\infty}{(1 + j\omega\tau)^{1-\psi}} \quad (\text{III.3})$$

This function depends on four variables: the static permittivity ϵ_s , ‘infinite frequency’ permittivity ϵ_∞ , the relaxation time τ and an experimental correction factor ψ ($0 < \psi < 1$). We can limit the values of relaxation time τ to ensure that relaxation is happening beyond the maximum frequency of the method. Finally, the parameter ψ modifies the width of the absorption peak. Its value is bounded by definition between 0 and 1. Note that when $\psi=0$, the Cole-Cole function becomes a Debye-type relaxation function [39].

Generalized permeability tensor model is used to represent the permeability tensor of the magnetic materials. This model has been discussed in detail in section II.2. This model describes the dynamic behavior of the permeability tensor components μ , κ , and μ_z in a predictive way by taking into account the hysteresis phenomenon and the dynamic interactions within the material. We can define the GPT model by the following function,

$$[\mu'(\omega), \mu''(\omega), \kappa'(\omega), \kappa''(\omega), \mu'_z(\omega), \mu''_z(\omega)] = GPT(H_{dc}, 4\pi M_s, H_a, \alpha, \omega). \quad (\text{III.4})$$

The input parameters of the GPT model are: saturation magnetization $4\pi M_s$, anisotropy field H_a , damping factor α , demagnetizing coefficient in the applied field direction N_z , and applied DC magnetic field H_{dc} . All of these are measurable physical parameters.

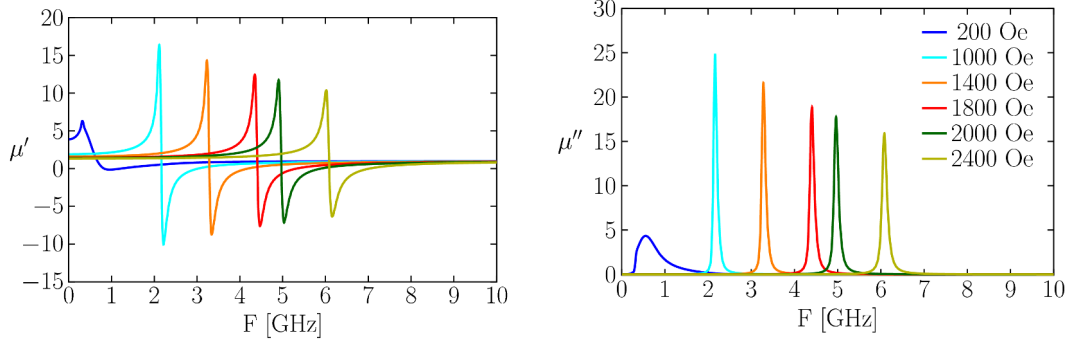


Figure III.4: Spectra of real and imaginary parts of the diagonal components of $\hat{\mu}$ tensor obtained using GPT model: Ferrite properties: $4\pi M_s=810$ G, $H_a=54$ Oe, $\alpha=0.0068$, $N_z=0.35$ and $H_{dc}=0-2400$ Oe

Most of the input parameters of the GPT model can be obtained using the standard static measurements. Hysteresis measurements are done using the vibrating sample magnetometer (VSM). The saturation magnetization is calculated from the measured hysteresis curve. The external magnetic field strength H_{dc} can be obtained by directly measuring the magnetic field inside the cell using a Hall effect probe. However we have retained parameter H_{dc} as an optimization variable in the inverse problem. This makes it possible, if necessary, to bridge the gap between reality and GPT model. In this case, H_{dc} parameter can be bounded between values close to those measured inside the cell.

With five input parameters, GPT model can simultaneously determine the frequency dependent, complex components of the permeability tensor μ , κ , and μ_z . This is not the case with the general mathematical formulations of permeability tensor components.

A typical response for the diagonal components of permeability tensor obtained with GPT model is shown in Figure III.4.

Thus, the usage of Cole-Cole model for permittivity, and GPT model for permeability in our optimization procedure ensures the uniqueness of the solution. In one hand we can choose initial points close to solution, and on the other hand, the optimization procedure will use realistic $\mu(\omega)$ and $\kappa(\omega)$ responses to search for the solution. This is made possible by the physical input parameters of the Cole-Cole model and GPT model (ϵ_s , ϵ_∞ , τ , $4\pi M_s$, H_a , α , N_z and H_{dc}) used in the direct problem.

III.2.3 Optimization algorithm

In Figure III.5, we present the optimization algorithm used to determine the constituent parameters of the sample material. The objective of this algorithm is to optimize the vector X which consists of the input parameters of the permeability and permittivity models (optimization variables).

The initial parameter H_{dc} can be set to the value of the magnetic field measured using the Gauss meter and saturation magnetization $4\pi M_s$ can be obtained from the hysteresis cycle measurement using vibrating sample magnetometer (VSM). Demagnetizing factor N_z is approximated from the sample dimensions (Chapter I, Section 2.1) and anisotropy field H_a can be approximated from gyromagnetic resonance frequency.

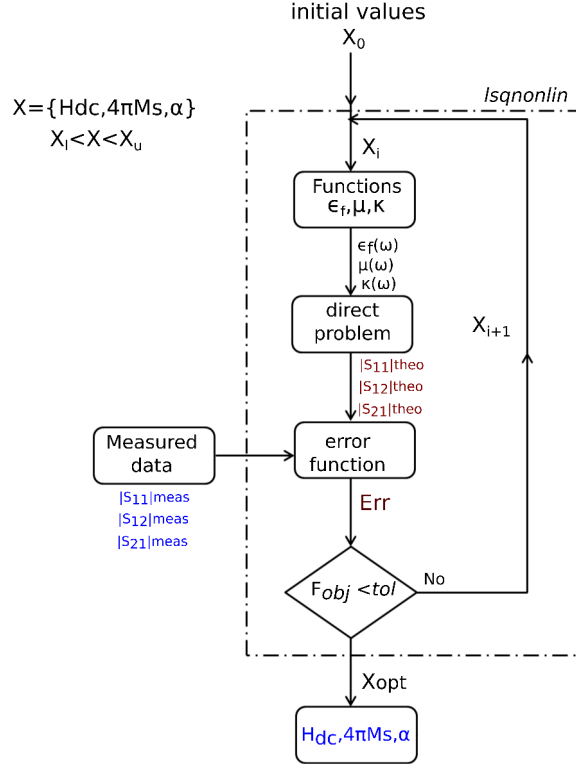


Figure III.5: Optimization algorithm. ($4\pi M_s$ is optional)

The limit values of the elements of the vector X are defined in the vectors X_{lb} and X_{ub} . If one of the parameters is not defined in the initial vector X_0 , the latter takes the mean value between its upper and lower limits. The value of the input parameter ψ in Cole-Cole permittivity model can be set to zero to convert it to a simpler Debye-type permittivity model.

The *lsqnonlin* subroutine initializes with the input vector X_0 which becomes the vector X_i to be optimized. The vector X_i is used to obtain the spectra of $\epsilon_f(\omega)$, $\mu(\omega)$, and $\kappa(\omega)$ using GPT model (Eq. III.4) and Cole-Cole model (Eq. III.3).

These spectra are then introduced into the direct problem to determine the theoretical S-parameters of the measurement cell containing the ferrite sample. Then the error (*Err*) between the magnitudes of theoretical ($|S|_{theo}$) and measured S-parameters ($|S|_{meas}$) are calculated.

The broadband error function is defined as,

$$\begin{aligned} Err(X, \omega) &= |S_{jk}(X, \omega)|_{theo} - |S_{jk}(\omega)|_{meas}, \\ j &= k = 1, 2. \end{aligned} \quad (III.5)$$

In order to converge the theoretical S-parameters with measured S-parameters, we must minimize this broadband error function over the entire frequency band used.

The objective function of subroutine *lsqnonlin* is defined as,

$$F_{obj}(X) = \sum_{f=fmin}^{fmax} \left(\sum_{j=1}^2 \sum_{k=1}^2 Err(X, \omega)^2 \right) \quad (III.6)$$

Then we get the broadband optimization problem of the form,

$$\min(F_{obj}) \quad \text{with limits } X_{lb} < X < X_{ub}.$$

A maximum tolerance value (eg : $tol=10^{-4}$) which represents the maximum difference that can be tolerated between two consecutive approximations of the solution is defined to ensure the convergence of S-parameters. From each i^{th} iteration, we obtain an approximation of the solution X_{i+1} . This approximation X_{i+1} becomes the variable X_i to close the algorithm (Figure. III.5). Once the tolerance level is reached (convergence of theoretical S-parameters with measured results), the iterative process ends resulting in the optimized vector X_{opt} . This vector contains the optimized values of the adjustment variables.

III.3 Measurement setup

The measurement cell is an APC7 standard coaxial line with inner conductor diameter 3.04 mm and outer conductor diameter 7 mm. A square toroidal shaped ferrite sample is inserted in between the inner and outer conductors of the measurement cell.

The sample is magnetized in the axial direction by placing the measurement cell between the poles of an electromagnet. This electromagnet controlled by the electric current provides a uniform magnetic field in between the poles. Experimental setup for coaxial line characterization of damping factor is shown in Figure III.6.

A current source Kepko Bop 20-20M is used to control the static magnetic field of the electromagnet. This setup provides a maximum magnetic field of 2200 Oe in between the poles of the electromagnet. The maximum magnetic field is limited to 2200 Oe by the minimum space required for placing the coaxial cell between the magnetic poles.

Intensity of the DC magnetic field in the coaxial cell is measured by using a Hall Effect probe. We use TE2M GN20000E Gauss meter to measure the static biasing magnetic field

strength. Under the action of static magnetic field, the material is magnetized and becomes anisotropic in nature.

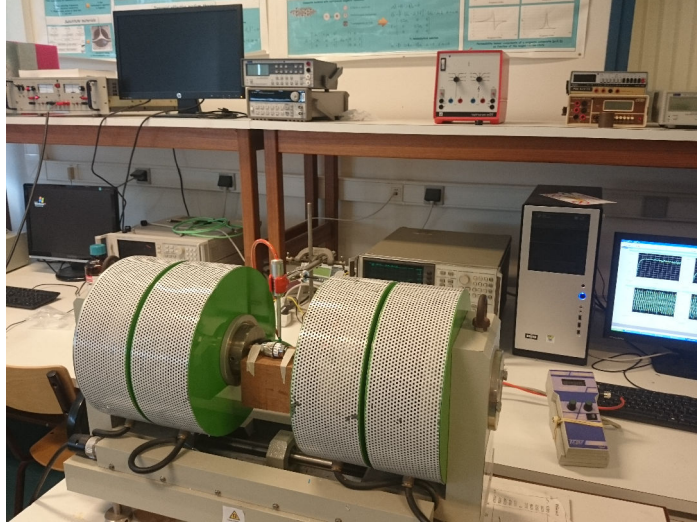


Figure III.6: Measurement setup

Scattering parameters S_{11} and S_{21} are then measured using a vector network analyzer HP8720 in the frequency band 130 MHz – 20 GHz. Hysteresis loop measurements are done using a vibrating sample magnetometer (VSM).

III.4 Measurement results

In order to validate the optimization procedure we first consider the case of the dielectric material. For dielectric materials, inverse problem optimizes only three quantities: ϵ_s , ϵ_∞ and τ , which correspond to the input variables of a Debye-type permittivity model ($\psi = 0$ in the Cole-Cole model) [39]. Diagonal components of permeability tensor is set to one and off-diagonal components are set to zero ($\mu = 1 - j0$ and $\kappa = 0 - j0$).

The sample under test is a dielectric sample Teflon of length 3 mm. The measurements are done for a frequency range from 130 MHz to 20 GHz. The inverse problem optimizes only three input quantities: ϵ_s , ϵ_∞ and τ , which correspond to the adjustment variables of a Debye type permittivity model. In the inverse problem only the magnitudes of the two measured S-parameters: $|S_{11}|_{mes}$ and $|S_{21}|_{meas}$ are used.

Measured and optimized S-parameters of the coaxial transmission line partially filled with teflon sample is shown in Figure III.7. A good agreement is found between the optimized and measured S-parameters.

Note that in this case, the optimized function in the inverse problem ϵ_{opt} represents an

effective value of permittivity. To determine the permittivity of the sample, we must take into account correction due to the $50 \mu m$ air gap between the sample and the measurement cell. The air gap correction is done by considering the sample with air gap as a set of series capacitors as described in the reference [46].

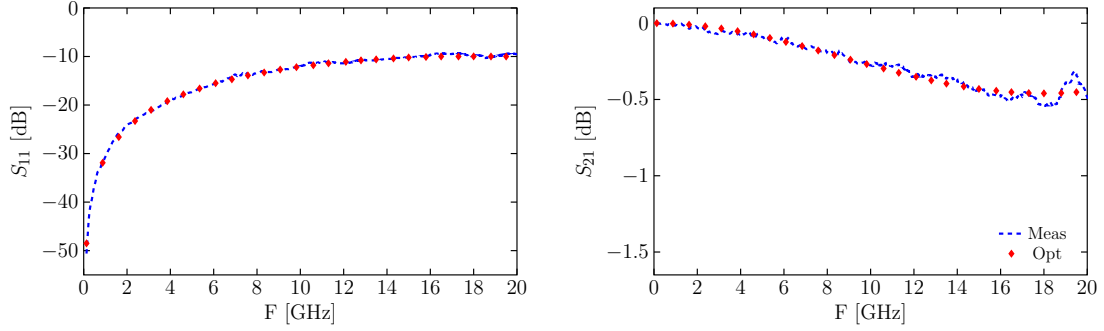


Figure III.7: Measured and optimized S-parameters of a Teflon sample of length 3 mm

We observe that results are completely consistent with the measurement carried out using a standard NRW characterization method [18, 19]. From this results it is clear that broadband inverse problem precisely determines the permittivity of the dielectric material using only the magnitudes of the S-parameters (avoiding the inaccuracies linked to the phase measurements of S-parameters).

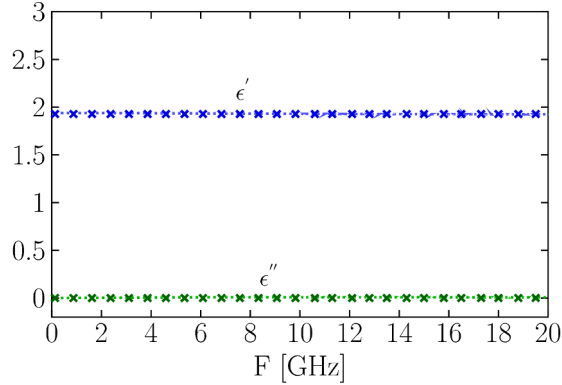


Figure III.8: Real and imaginary parts of effective permittivity ϵ of the dielectric sample - Teflon (--- : NRW method, \times : Optimization).

To ensure correct operation of the inverse problem, we must limit the occurrence of air gaps between the sample and the cell. These results validate the inverse problem of the proposed measurement method.

In the case of magnetic materials, permittivity and permeability spectra are unknown. The permittivity of the material can be obtained from coaxial line NRW method [18, 19] in

the demagnetized state. But the direct problem needs to calculate the permittivity of the material for any given frequency value. So we chose a theoretical permittivity model, Debye model [39] that fits the experimental permittivity of the demagnetized sample to represent permittivity spectra in the direct problem. The input parameters of the Debye permittivity model are ϵ_s , ϵ_∞ and τ .

The inverse problem uses GPT model [36] to describe the permeability tensor components. The input parameters for GPT model are saturation magnetization $4\pi M_s$, anisotropy field H_a , demagnetizing coefficient N_z , applied magnetic field H_{dc} and the damping factor α . All the input parameters except damping factor α can be calculated from other static measurements. Saturation magnetization $4\pi M_s$ is obtained from the hysteresis measurement and anisotropy field H_a can be approximated from the gyromagnetic resonance frequency measurements in the demagnetized state. The demagnetizing factor N_z can be approximated from the sample dimensions (Chapter I, Section 2.1).

Given the complexity of the system and the mathematical functions used (Debye and GPT models), the inverse problem in the case of magnetic material requires significant computation time and presents problems of non-uniqueness of the solution. To overcome these difficulties, we have established a characterization protocol for the measurement of magnetic samples. We define two inverse problems - first one is to measure the static permittivity ϵ_f of the material and the second one is to determine the dynamic quantity, the damping factor α .

To find the input parameters of the Debye model, we can either fit the theoretical permittivity values with experimental values measured using NRW method or we can define an inverse problem in the high frequency region. To find the permittivity spectra of the ferrite material, we chose to define an inverse problem of purely dielectric type in the frequency band where only the dielectric properties of the magnetic material will have an influence on the characteristics of the measurement cell. To achieve this, we consider the high frequency region well above the gyromagnetic resonance of the demagnetized ferrite material where the sample shows dielectric behavior. In this frequency band, we can assume that there is no magnetic effects present ($\mu(\omega) = 1 - j 0$ and $\kappa(\omega) = 0 - j 0$). Permittivity spectrum of the magnetic sample $\epsilon_f(\omega)$ is measured from optimized values of ϵ_s , ϵ_∞ and τ . These values are then compared with the measured permittivity using NRW method in order to validate the inverse problem and the input parameters of the Debye model.

Once the permittivity values are obtained, a second inverse problem is realized in order to determine the dynamic damping coefficient α . Since the permittivity of the magnetic materials is independent of the static magnetic field, $\epsilon_f(\omega)$ measured in the first inverse problem remains unchanged for all states of magnetization. The variables to be optimized are α and H_{dc} which correspond to the input variables of the GPT model.

III.4.1 Composite ferrites

Sample under test is a composite material of Yttrium Iron Garnet (YIG 39- TEMEX ceramics) powder and epoxy with relative permittivity 7.70.

Properties of the ferrite are given by,

$$4\pi M_s = 800 \text{ G}$$

$$\text{Magnetic volume fraction} = 70 \%$$

$$\text{thickness} = 2.93 \text{ mm}$$

$$\epsilon' = 7.7$$

$$\tan\delta < 1.2 \times 10^{-4}.$$

We use this data to initialize the variables to be optimized in the inverse problem. Anisotropy field H_a is approximated from the demagnetized ferromagnetic resonance measurement to be around 54 Oe. We initialize the demagnetizing coefficient N_z of the square toroidal sample to be 0.42 which is the approximate value calculated using the method described in [9] (Chapter I, Section 2.1). Magnetic volume fraction is taken into account in the GPT model for computing the permeability tensor components.

The optimization variables are damping factor α and applied magnetic field H_{dc} . Table III.1 summarizes the initial values and the limits imposed on each of the variables to be optimized in the inverse problem.

Parameter	Initial value	Lower limit	Upper limit
H_{dc}	H_{meas}	$H_{meas}-200 \text{ Oe}$	$H_{meas}+ 200 \text{ Oe}$
α	0.06	0	1

Table III.1: Composite material of YIG 39- Initial values and boundaries of the optimization variables

An APC7 standard coaxial line of length 30 mm is loaded with the toroidal ferrite sample and scattering parameters are measured for static magnetic field values ranging from 0 Oe to 1700 Oe. The measurements are carried out in a frequency range from 130 MHz - 20 GHz.

Maximum offset losses show an expected shift to high frequency values when the static magnetic field is increased. The optimization procedure allow us to match the theoretical S-parameters with the measured results by adjusting two parameters - the damping factor α and the applied magnetic field H_{dc} .

In the first phase of inverse problem, we optimize the complex permittivity of the ferrite in the high frequency region where sample shows pure dielectric behavior ($\mu(\omega) = 1 - j 0$ and $\kappa(\omega) = 0 - j 0$).

Figure III.9 presents the measured and optimized S-parameters in frequency region where the YIG sample shows pure dielectric behavior.

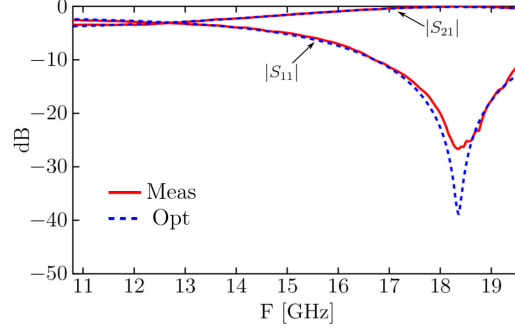
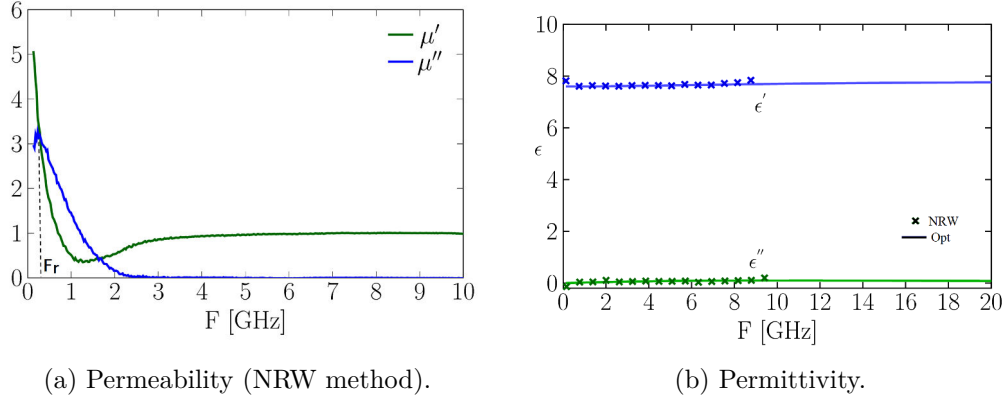


Figure III.9: Measured and optimized S-parameters of the demagnetized YIG 39 composite material in the high frequency region.

The results obtained from the inverse problem are then compared with the permittivity values obtained using NRW method [18, 19] in the demagnetized state. The optimized results show good agreement with the measured value using the standard NRW method (Figure III.10b). Real and imaginary parts of optimized permittivity are shown in Figure III.10b. These results validate the inverse problem and initial parameters.



(a) Permeability (NRW method).

(b) Permittivity.

Figure III.10: Real and imaginary parts of scalar permittivity, and permeability spectra in the demagnetized state. Sample: YIG 39 composite material.

Since the permittivity of the magnetic materials is independent of the static magnetic field, $\epsilon_f(\omega)$ measured in the first inverse problem is used to represent the permittivity of YIG composite ferrite material in all the magnetization states. In the second step, we solve the inverse problem to measure the damping factor α for different values of the static magnetic fields H_{dc} .

For each applied field values, the inverse problem will give a vector X_{opt} which contains the optimized values of the variables α and H_{dc} .

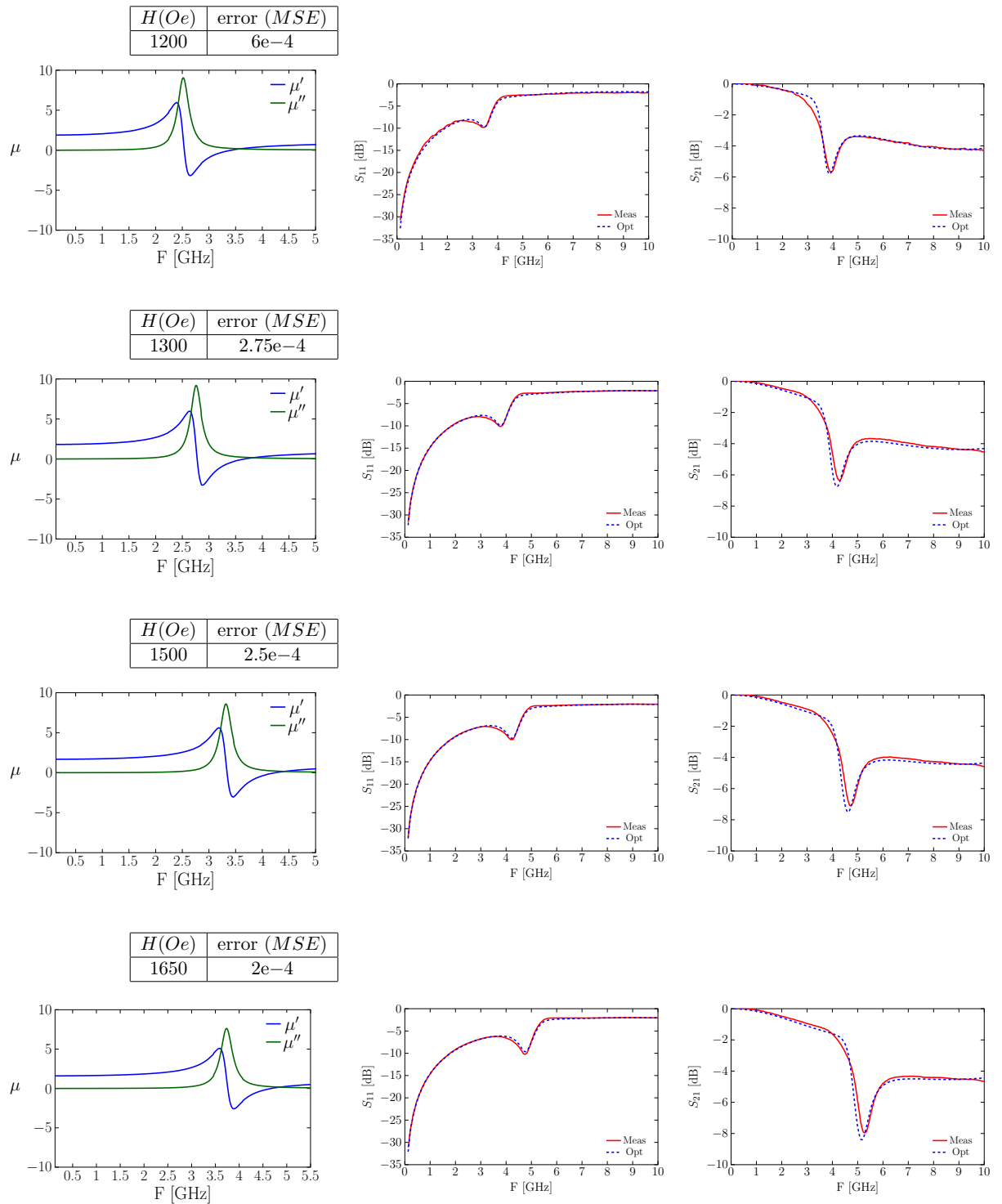


Figure III.11: Optimized permeability spectrum and S-parameters of Y39 composite material for different DC magnetic field (H_{dc}) values. Sample properties: $4\pi M_s = 800$ G, $H_a = 54$ Oe, $N_z = 0.42$.

As with any optimization procedure, it is necessary to define criteria for the validation of the optimized solution. Therefore, we have established criteria to validate or reject an optimized solution - mean square error (MSE). MSE represents the average of the squares of errors or deviations between the optimized values and the measured data. The mean square error (MSE) is estimated for each optimized S parameter, and this indicates the extent to which the optimized curve is dispersed from the measured curve. MSE value less than 2×10^{-3} indicates that the optimized curve passes through most points of the measured curve.

$$MSE = \frac{1}{n} \sum_{i=1}^n (|S|_{opt} - |S|_{meas})^2, \quad (III.7)$$

where n is the number of frequency points.

Figure III.11 presents the measured and optimized S-parameters resulting from the resolution of the inverse problem for different magnetization fields H_{dc} well above saturation.

The optimized values for damping coefficient for different applied field values are plotted in Figure III.12. A small variation observed in the damping factor values is due to the simplifying assumptions used in the direct problem. The damping coefficient seems to be reaching a constant value at high applied values when the material is saturated. To make sure that sample is saturated, only the optimization results for applied field values above 1000 Oe are presented.

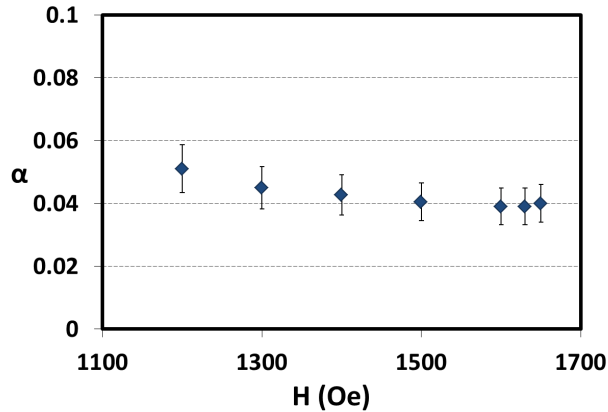


Figure III.12: YIG 39 sample- Optimized damping coefficient

The measured values of damping coefficient are quite high compared to those traditionally observed for bulk ferrites. These high values are due to the sample's composite nature in which the non-homogeneities, random orientation of grains or the demagnetization effects lead to an expansion of the power absorption spectrum.

III.4.2 Bulk ferrites

Using the same characterization protocol as described above, we also measured the EM properties of a YIG-type ferrite (Yttrium Iron Garnet - Y39, supplied by EXXELIA TEMEX).

An APC7 coaxial line of length 7 mm is taken as the measurement cell. S-parameters of the measurement cell loaded with ferrite samples are recorded for static magnetic values ranging from 0 *Oe* to 2000 *Oe*. Measurements are done in a frequency range from 130 MHz to 20 GHz.

The sample under test is a bulk ferrite material Yttrium Iron Garnet-Y39 (EXXELIA TEMEX) of thickness 4 mm.

Properties of the ferrite are given by,

$$\begin{aligned} 4\pi M_s &= 810 \text{ G} \\ \text{thickness} &= 4 \text{ mm} \\ \epsilon' &= 14.3 \\ \tan\delta &< 1.2 \times 10^{-4}. \end{aligned}$$

We use this data to initialize the variables to be optimized in the inverse problem. Finally, we initialize the demagnetizing coefficient N_z of the square toroidal sample to be 0.35 which is the approximate value calculated using the method described in [9] (Chapter I, Section 2.1).

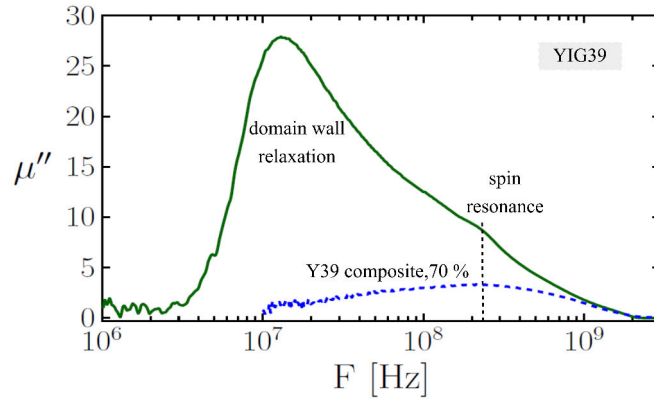


Figure III.13: Imaginary part of permeability μ'' of YIG 39 sample

Initial permeability of multi domain ferrite samples has two main contributions, one from the relaxation behavior of domain walls and the other due to the magnetization rotation. This domain wall relaxation contribute a significant part to the initial permeability of the bulk ferrite samples at low frequencies.

Figure III.13 shows the imaginary parts of permeability of YIG 39 ferrite material measured in the demagnetized state using NRW method.

From the Figure III.13, it is clear that initial permeability of our sample is mainly due to the domain wall contribution and it is difficult to differentiate the contributions from rotational resonance.

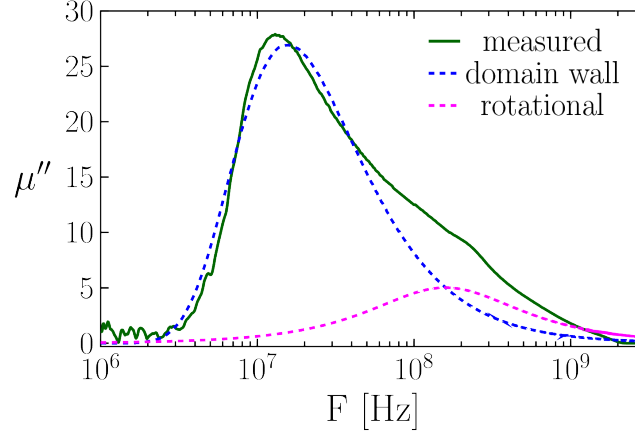


Figure III.14: YIG 39 sample- Domain wall relaxation and gyrotropic response.

The loss peak observed at 11 MHz, corresponding to a wall resonance is no longer exists in the YIG 39 composite sample with a magnetic volume fraction of 70%. The second resonance around 160 MHz corresponds to the gyromagnetic resonance which is masked by the wall relaxation.

GPT model which we used in the direct problem, does not take into account the domain wall motions in the calculation of permeability tensor components. The initial permeability can be described as a sum of contributions from domain wall motions and gyrotropic response (see Figure III.14).

Mathematical distribution functions like Log-normal distribution or Fisher distribution can be used to describe the domain wall contributions in the imaginary part of permeability. The contribution of magnetization rotation in the initial permeability can be described by the GPT model.

In GPT model, dynamic magnetization vector \vec{m}_i is calculated as a function of microwave field \vec{h}_i , the applied magnetic field (H_{dc}, ϑ) and the demagnetizing coefficients of the grain (n_g) and the domain (n_d).

$$\vec{m}_i = (H_{dc}, \vartheta, \vec{h}_i, n_g, n_d) . \quad (\text{III.8})$$

In order to calculate the permeability tensor $\hat{\mu}$ of a bulk ferrite sample, a statistical summation of the local dynamic magnetizations is performed. This summation takes into account the possible directions of the vector \vec{m}_i described by the angles ϑ and φ and the possible grain and domain shapes (Eq. III.9).

$$\langle \vec{m}_i(\vec{h}, H_{dc}) \rangle = \int_{\varphi} \int_{\vartheta} \int_{n_g} \int_{n_d} P_1 \cdot P_2 \cdot P_3 \vec{m}_i \, dn_d dn_g d\vartheta d\varphi, \quad (\text{III.9})$$

$$P_1 = P_1(\varphi, \vartheta), \quad P_2 = P_2(n_g), \quad P_3 = P_3(n_d) \quad .$$

The functions P_1 , P_2 and P_3 are the distribution functions chosen as a function of the easy axes orientation and the grain and domain shapes. GPT model uses two empirical probability distributions to describe the grain and domain shapes in the polycrystalline ferrite materials. These distributions can be represented by linear or Gaussian distribution functions.

For the case of bulk ferrite samples where initial permeability is mainly due to domain wall motions, empirical distribution functions used to describe the grain and domain shapes show major influence in the description of permeability tensor components. The imaginary part of permeability shows a wider response and the gyromagnetic resonance is shifted to a comparatively higher frequency value.

For bulk ferrite materials in which domain wall contributions are prominent, GPT model have a major limitation in describing the permeability tensor components in the demagnetized state. Contributions of empirical distribution functions overshadows the contributions from the damping factor in the low applied field regions. This limitation of GPT model makes it difficult to use the direct problem proposed in Chapter II, for multi-domain ferrite material in low magnetic field regions.

Domain wall contribution will disappear when the applied field is increased. Once the material is saturated, the proposed coaxial line method can be used for the damping factor measurements.

In the first phase of inverse problem (pure dielectric behavior of the sample, $\mu(\omega) = 1 - j 0$ and $\kappa(\omega) = 0 - j 0$), we optimize the complex permittivity of the ferrite in the demagnetized state. The optimized permittivity values are then compared with the measured values in order to validate the inverse problem.

The optimization procedure matches theoretical S-parameters with measured parameters in the high frequency region where only the dielectric properties of the material will have an influence on the characteristics of the measurement cell.

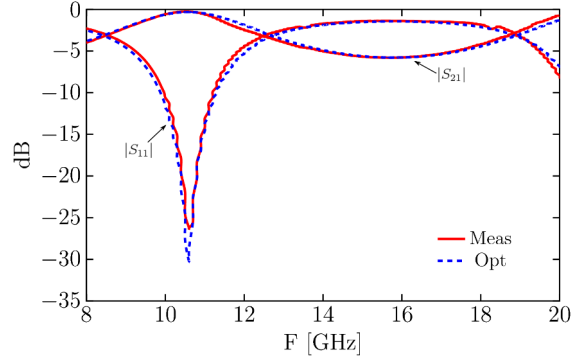


Figure III.15: Measured and optimized S-parameters of the demagnetized YIG 39 (EXXELIA TEMEX) ferrite sample of length 4 mm in the high frequency region.

Measured and optimized S-parameters of the demagnetized YIG 39 ferrite in the high frequency region are given in Figure III.15.

It is to be noted that the optimization procedure gives the effective value of the permittivity in the demagnetized state. There is an air gap of $20 \mu\text{m}$ between the sample and conductors of the measurement cell. In order to find the actual permittivity we have to take into account the air gap between the sample the inner and outer conductors of the measurement cell. The air gap correction is done by considering the sample with air gap as a set of series capacitors as described in the reference [46].

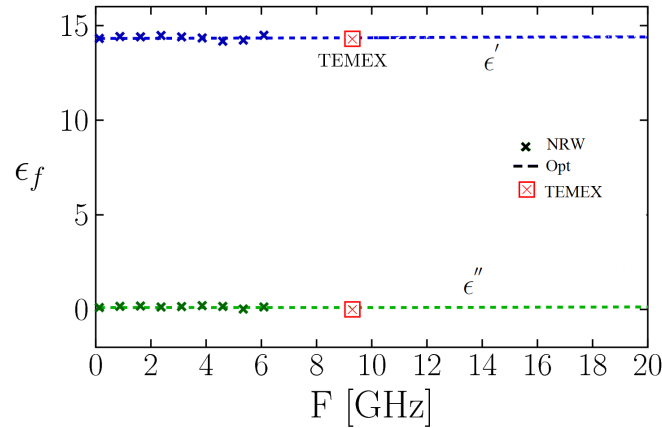


Figure III.16: Real and imaginary part of measured permittivity spectra, ϵ_f of the ferrite material of length 4 mm (considering the air gap correction using a layered capacitor model).

Figure III.16 presents the optimized broadband permittivity spectrum of the YIG 39 ferrite material in the high frequency region considering air gap correction [46]. The optimized permittivity of the material coincides with the value provided by the supplier EXXELIA TEMEX ceramics (Figure III.16) and the permittivity value measured using NRW method.

These results validate the inverse problem and optimized permittivity spectrum.

As the second step, we solve the inverse problem to measure the damping factor α for different values of the static magnetic fields H_{dc} well above saturation. The optimization variables are damping factor α and applied magnetic field H_{dc} . The anisotropy field H_a can be approximated from the gyromagnetic resonance in the composite sample to be around 54 Oe.

Table III.2 summarizes the initial values and the limits imposed on each of the variables to be optimized in the inverse problem.

Parameter	Initial value	Lower limit	Upper limit
H_{dc}	H_{meas}	$H_{meas}-200$ Oe	$H_{meas}+ 200$ Oe
α	0.006	0	0.1

Table III.2: YIG 39- Initial values and limits of the optimization variables

Figure III.18 presents the measured and optimized S-parameters different magnetization fields H_{dc} .

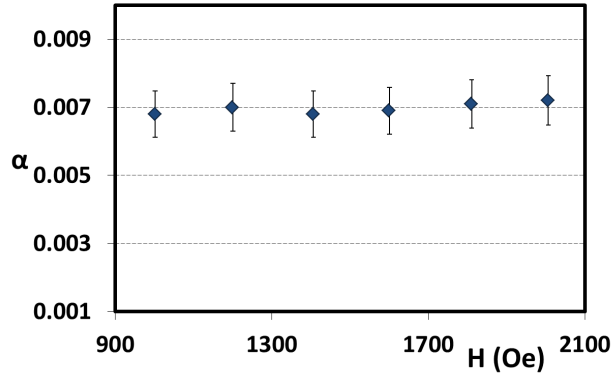


Figure III.17: YIG 39 sample- Optimized damping coefficient

For each applied field value, the inverse problem will give a vector X_{opt} which contains the optimized values of the variables α and H_{dc} .

The optimized values of damping factor α for different applied field values are plotted in Figure III.17. When the material is saturated, the damping factor α shows a constant behavior with value close to 0.0068.

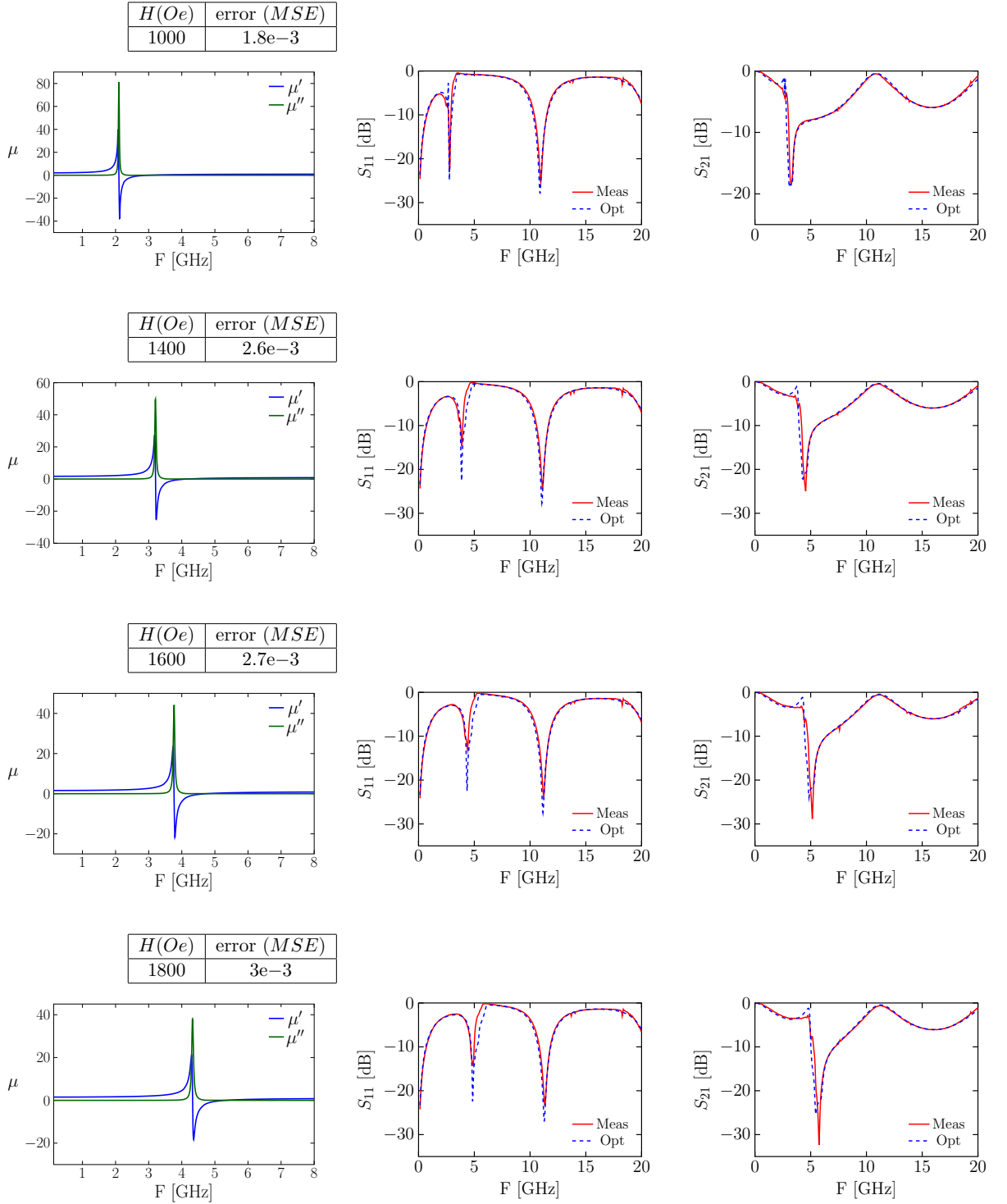


Figure III.18: Optimized permeability spectrum and S-parameters of YIG 39 ferrite material for different DC magnetic field (H_{dc}) values. Sample properties: $4\pi M_s = 810$ G, $H_a = 54$ Oe, $N_z = 0.35$.

III.4.3 Validation of results

Saturated state

In the saturated state damping factor α is directly related to resonance linewidth ΔH by Polder formulations [35].

$$\alpha = \frac{\gamma \Delta H}{2\omega}, \quad (\text{III.10})$$

where γ is the gyromagnetic ratio 2.8 MHz/Oe and ω is the angular frequency. This relation is only valid in the saturated state.

In order to validate the inverse problem results, resonance linewidth ΔH is calculated from the optimized damping factor value of a commercially available ferrite sample (Yttrium Iron Garnet-Y39 from TEMEX).

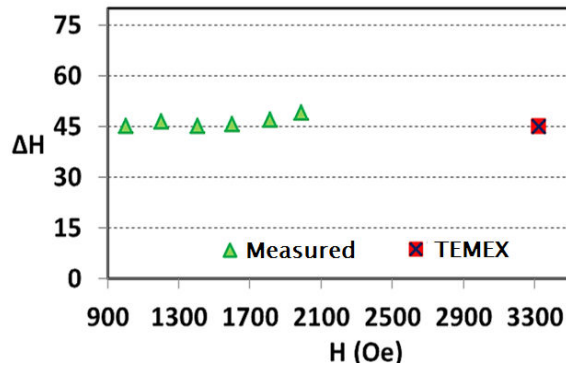


Figure III.19: Measured resonance linewidth ΔH of Y39 ferrite material . 'x' - value provided by EXXELIA TEMEX

The result are then compared with the ΔH value provided by the supplier data sheet. Figure III.19 shows the resonance linewidth ΔH calculated for the Y39 sample of length 4 mm in the saturated state. Mark 'x' represents the value provided by the supplier data sheet. TEMEX data sheet gives the resonance linewidth ΔH around 45 Oe (+/- 20%) at 9.3 GHz. From the Figure III.19, it is clear that the resonance linewidth calculated using the proposed method shows very good agreement with supplier data.

EXXELIA TEMEX also provided us with the experimental power absorption data measured in the resonance cavity using a spherical sample. The resonance linewidth is calculated from this experimental data and found to be 44 Oe.

Power absorption has linear relationship with the imaginary part of permeability μ'' .

$$P \propto \mu'' \quad (\text{III.11})$$

In a single computation procedure GPT model is able to predict the permeability tensor components for different applied values from a few input parameters. By using the dynamic damping coefficient α calculated using inverse problem, along with other static input parameters ($4\pi M_s$, H_a , etc.) GPT model is able to describe the permeability tensor components in a broad frequency band for different applied field values.

Input parameters to the GPT model are: saturation magnetization $4\pi M_s = 810$ G, anisotropy field $H_a = 54$ Oe, damping factor $\alpha = 0.0068$, and demagnetizing coefficient $N_z = 0.35$. From this permeability spectra, we can deduce the dynamic losses as a function of applied magnetic fields for every frequency value.

The absorbed power calculated for different applied field values at the frequency 9.3 GHz are then compared with the measured data provided by EXXELIA TEMEX. Figure III.20 shows the measured power absorption in the resonant cavity and the power absorption calculated from the imaginary part of permeability obtained using GPT model.

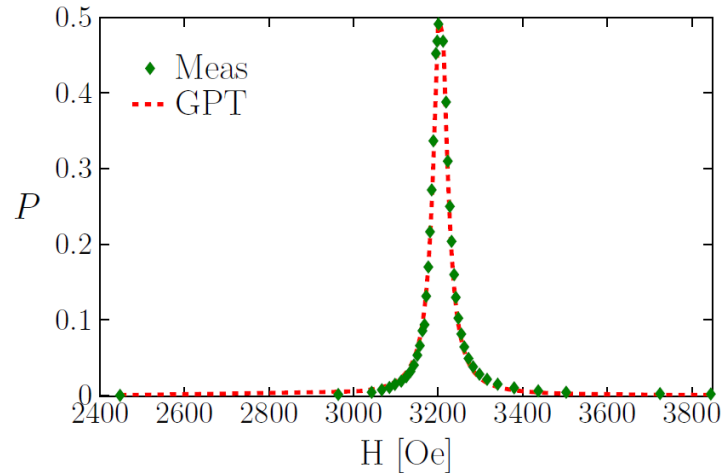


Figure III.20: YIG 39 sample- Measured and calculated power absorption

From the Figure III.20, it is clear that with the measured damping factor α , GPT model is able to accurately describe the dynamic losses in the spin resonance region. These results validate the inverse problem in the saturated states. This method shows some limitations for multi-domain ferrite materials in low magnetic field regions where the domain wall relaxation is prominent. This is due to the limitation of the GPT model to describe the domain wall contributions in the demagnetized permeability spectrum.

From the above results it is clear that proposed method is well suited for damping factor α measurement in the magnetized state. This broadband characterization method can be used from DC to millimeter wave frequencies since the dominant mode propagated in the empty coaxial line is TEM mode which has no cut-off frequency. Standard resonant cavity methods are limited to a single frequency corresponds to the resonant frequency of the measurement cavity, and these methods require the sample to be spherical in shape and sample length to be small compared to one quarter of the wavelength of the microwave radiation in the sample. This coaxial line method eliminates the shape and size constraints related to the resonant cavity and the samples imposed by the standard resonant cavity methods. The damping factor α is a more realistic representation of dynamic losses of ferrites than the parameters currently used: ΔH and ΔH_{eff} .

III.5 Conclusion

Inverse problem of the proposed coaxial line damping factor measurement method is presented and the method is validated by comparing the results with the supplier's data sheet. This coaxial line method eliminates the size and shape constraints related to the cavity and the sample imposed by standard measurement methods. More over this coaxial line method is a broadband method and easy to implement. Knowledge of a unique parameter representing dynamic losses would assist engineers in optimizing design and adjustment procedures for ferrite-based microwave devices. This unique dynamic property α combined with the static characteristics (saturation magnetization, anisotropy field, etc.) would be the input parameters of theoretical tool describing the dynamic properties of the ferrite material.

In the next chapter, we will present a theoretical EM tool incorporating a magneto-static analysis, a general permeability tensor model, and a commercial EM simulation software Ansys HFSS, for accurate description of dynamic behavior of ferrite based devices. This theoretical modeling approach will combine experimental techniques to find the physical parameters of the ferrites (saturation magnetization, damping factor, etc.), and a theoretical permeability model which will use these physical parameters to describe the dynamic behavior of ferrites at any magnetization state.

Chapitre 3. Résumé

Dans ce chapitre, nous présentons le problème inverse de la méthode proposée en ligne coaxiale et les résultats expérimentaux obtenus. L'objectif général du problème inverse est d'extraire par une procédure d'optimisation le facteur d'amortissement α du matériau testé en comparant les paramètres S théoriques obtenus à partir d'un problème direct, avec les paramètres S mesurés. D'un côté, les paramètres S théoriques sont calculés en utilisant l'analyse EM directe de la cellule de mesure. De l'autre côté, la procédure d'optimisation numérique est définie pour faire correspondre les paramètres S théoriques avec les paramètres S mesurés. Cette procédure d'optimisation est basée sur la minimisation d'une fonction erreur large bande (Err).

Les variables d'optimisation sont les paramètres d'entrée des fonctions analytiques choisies dans le problème direct. L'objectif de la procédure d'optimisation est de faire correspondre les paramètres S théoriques aux paramètres S mesurés en ajustant de manière itérative les paramètres d'entrée des fonctions analytiques représentant les propriétés du matériau: permittivité et perméabilité. Une fois que l'erreur entre les paramètres S théoriques et mesurés est minimisée ($Err \approx 0$), les fonctions optimisées représentent les paramètres EM de l'échantillon à caractériser. Les variables d'optimisations correspondent alors aux valeurs des paramètres recherchés.

Le nombre de paramètres d'ajustement dépend des fonctions analytiques choisies dans le problème direct. Notre problème inverse n'utilise que deux variables d'optimisation : le champ statique appliqué H_{dc} et le facteur d'amortissement α . Tous les autres paramètres d'entrée ($4\pi M_s$, H_a , etc.) sont déterminés au préalable par des mesures statiques standard.

La procédure d'optimisation ajuste les valeurs des paramètres H_{dc} et α en faisant correspondre les modules des paramètres S théoriques avec ceux mesurés. Cette comparaison théorie/mesure est réalisée, non pas fréquence par fréquence, mais sur l'ensemble des valeurs de la bande de fréquence mesurée. En prenant en compte uniquement les amplitudes des paramètres S, les incertitudes sur les phases liées aux résonances de dimension sont évitées. Au contraire, notre problème inverse exploite ces résonances lorsqu'elles existent pour faire converger les paramètres S plus rapidement et plus précisément.

Nous résolvons notre système d'équations en utilisant les techniques de type *curve fitting*. Pour cela, nous utilisons le sous-programme *lsqnonlin* de la boîte à outils d'optimisation MATLAB®. Pour s'assurer de trouver la solution correcte de notre système d'équations, nous devons vérifier que le sous-programme *lsqnonlin* fonctionne avec des solutions physiques (réalistes). Pour ce faire, nous devons garantir deux conditions: premièrement la détermination d'un point initial (pour les variables d'optimisation) qui n'est pas trop éloigné de la solution physique et deuxièmement la définition de valeurs limites physiques pour les variables d'optimisation. Il est possible de respecter ces conditions en choisissant des modèles réalistes de permittivité et de perméabilité basés sur des paramètres physiques.

Afin de tenir compte de sa nature dispersive, le modèle Cole-Cole est utilisé pour représenter la permittivité du ferrite dans le problème direct. Le modèle «Generalized Permeability Tensor (GPT)» est lui utilisé pour représenter le tenseur de perméabilité des matériaux magnétiques. Ce modèle décrit le comportement dynamique des composants du tenseur de perméabilité de manière prédictive en tenant compte du phénomène d'hystérésis et des interactions dynamiques dans le matériau.

La plupart des paramètres d'entrée du modèle GPT peuvent être obtenus par des mesures statiques standards. Les mesures d'hystérésis sont effectuées à l'aide d'un VSM (Vibration Sample Magnetometer). L'aimantation à saturation est déduite du cycle d'hystérésis mesuré. L'intensité du champ magnétique externe H_{dc} est mesurée directement à l'intérieur de la cellule à l'aide d'une sonde à effet Hall. Cependant, nous avons choisi de conserver le paramètre H_{dc} comme variable d'optimisation dans le problème inverse. Cela permet, si nécessaire, de corriger les écarts entre la réalité et le modèle GPT. Dans ce cas, le paramètre H_{dc} sera limité entre des valeurs proches de celles mesurées à l'intérieur de la cellule.

L'utilisation de modèles physiques comme celui de Cole-Cole pour la permittivité et celui de GPT pour la perméabilité dans notre procédure d'optimisation permet de garantir les réalités physiques des solutions trouvées.

L'avantage du modèle GPT est de déterminer par une procédure de calcul unique, les composantes du tenseur de perméabilité. En utilisant le coefficient d'amortissement dynamique issu du problème inverse, et les paramètres statiques ($4\pi M_s$, H_a , etc.), le modèle GPT est capable de décrire les composants du tenseur de perméabilité dans une large bande de fréquences et pour différentes valeurs de champ appliqués.

La cellule de mesure est une ligne coaxiale standard APC7. Un échantillon de ferrite de forme toroïdale est inséré entre les conducteurs interne et externe de la cellule de mesure. L'échantillon est aimanté dans la direction axiale en plaçant la cellule de mesure entre les pôles d'un électro-aimant. Les paramètres S_{11} et S_{12} sont ensuite mesurés à l'aide d'un analyseur de réseau vectoriel HP8720 dans la bande de fréquences de 130 MHz à 20 GHz.

Dans le cas saturé, le facteur d'amortissement peut être directement relié à la largeur à mi-hauteur des pertes selon les formulations de Polder. La largeur à mi-hauteur mesurée selon la méthode proposée montre un très bon accord avec les données des fournisseurs. La méthode de ligne coaxiale proposée est bien adaptée à la mesure du facteur d'amortissement à l'état aimanté. Cette méthode élimine les contraintes liées aux cavités résonantes et aux dimensions d'échantillon imposées par les méthodes de mesure standard. La connaissance d'un paramètre unique « α » représentant des pertes dynamiques devrait aider les concepteurs à optimiser les procédures de conception et de réglage des dispositifs micro-ondes à base de ferrite.

Cette méthode montre cependant certaines limites pour les matériaux multi-domaine dans les régions de champs magnétiques faibles où les relaxations de parois sont importantes. En effet, le modèle GPT, utilisé dans le problème direct, ne prend pas en compte l'aimantation par mouvements de parois dans le calcul des composants du tenseur de perméabilité. Cela limite l'utilisation de la méthode proposée pour le cas des ferrites multi-domaines dans la région du champ magnétique faible.

Chapter IV

EM Modeling Of Anisotropic Ferrites - Application To Y-Junction Microstrip Circulators

Contents

IV.1 Introduction	124
IV.2 Anisotropic ferrites - Non-homogeneous internal fields	124
IV.2.1 Demagnetizing field effects	124
IV.2.2 Effect of non-uniform internal fields in the power absorption spectrum	128
IV.2.3 Commercial software solutions: Magneto-static simulations using Ansys Maxwell 3D	129
IV.3 Electromagnetic modeling tool	131
IV.3.1 Magneto-static solver (Lab-STICC)	132
IV.3.2 EM modeling of anisotropic ferrites – Ansys HFSS	136
IV.4 Application - Microstrip Y-junction circulator	144
IV.4.1 Circulator Design	146
IV.4.2 Experimental results	147
IV.4.3 Non-uniform biasing fields- Electromagnetic analysis	149
IV.5 Conclusion	152

IV.1 Introduction

In this chapter we present a theoretical electromagnetic (EM) tool for accurately describing the dynamic behavior of ferrite based devices by taking into account the internal polarizing fields of anisotropic ferrite materials. This theoretical tool will combine a magneto-static analysis and the general permeability tensor model with a commercial simulation software.

Most of the input parameters of this theoretical tool are the static properties of the ferrite material except the damping factor. In first part of this thesis, we have developed a coaxial line technique for the determination of damping factor. All other input parameters of the EM tool can be determined by standard characterization methods. By considering the inhomogeneity of the internal polarizing fields, proposed theoretical tool will be able to predict the dynamic behavior of ferrite devices more accurately, at all magnetization states.

First, we discuss the non-homogeneity of the internal magnetic fields and its effect on the dynamic response of the anisotropic ferrite materials. Secondly we present the theoretical EM tool which combines a magneto-static analysis, a general model of permeability and commercial simulation software Ansys HFSS. Finally, proposed tool is validated by modeling and realizing a microstrip Y-junction circulator and comparing the results with measurements and Ansys HFSS-Maxwell 3D simulations.

IV.2 Anisotropic ferrites - Non-homogeneous internal fields

Dynamic response of an anisotropic ferrite material is dependent on the shape of the sample. The permeability of a sample ring is not the same as that of a wafer. In addition, for non-ellipsoidal magnetic material which is the case most commonly encountered in ferrite devices, the internal static biasing field is not uniform.

In a previous study in Lab-STICC, it is seen that in most common microwave applications, unsaturated regions in ferrimagnetic materials exist even when strong fields are applied [29]. This is due to the inhomogeneous nature of the internal magnetic fields within the non-ellipsoidal samples.

IV.2.1 Demagnetizing field effects

When the dielectric losses in ferrite materials are very small and constant, ferromagnetic losses can be represented by the power absorption in the system. A 30 mm APC7 standard coaxial line is taken as the measurement cell. The coaxial line is partially filled with toroidal shaped ferrite material and inserted between the poles of an electromagnet.

The S-parameters of the measurement cell loaded with toroidal ferrite samples are recorded using a vector network analyzer (VNA) for static magnetic values ranging from 0 Oe to 1700 Oe. The measurements are done in a frequency range from 130 MHz to 10 GHz.

The measurements are done for the composite Yttrium Iron Garnet ferrite sample- Y39 (magnetic volume fraction 70%) of thickness 2.93 mm.

The power absorption can be obtained from the S-parameters using the relation,

$$P = 1 - |S_{11}|^2 - |S_{21}|^2. \quad (IV.1)$$

Figure IV.1 shows the power absorption spectra of the coaxial line loaded with 2.93 mm thick YIG 39 composite material for different applied DC field values.

Maximum offset losses show an expected shift to high frequency values when the static magnetic field is increased. For each field value, optimization procedure proposed in Chapter III.2 allows us to match the theoretical curves with experimental data by minimizing a broadband error function.

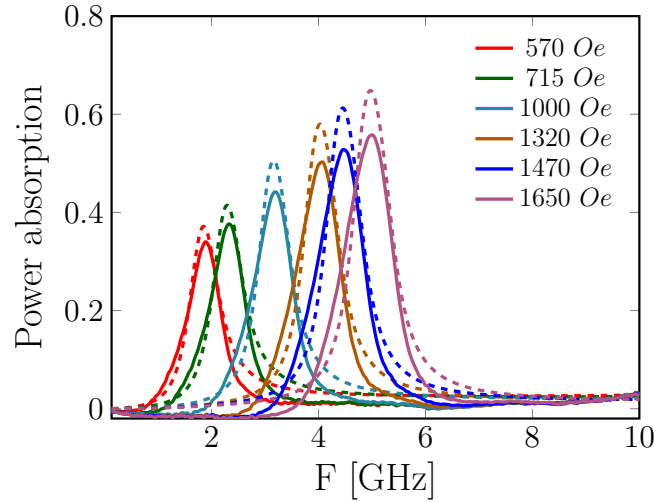


Figure IV.1: Evolution of the measured (-) and simulated (—) power absorption spectra of a coaxial line loaded with a YIG ferrite material (Y39 composite) as function of the applied DC magnetic field.

The frequency of maximum power consumption follows a linear law as a function of the internal field in the material,

$$F_r \propto H_{in}. \quad (IV.2)$$

The internal static field seen by the magnetic moments in the sample is decreased by the demagnetizing field which is a function of the demagnetizing coefficient N ,

$$H_{in} = H_{DC} + H_a - N.M_z, \quad (IV.3)$$

where H_{DC} is the applied static magnetic field, H_a is the magneto-crystalline anisotropy field and M_z the magnetization of the material in the z-direction.

Indeed in the proposed coaxial line method we assume to know the exact value of the internal magnetic field. To get accurate results with the EM analysis, we have to calculate the internal field inside the material. One challenge lies in the evaluation of the demagnetizing fields inside the sample. In our samples the demagnetizing coefficient in the longitudinal direction, depends on the sample thickness. Thinner the sample, stronger are the demagnetizing fields.

In the composite YIG 39 ferrite, demagnetizing fields are local and each grains can be assumed to be magnetized uniformly. To estimate the macroscopic demagnetization effects due to the shape of the sample and not to its composition, we measured power absorption spectra of bulk ferrite samples with identical composition (Yttrium Iron Garnet) but different thicknesses 2 mm, 3 mm, 4 mm, 5 mm, and 6 mm. Since the samples are finite in size, they have demagnetizing fields associated with their shape. The internal static magnetic field seen by the magnetic moments in the sample is reduced by the demagnetizing field effects.

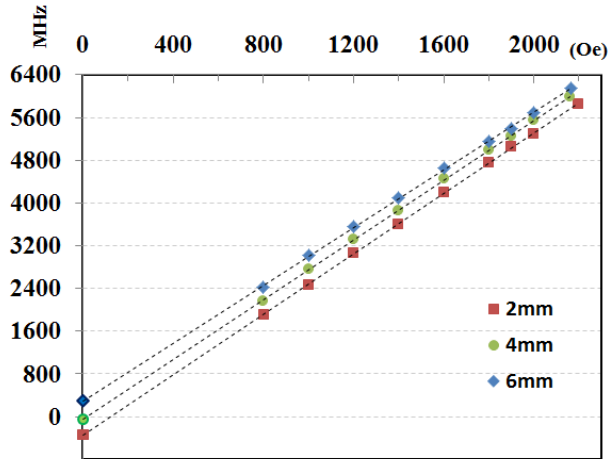


Figure IV.2: Evolution of the maximum power absorbed by bulk ferrite materials (YIG 39- different thickness) with the applied magnetic field.

A 7 mm long APC7 coaxial line is taken as the measurement cell. The measurement cell is partially filled with ferrite sample and placed between the poles of an electromagnet.

Choice of a smaller measurement cell helps to reduce the space between the magnet poles and thereby allows us to apply stronger DC fields. The S-parameters of the measurement cell loaded with ferrite samples are recorded for static magnetic values ranging from 0 Oe to 2100 Oe. The measurements are done for bulk Yttrium Iron Garnet-Y39 (EXXELIA TEMEX) samples of thickness 2, 3, 4, 5, 6 mm. The samples are with permittivity value 14.3 and saturation magnetization equal to 810 G. For each sample, measurements are repeated in a frequency range from 130 MHz to 20 GHz.

The maximum offset values for power absorption are moved to higher frequencies when applied field increases. We know that the resonant frequency has a direct proportionality with the internal field in the material. When the material is saturated, the relationship between the resonant frequencies and applied field follows the equation of a straight line with positive slope close to the value of the gyromagnetic ratio, 2.8 MHz/Oe.

From Figure IV.2, it is clear that, for samples with different thickness, variation of frequency corresponds to maximum offset losses with applied field, shows parallel behavior with similar slope. These lines show same slope, but different Y intercept which can be translated to different demagnetizing factor N_z .

Thinner the sample, the demagnetizing coefficient becomes higher, leading to a lower Y intercept with lower origin. From the calculated Y intercept we can deduce a relation between the demagnetization coefficients of samples with identical composition and different thickness, assuming all the samples have same anisotropy field and saturation magnetization.

Theoretical calculation of demagnetization coefficient is not easy for non-ellipsoidal samples. Exact calculation of N factor is only possible in the case of ellipsoidal forms and uniform magnetization [6, 7]. Several studies have proposed formulations to calculate the demagnetization coefficient of hollow cylinder (thick ring) [8, 9]. These formulations give an effective value for the demagnetizing coefficient N . They are based on different approximations, and not often lead to similar results.

Thickness	2 mm	3 mm	4 mm	5 mm
N	0.562	0.414	0.346	0.296

Table IV.1: Demagnetizing factors calculated for the samples with different thickness

As an example, Table IV.1 shows the values of demagnetizing factors calculated with the method proposed in [9] for our sample of APC7 standard (outer diameter, $D_o = 7$ mm, inner diameter $D_i = 3.04$ mm). These results are consistent with the observed linear variation of maximum offset losses with applied fields as shown in Figure IV.2. Ratio of the theoretical demagnetization coefficients of samples with different thickness gives a value very close to the ratio of the demagnetizing fields calculated from the experimental Y-intercepts.

For example consider N_2 and N_3 as the theoretical demagnetization coefficients calculated for samples with thickness 2 mm and 3 mm respectively, ratio N_2/N_3 gives a value 1.365 which is in good agreement with ratio of the demagnetization fields calculated from the Y-intercept 1.37. But an in-depth study is necessary to describe the demagnetizing field effects more accurately and to determine the internal magnetic fields in the ferrite material.

IV.2.2 Effect of non-uniform internal fields in the power absorption spectrum

Power absorption spectra of toroidal shaped bulk ferrite materials show the presence of secondary resonance peaks as shown in Figure IV.3. These secondary peaks results in a broadening of the power absorption near the resonance. Standard measurement methods use spherical shaped samples to avoid these demagnetizing effects because spheres are the only shape providing uniform magnetization.

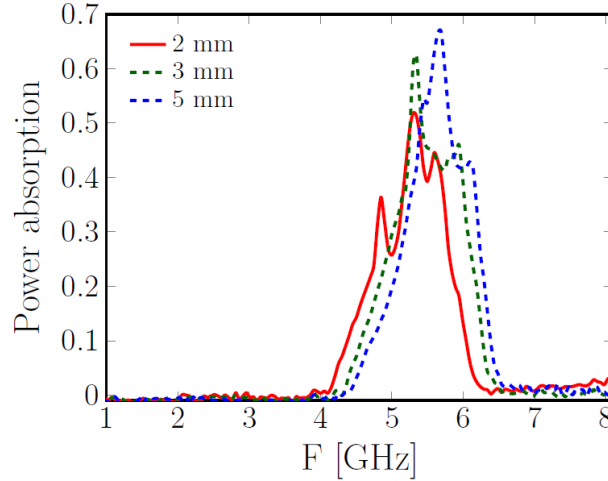


Figure IV.3: Power absorption spectra of YIG 39 (EXXELIA TEMEX) samples of different thickness, $4\pi M_s = 810$ G, $\epsilon = 14.3$, $\alpha = 0.0068$, $H_{DC} = 2000$ Oe.

These peaks follow an expected behavior - when the static field increases resonant peaks shift towards higher frequencies. After saturation, each resonance peak shows a linear variation in frequency with the increase in static field.

Initial EM analysis of the measurement cell with quasi-TEM approximation does not predict all these secondary peaks in the absorbed power spectrum. Classical frequency domain simulation using uniform biasing in HFSS produces similar results as the quasi-TEM analysis, and it cannot account for the broadness of the power absorption near the resonant frequency.

Indeed these simulations consider an approximate value for the demagnetizing coefficient, and uniform magnetization inside the sample, but in reality demagnetization fields vary

in space, and in direction inside the sample. This leads to inhomogeneous internal fields inside the ferrite material. In many cases, a numerical magneto-static simulation is the only capable way of describing the reality of the internal static fields.

Several software solutions are available to compute the internal magnetization as a function of the applied DC magnetic field. However the valid range of application of these software products is limited.

IV.2.3 Commercial software solutions: Magneto-static simulations using Ansys Maxwell 3D

A magneto-static study using Ansys Maxwell 3D can be used to find the non-uniform internal fields inside the ferrite material. In Maxwell 3D magneto-static simulations, the sample is defined as a non-linear anisotropic material.

In order to describe the evolution of ferrite magnetization with magnitude and direction of applied magnetic field, Maxwell 3D uses a single (B -H) hysteresis curve. The B-H curve used is often extracted from the measured hysteresis cycle and it is applied to the whole volume of the ferrite sample under study. The permeability in each direction is calculated from the hysteresis (B-H) curve based on the magnitude of the applied DC magnetic field. Specific boundary conditions are used to define uniform external magnetic field along the propagation direction.

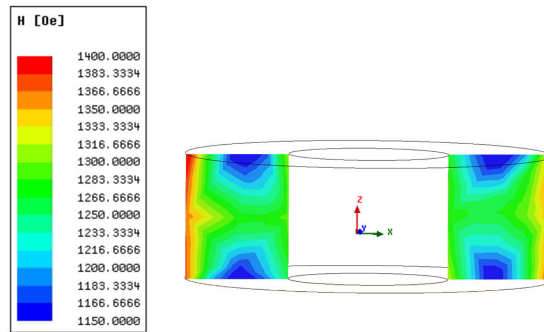


Figure IV.4: Internal fields calculated inside a 2 mm YIG ferrite sample using the Maxwell 3D, when an external DC magnetic field $H_{DC}=1600$ Oe is applied uniformly on the ferrite material.

Figure IV.4 shows the internal magnetic fields inside YIG ferrite material of thickness 2 mm calculated using the Maxwell 3D analysis. An external DC magnetic field $H_{DC}=1600$ Oe is applied uniformly on the ferrite sample. From the Figure IV.4, it is clear that internal fields inside the sample material is not uniform and varies in space inside the sample. In order to consider the non-homogeneity of the internal magnetic fields inside the ferrite material in frequency domain simulations, we combine Maxwell 3D simulations with Ansys HFSS.

The non-uniform internal biasing fields of ferrite material in HFSS is defined using the field values obtained from the Maxwell 3D simulation. Once the non-homogeneous internal DC magnetic fields inside the ferrite are obtained from the Maxwell 3D simulations, they are used to compute the permeability spectra of the ferrite material in HFSS. These internal field values in association with saturation magnetization $4\pi M_s$, and resonance linewidth ΔH , are used in classical Polder model to define the frequency dependent permeability tensor of the sample material.

S-parameters are calculated using the frequency domain solver in HFSS. Measured and simulated power absorption spectra of a coaxial line loaded with 2 mm sample are shown in Figure IV.5, for different applied field values.

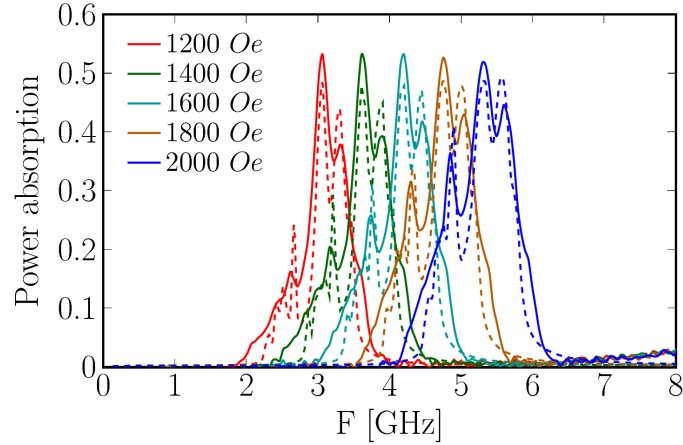


Figure IV.5: Measured (-) and Simulated (- -) power absorption of 2 mm sample for various applied DC magnetic fields.

Power absorption spectra simulated using the combination of Maxwell 3D and HFSS show multiple peaks and they are in good agreement with the measurement results. From these results it is clear that multiple peaks and the broadening of losses in the power absorption spectra are due to the non-uniformity of the internal fields inside the ferrite material. This study concludes that the demagnetizing fields effects due to the size and shape of the sample is prominent in non-ellipsoidal samples. It is necessary to evaluate the demagnetizing field effects and accurately calculate the non-homogeneous internal fields in the ferrite material to get better results with EM simulations.

The association of Maxwell 3D with HFSS produces satisfactory results in the case of saturated ferrite materials. HFSS software uses Polder model to describe the permeability tensor of the anisotropic ferrite and always uses saturation magnetization ($4\pi M_s$) to describe the magnetization inside the sample. This presents a limitation for this approach.

The intensity of the internal magnetic field can be too low in some regions of the material

and totally saturated medium assumed by the Polder model is not valid in those cases. Moreover, for a given static field value, there may be several possible states of magnetization depending on the magnetization history. But HFSS cannot take this phenomenon into account, because one can only define a single B-H curve to represent the static magnetic behavior of the whole sample.

This description of magnetization is sufficient for ferrite materials in saturated state but not suitable for the general description of the ferrite magnetization. Dynamic behavior of ferrite in remanent or partially magnetized states cannot be described by this theoretical approach.

IV.3 Electromagnetic modeling tool

Design of the new classes of ferrite devices has to be based on the combination of experimental techniques to find the physical parameters of the ferrites and theoretical tools capable of describing the dynamic EM behavior of the ferrites in all magnetization states. Within the Lab-STICC, Gelin and Queffelec have developed a model to determine permeability tensor components in any state of magnetization [36]. Most of the input parameters of the generalized permeability tensor model are the static properties of the ferrite like saturation magnetization $4\pi M_s$, anisotropy field H_a , etc. except the damping factor α used to represent the dynamic losses.

In Chapter II, we presented a broadband coaxial line technique to measure the damping factor α . Static input parameters like saturation magnetization $4\pi M_s$, anisotropy field H_a , etc., can be measured using standard measurement methods. Now we have experimental methods to find the physical parameters of the ferrites and theoretical model which will use these parameters to describe the dynamic behavior of ferrites at any magnetization state. A dynamic EM analysis of the structure considering inhomogeneous internal fields and a generalized permeability tensor model would enable us to understand the internal field distribution and the demagnetizing field effects on the performances of ferrite devices.

In this section, we are presenting a rigorous theoretical tool to determine the EM properties of ferrites in a predictive way, whatever their magnetization state is, and takes into account the inhomogeneity of the internal field polarization. This tool combines a magneto-static analysis, a general model for permeability tensor and a commercial simulation software-Ansys HFSS.

A magneto-static analysis is carried out to find the internal biasing field in the ferrite sample. The sample is then divided into finer zones where the internal field can be considered

uniform. Permeability tensor is calculated for each zone using Generalized permeability tensor model [36] taking into account corresponding demagnetizing tensor and internal field magnitude and direction.

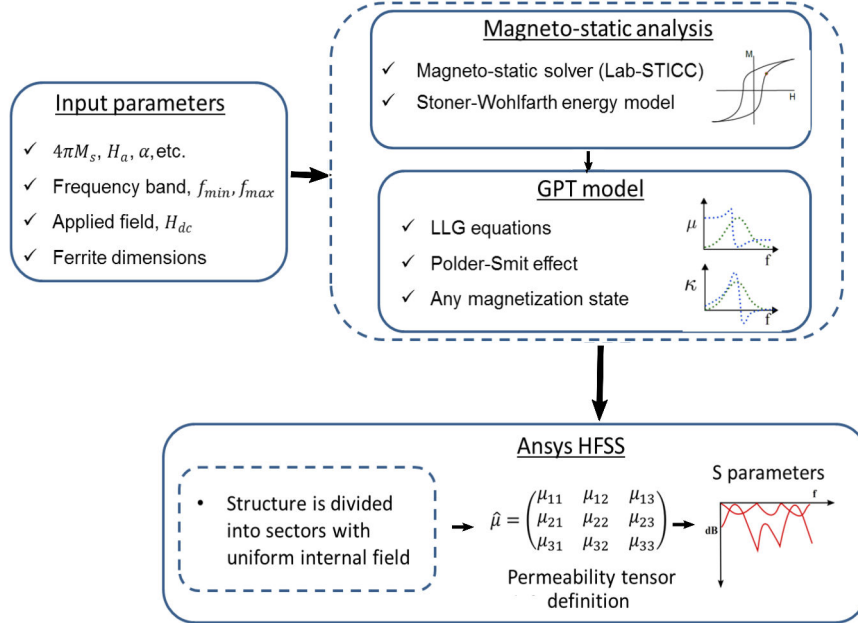


Figure IV.6: Predictive electromagnetic modeling tool.

In HFSS design, these zones are then defined as different materials or simply as computational regions in which material is the same but with different internal magnetic biasing fields.

For each region, real and imaginary parts of the permeability tensor components are defined as frequency dependent functions in HFSS. S-parameters are then calculated using the frequency domain solver.

In the following, we will discuss in detail about the magneto-static solver and the integration of the permeability models with HFSS. The results will be validated by comparing them with measurements and HFSS-Maxwell simulations.

IV.3.1 Magneto-static solver (Lab-STICC)

In order to study the inhomogeneity of the internal static magnetic fields in ferrite materials, a magneto-static solver has been developed in Lab-STICC [47]. This magneto-static solver developed by G.Verissimo, a post-doctoral fellow in Lab-STICC, is based on the discretization of the Poisson equation using the finite difference method.

Considering analogy to the polarization of electric dipoles,

$$\Delta V_m = -\rho_m \quad , \quad (IV.4)$$

where V_m is the scalar magnetic potential, and ρ_m is the magnetic charge density. Magnetic charge density ρ_m is calculated from the magnetization vector \vec{M} by the relation,

$$\rho_m = -div(\vec{M}) \quad , \quad (IV.5)$$

The finite difference algorithm gives a system of equations,

$$\bar{A}\vec{V}_m = -\vec{\rho}_m \quad , \quad (IV.6)$$

where \bar{A} is a square matrix of the order N_l (number of free nodes of the mesh), V_m is the scalar magnetic potential on each free nodes, and ρ_m is the magnetic charge density on each free node.

The algorithm used is a differential method, so we have to define an air box including the ferrite sample. The nodes are defined on the edges of the mesh. An integral method based on the knowledge of ρ_m at all nodes of the mesh, is used to model the free space opening.

Magnetic potential V_m is computed from the charge density ρ_m ,

$$\vec{V}_m = -\bar{A}^{-1} \times \vec{\rho}_m \quad , \quad (IV.7)$$

The demagnetizing field is then obtained from the relation between magnetic field intensity and scalar magnetic potential,

$$\vec{H}_m = -\nabla V_m \quad , \quad (IV.8)$$

The magnetic field and the magnetization are computed in the center of each mesh cell unlike scalar potentials and magnetic charge density. The magnetization M is computed as a function of total DC magnetic field \vec{H}_t ,

$$\vec{H}_t = \vec{H}_0 + \vec{H}_m. \quad (IV.9)$$

For each mesh cell, this solver takes into account a hysteresis cycle based on Stoner-Wohlfarth energy model [38]. This approach enables us to model the magnetization states of polycrystalline ferrites containing domains by considering the magnetic domains as uniaxial anisotropic particles. Since this is a numerical model the system of equations Eq. IV.6 becomes nonlinear in nature.

An iterative Broyden algorithm (Quasi-Newton method) is used to solve the system of equations, which comprises the use of a Jacobian matrix (\bar{J}) approximation.

For k^{th} iteration,

$$\vec{F}_k = \bar{A}\vec{V}_{mk} + \vec{\rho}_{mk} = 0. \quad (IV.10)$$

- Initial point

$$\vec{V}_{mk} = 0, \vec{H}_{mk} = 0, \bar{J}_k = \bar{A}, \quad (IV.11)$$

$$\vec{B}_k = stoner(\vec{H}_0), \vec{\rho}_{mk} = -div(\vec{B}_k).$$

stoner = Stoner-Wohlfarth model.

- If error is greater than tolerance level,

$$d\vec{V} = -\bar{J}_k^{-1}\vec{F}_k,$$

$$\vec{V}_{mk+1} = \vec{V}_{mk} + d\vec{V},$$

$$\vec{H}_{mk+1} = -\nabla V_{mk+1},$$

$$\vec{B}_{k+1} = stoner(\vec{H}_t),$$

(IV.12)

$$\vec{\rho}_{mk+1} = -\nabla \cdot \vec{B}_{k+1},$$

$$\vec{F}_{k+1} = \bar{A}\vec{V}_{mk+1} + \vec{\rho}_{mk+1}$$

$$error = |\vec{F}_{k+1}|.$$

For the next iteration, \vec{J}_{k+1} is calculated using Broyden formulations.

When the algorithm is converged, in each mesh cell we obtain the microscopic quantities such as local domain magnetization (computed using the Stoner and Wohlfarth model) along with macroscopic quantities (\vec{H}_m, M).

In order to validate the results obtained with our magneto-static solver, we consider the case of an APC7 standard hollow cylindrical shaped ferrite uniformly magnetized along the axial direction. Internal static biasing fields are calculated using the magneto-static analysis and the results are compared with a commercial software solution- Ansys Maxwell 3D.

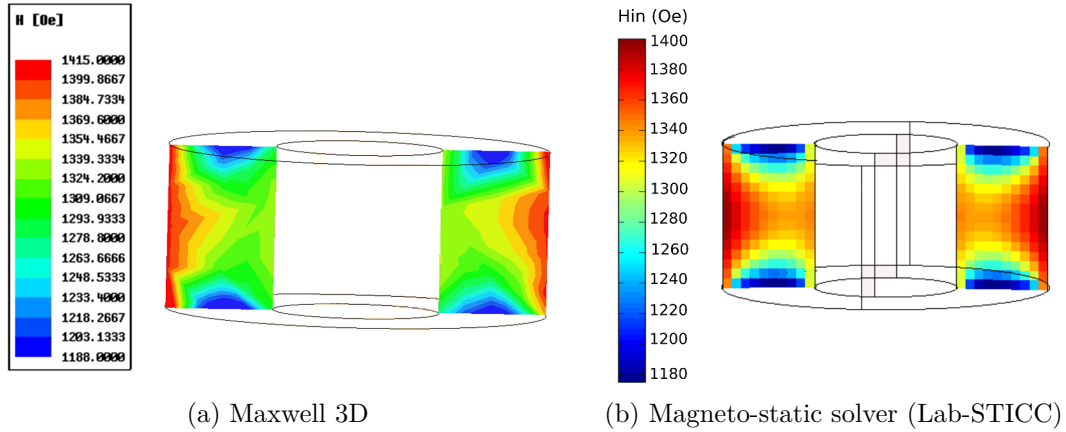


Figure IV.7: Internal fields calculated inside a 3 mm YIG ferrite using the magneto-static analysis, when an external DC magnetic field $H_{DC}=1600$ Oe is applied uniformly on the ferrite material.

Figure IV.7 shows the calculated internal DC biasing fields of the coaxial line loaded with a 3 mm thick YIG ferrite when the material is magnetized along the z-direction with an applied DC magnetic field 1600 Oe. In Maxwell 3D simulations, the whole ferrite material is represented by a single hysteresis curve.

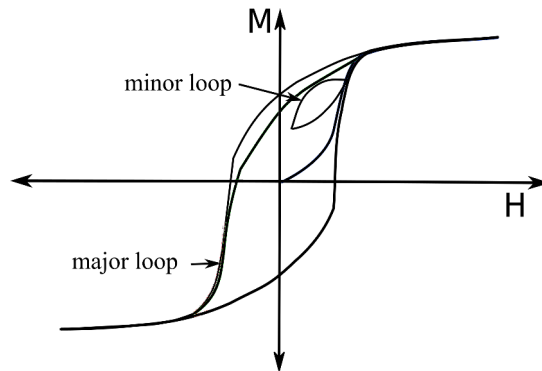


Figure IV.8: Illustration of major and minor hysteresis loops- Stoner and Wohlfarth model.

For an applied field, there can be several states of magnetization depending on the magnetization history. But Maxwell 3D cannot take this phenomenon into account, because a single B-H curve is used to represent the whole sample. Our magneto-static analysis presents a more realistic description of internal DC fields. Each mesh cell can follow a different hysteresis cycle (major or minor) and is applicable for all magnetization states.

IV.3.2 EM modeling of anisotropic ferrites – Ansys HFSS

Anisotropic nature of the ferrite material can be modeled using Ansys HFSS either by using Polder formulations or by using user defined permeability tensor. Conventionally HFSS software uses Polder model - a small signal approximation of Landau-Lifshitz equations [35]. As we have seen in Chapter II, these formulas are established for a single spin magnetic moment subjected to a static magnetic field H_{DC} , and to a perpendicular microwave magnetic field \vec{h} . This approximation is only valid for the case of saturated ferrites where all the magnetic moments are aligned parallel to each other.

Internal DC magnetic field (magnetic biasing) can be defined as uniform or non-uniform. For the case of uniform magnetic biasing, the internal static field is corrected using the Kittel formula to take into account the demagnetizing fields related to the finite dimensions of the ferrite.

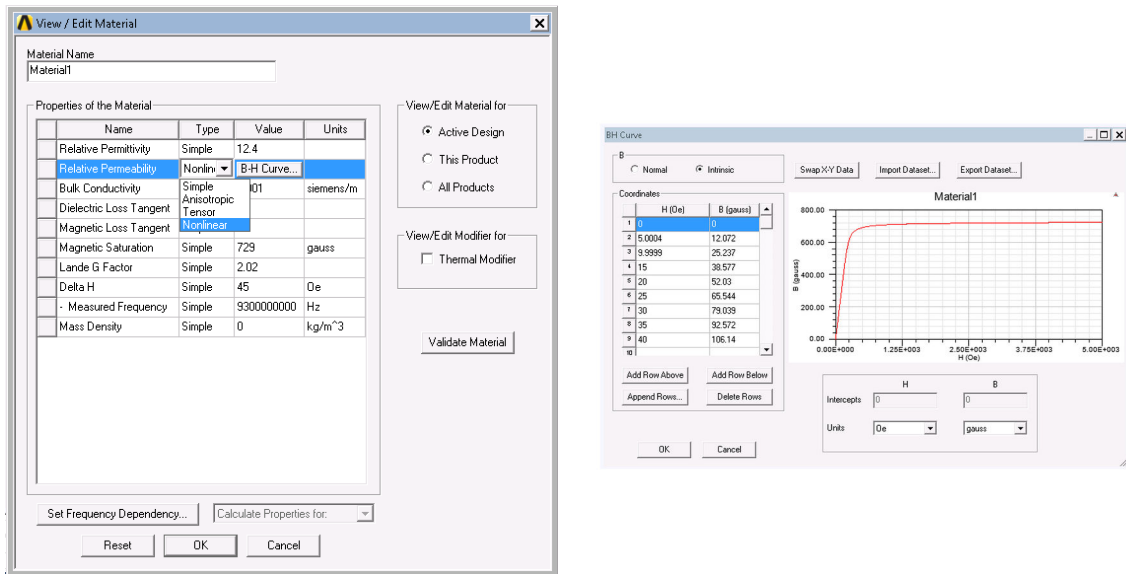


Figure IV.9: Material definition - Ansys HFSS.

Ferrite material can also be defined as a non-linear material by using a B-H hysteresis curve (for example first magnetization curve). Another option is to define the material property as anisotropic, where HFSS allows us to define the diagonal components of the anisotropic tensor. The diagonal components can be defined as a simple value, a constant, a variable or a non-linear B-H curve.

A combination of Maxwell 3D simulations with Ansys HFSS can be used to define the non-uniform biasing in frequency domain simulations. The internal bias field and local coordinate system are calculated on a tetrahedron by tetrahedron basis from magneto-static

analysis using Maxwell 3D software.

Ansys Electronic Desktop version 2016.2 and above also offers an option to define all the nine components of permeability and/or permittivity tensor. This function allows the user to independently define the real and imaginary parts of the nine elements of the tensor. It is also possible to define these elements as being frequency dependent functions or as project variables. This opens up an opportunity to use theoretical permeability tensor models other than Polder model with HFSS.

IV.3.2.1 Integration of theoretical permeability tensor models with HFSS

Conventionally, Ansys HFSS use Polder model to calculate the permeability tensor components. As we have discussed in the previous sections, Polder model is only valid in the saturated state. Several theoretical models have already been proposed in the literature to describe the complex permeability tensor components - Schloemann [30] for demagnetized ferrites, or Rado [31], Green and Sandy [32], and Igarashi and Naito [33, 34] for partially magnetized ferrites. Within the LabSTICC, Gelin and Queffelec have developed a model to determine permeability tensor components in any state of magnetization [27, 36].

When the applied field is along z direction, permeability tensor can be defined as,

$$\hat{\mu} = \begin{bmatrix} \mu' - j\mu'' & -j(\kappa' - j\kappa'') & 0 \\ j(\kappa' - j\kappa'') & \mu' - j\mu'' & 0 \\ 0 & 0 & \mu'_z - j\mu''_z \end{bmatrix} \quad (\text{IV.13})$$

HFSS offers a function to define datasets with user defined points. These data sets can be used in the piecewise linear intrinsic functions of HFSS.

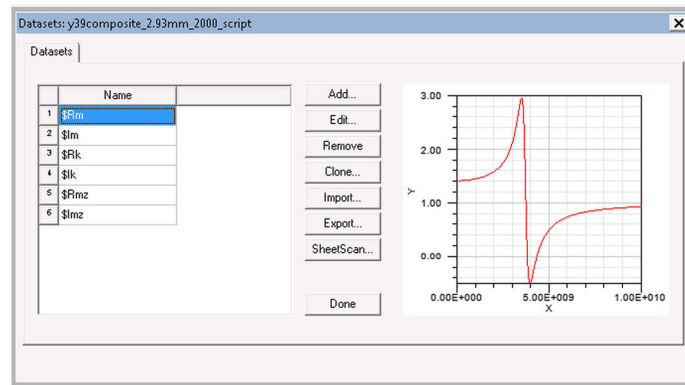


Figure IV.10: Definition of datasets in HFSS.

The property of the material can be defined as being frequency dependent, using the dataset as first parameter to the piecewise linear interpolation function (*pwl (dataset_expression, variable)*).

Frequency domain solver in HFSS must be able to calculate the value of the permeability tensor components at any frequency value. Our approach involves the definition of (user defined) data points and linear interpolation of the defined data points into frequency dependent functions. We use theoretical models to compute the permeability tensor components and interpolate them as frequency dependent functions.

Material permeability is defined by using the Tensor function in HFSS. Real and imaginary parts of the permeability tensor components are calculated using theoretical models and imported as separate data sets in HFSS. Each data set is interpolated into frequency dependent functions using intrinsic piecewise linear interpolation function. These frequency dependent functions are then used to define the complex components of the permeability tensor.

IV.3.2.2 Ansys HFSS – Macro programming

HFSS can be controlled via scripts in Microsoft Visual Basic programming language. These scripts can be used, for example, to create libraries, datasets or to do automated tasks (create 3D objects, material definition etc.). VB scripting is a fast and effective way to do repetitive tasks.

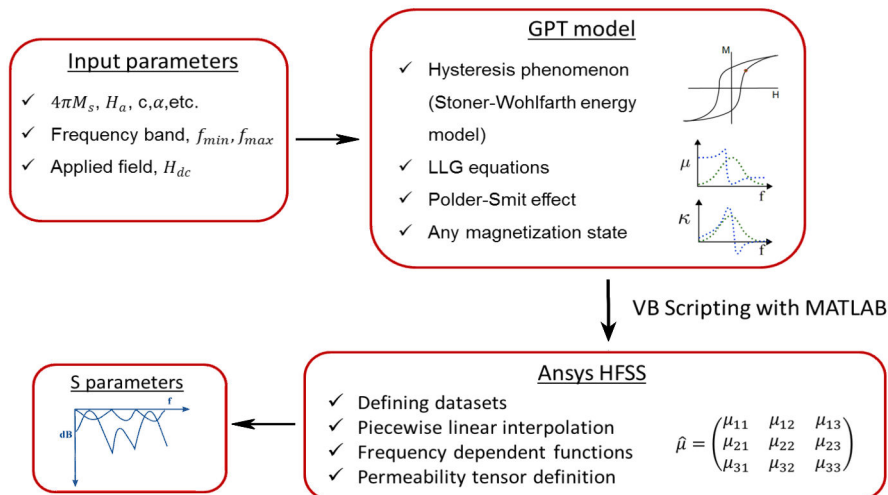


Figure IV.11: Integration of GPT model with HFSS.

Scripts can be written using any text editor or we can record a script from the ANSYS

Electronics Desktop interface. Scripts can also be executed from command line if they are written in any language that supports Microsoft COM methods. This provides an opportunity to create, control and execute HFSS simulations with MATLAB.

Using these functions we can create new materials in HFSS and it is possible to define the nine elements of the permeability tensor from MATLAB environment. This allows us to define the real and imaginary parts of nine components of permeability tensor calculated using theoretical models other than Polder model in HFSS.

Permeability tensor is calculated using generalized permeability tensor (GPT) model. A set of MATLAB functions is created to integrate the GPT model with HFSS. A VB Script is created using MATLAB to add or edit a material definition in HFSS. Permeability of the material is defined by tensor function and each component of the permeability tensor is defined by frequency dependent functions.

Real and imaginary parts of permeability tensor components are defined as dataset points. These data points are interpolated using inbuilt piecewise linear interpolation function of HFSS software. Scripting with MATLAB allows us easy control over the material definition in HFSS simulations.

IV.3.2.3 Validation of results

IV.3.2.4 Comparison with classical HFSS simulations

Polder model

In order to validate the new approach involving the manipulation of datasets, we consider the case where a ferrite sample is inserted between the inner and outer conductors of a coaxial line. The sample is magnetized to saturation by using an electromagnet.

The coaxial line is of APC7 standard and the sample is a ferrite material with relative permittivity 8.3, saturation magnetization $4\pi M_s = 800$ G, anisotropic field $H_a = 54$ Oe, demagnetizing coefficient $N_z = 0.42$ and $\Delta H = 300$ Oe.

For an applied magnetic field $H_{dc} = 1400$ Oe, permeability tensor is calculated with Polder model. Real and imaginary parts of permeability tensor components are saved as the frequency dependent datasets in HFSS. Real and imaginary parts of permeability tensor components are then interpolated into frequency dependent functions using the intrinsic *pwl* function in HFSS.

These frequency dependent functions are then used to define the user defined permeability tensor in HFSS. Each complex component of the permeability tensor is defined using the frequency dependent functions. S-parameters are calculated using frequency domain solver in HFSS. The simulations are done for a frequency range from 130 MHz up to 20 GHz.

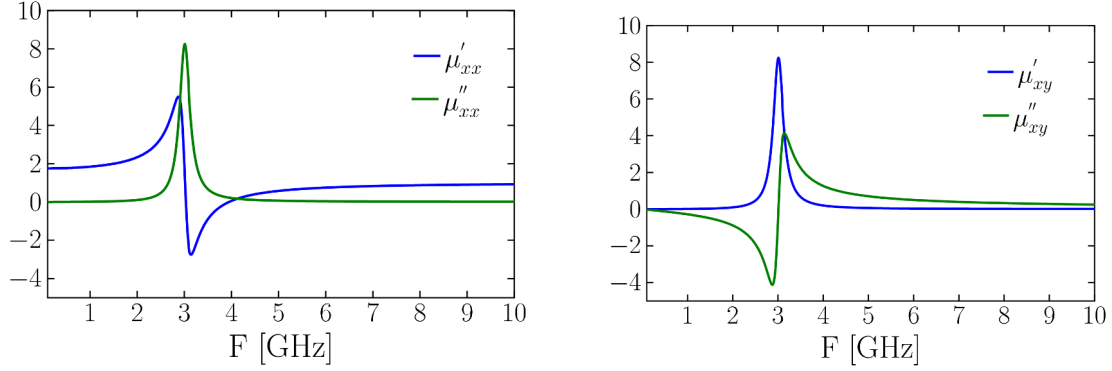


Figure IV.12: Spectra of the real and imaginary parts of the diagonal μ and off-diagonal κ components of permeability tensor computed using Polder model. $4\pi M_s = 800$ G, $H_a = 54$ Oe, $N_z = 0.42$ and $\Delta H = 300$ Oe. Sample thickness = 2.9 mm.

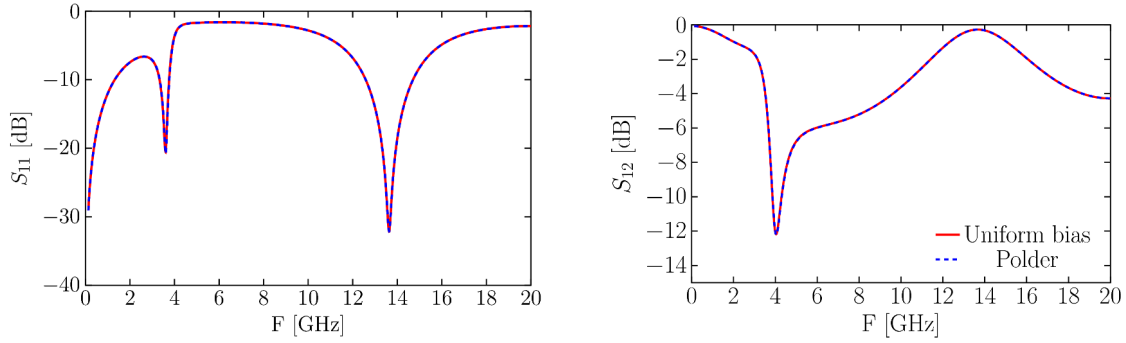


Figure IV.13: Simulated S-parameters of a coaxial line (APC7 standard) loaded with a magnetized ferrite (Polder model) - Sample properties: $4\pi M_s = 800$ G, $H_a = 54$ Oe, $N_z = 0.42$ and $\Delta H = 300$ Oe. Sample thickness = 2.9 mm.

S-parameters obtained from the frequency domain simulations are shown in Figure IV.13. Results are then compared with the conventional HFSS simulations (uniform biasing) using inbuilt Polder model. For the case of uniform magnetic biasing in HFSS, the internal magnetic field is corrected using the Kittel formula [37] to take into account the demagnetizing fields. From these results it is clear that the use of tensor permeability gives very good agreement with the conventional simulations using uniform biasing assumption.

GPT model

In saturation GPT model [36] gives similar results with Polder model. For the same conditions as above permeability tensor is calculated using the GPT model.

Real and imaginary parts of all the nine components of the permeability tensor are then imported as datasets in HFSS. Intrinsic piecewise linear interpolation function of HFSS

(*pwl*), is then used to interpolate these datasets as frequency dependent functions. These functions are then used to calculate the user defined permeability tensor in HFSS.

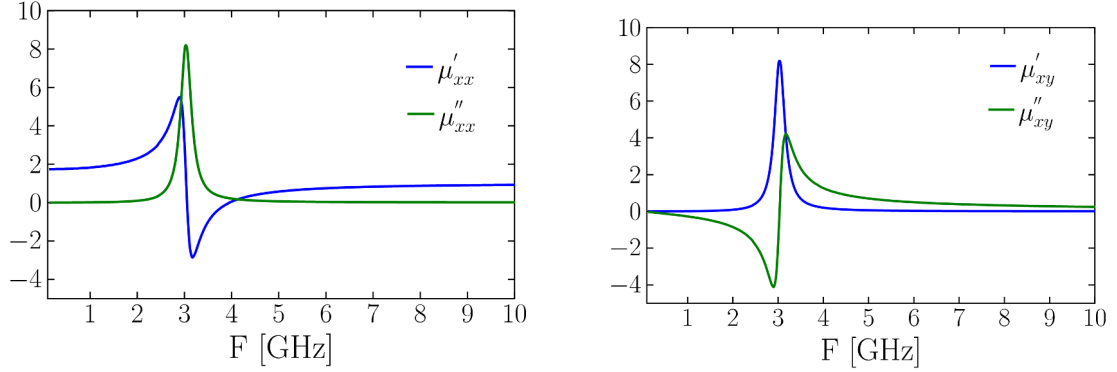


Figure IV.14: Spectra of the real and imaginary parts of the diagonal μ and off-diagonal κ components of permeability tensor computed using GPT model. Sample properties: $4\pi M_s = 800$ G, $H_a = 54$ Oe, $N_z = 0.42$ and $\Delta H = 300$ Oe. Sample thickness = 2.9 mm.

S-parameters are calculated using frequency domain solver in HFSS. The simulations are done for a frequency range from 130 MHz to 20 GHz. Results are then compared with the conventional HFSS simulations (uniform biasing) using inbuilt Polder model.

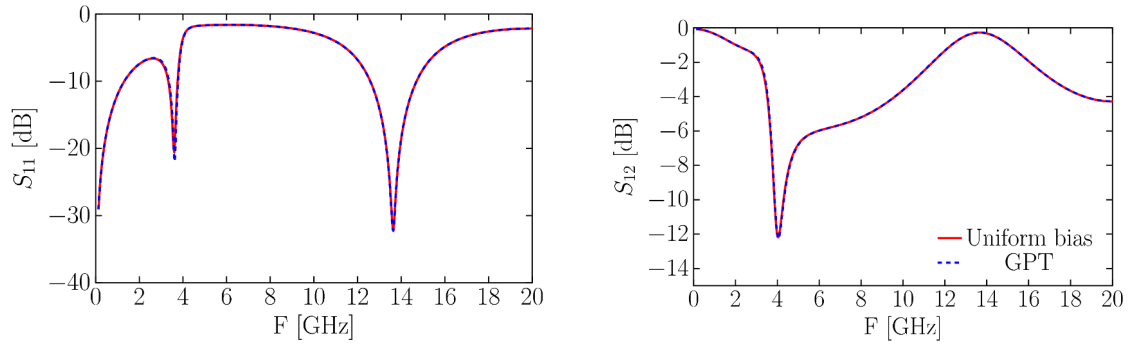


Figure IV.15: Simulated S parameters (GPT model + HFSS). Sample properties: $4\pi M_s = 800$ G, $H_a = 54$ Oe, $N_z = 0.42$ and $\Delta H = 300$ Oe. Sample thickness = 2.9 mm.

From Figure IV.14, it is clear that the new approach with GPT model gives very good agreement with the conventional simulations using Polder model with uniform biasing assumption. These results validate the proposed approach using Tensor function in HFSS.

IV.3.2.5 Non-Uniform biasing – Comparison with Maxwell 3D simulations

In order to validate the proposed approach in the case of non-uniform biasing fields, we studied the power absorption spectra of a coaxial line partially filled with toroidal ferrite sample. The sample is in hollow cylindrical in shape and it is magnetized to saturation with an electromagnet.

The coaxial line is of APC7 standard and the sample is a YIG39 ferrite material (from EXXELIA TEMEX) with relative permittivity 14.3, saturation magnetization $4\pi M_s = 810$ G, anisotropic field $H_a = 54$ Oe, and damping coefficient $\alpha = 0.0068$.

Power absorption spectra of a coaxial line loaded with bulk ferrite materials show the presence of secondary resonance peaks. These secondary peaks result in a broadening of the power absorption curve near the resonance. Initial EM analysis of the measurement cell with quasi-TEM approximation does not predict all these secondary peaks in the absorbed power spectrum. Classical frequency domain simulation using uniform biasing in HFSS produces similar results as the quasi-TEM analysis, and it cannot account for the broadness of the power absorption near the resonant frequency. Indeed these simulations consider an approximate value for the demagnetizing coefficient and uniform magnetization inside the sample but in reality internal fields are non-homogeneous in nature.

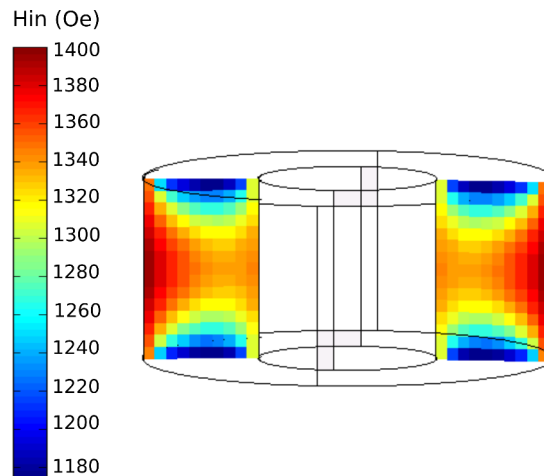


Figure IV.16: Internal DC magnetic fields calculated inside a 3 mm YIG ferrite using the magneto-static analysis, when a uniform DC magnetic field $H_{DC} = 1600$ Oe is applied on the sample.

The inhomogeneity of the internal static magnetic fields in the ferrite, is studied using the magneto-static solver previously developed in Lab-STICC [47]. This magneto-static analysis presents a more realistic description of internal DC fields. For each mesh cell, this solver takes into account a hysteresis cycle based on Stoner-Wohlfarth energy model [38]. Each mesh cell can follow a different hysteresis cycle (major or minor) and is applicable for all magnetization states.

Internal biasing fields inside the ferrite are determined using a magneto-static solver. The internal static fields of a 3 mm YIG sample for applied magnetic field, $H_{DC}=1600$ Oe are shown in Figure IV.16.

The magneto-static study of sample shows that demagnetizing fields are space dependent and internal DC fields are inhomogeneous in nature. The internal fields show no variation along the θ direction. In order to consider the variation in direction and magnitude of the demagnetizing fields, ferrite sample is divided into different concentric annulus regions in which the internal DC field can be considered uniform (Figure IV.17).

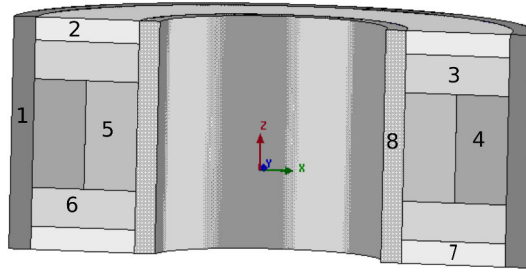


Figure IV.17: Cross section of the ferrite sample- Definition of different regions where internal DC magnetic fields can be considered as uniform.

In each annulus sector, the internal field is considered uniform and a permeability tensor is then calculated for each sector using GPT model by taking into account its demagnetizing fields. GPT model allows us to determine the permeability tensor components in a predictive way at all magnetization states.

In this study, the generalized permeability tensor (GPT) model is used to describe the permeability tensor components of the ferrite material. This model is based on the classical Landau-Lifshitz-Gilbert equations and takes into account the inherent physical phenomena in polycrystalline ferrites such as the Polder-Smit effect, the hysteresis phenomenon, and statistical distribution on the shape of grains and domains. The input parameters are the static parameters like saturation magnetization ($4\pi M_s$), anisotropic field (H_a), etc., and the damping factor (α) which represents the magnetic losses of the material.

GPT model is used to define the full (nine element tensor) tensor permeability of the ferrite material in HFSS software. The frequency domain solver in HFSS needs to be able to calculate the permeability tensor components at any frequency value. Real and imaginary parts of each element of the permeability tensor is defined as the frequency dependent functions by using the piecewise linear interpolation of the data points in HFSS. S-parameters are then calculated using the frequency domain simulations. Simulations are done in a frequency range from 130 MHz up to 20 GHz.

Power absorption can be calculated from the simulated S-parameters. Simulated and measured power absorption spectra of coaxial line loaded with a 3 mm-thick YIG sample for different applied DC magnetic field values are shown in Figure IV.18. The power absorption results are also compared with results obtained using the Maxwell 3D simulations as shown in Figure IV.18.

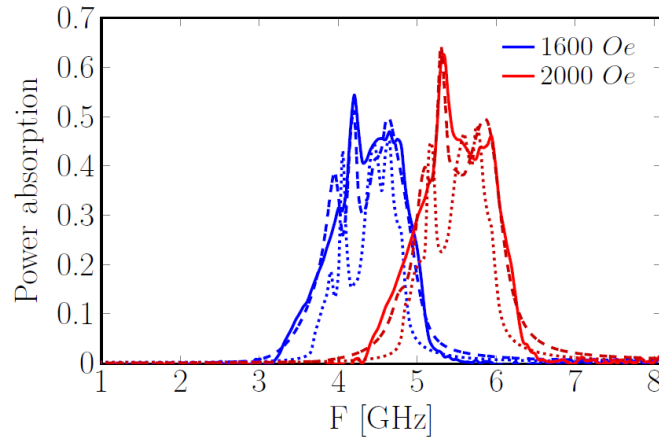


Figure IV.18: Measured (-) and simulated power absorption spectra of 3 mm YIG ferrite (Maxwell 3D (...), GPT+HFSS (- -)).

A very good agreement is found between the measured and simulated results. From the Figure IV.18, it is clear that results obtained from our theoretical tool are closer to the measurement results than those predicted by Maxwell-HFSS simulations. Integration of magneto-static analysis enhances the predictive nature of GPT model.

By taking into account the inhomogeneity of the internal polarizing fields, proposed theoretical tool can predict the dynamic behavior of anisotropic ferrites more accurately, at all magnetization states.

IV.4 Application - Microstrip Y-junction circulator

Circulators play an important role in the microwave communication systems for civil and military applications. The working of ferrite circulators/isolators is based on the nonreciprocal behavior of EM wave propagation in magnetized ferrites [48, 49]. Circulators are generally used for full duplex communications whereas isolators (one port is ended with a matched load) are used to protect the transmission components from parasitic radiations or impedance mismatch.

The circulator is composed of at least three ports around a central junction. The propagation of the EM wave takes place in a predetermined direction. This is due to the

nonreciprocal behavior of wave propagation in magnetized ferrite placed at the center of the structure. The S-parameter matrix of an ideal circulator is shown in Figure IV.19.

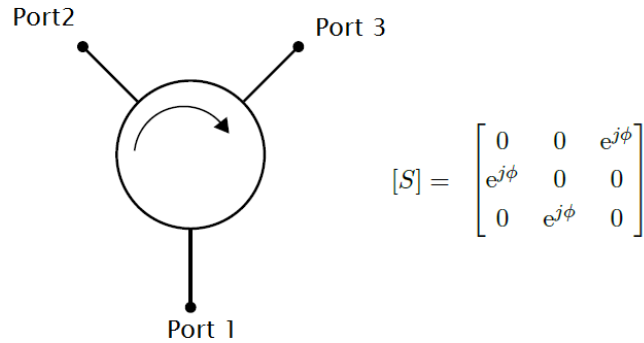


Figure IV.19: Symbol and S parameter matrix of an ideal circulator.

To meet the requirements for the rapid growth of microwave communication systems, design of circulators has to be based on new materials (low sintering temperature ferrites, hexaferrites) [50, 51], new technologies [52] (LTCC, 3D printing) and predictive EM simulation tools. Due to its complex nature (nonreciprocal behavior, anisotropic properties of magnetic materials, heterogeneous configuration etc.), design of circulators which meet the miniaturization conditions with good EM performances, requires better understanding of the physical processes involved. This requires the development of new theoretical tools to predict the dynamic behavior of ferrite devices.

One of the important parameters that affect the performance of circulators is the non-uniformity of the DC biasing field. The reduction of transmission band in Y-junction circulators due the DC field non-homogeneity within the ferrite is already discussed by How et al [53]. In most ferrite devices, ferrite sample is non-spherical in shape, i.e. non-homogeneity of static biasing field is quite common in those devices.

Conventional junction circulators require strong magnetic fields to bias the ferrite integrated in the device [49]. These bias fields are provided by the permanent magnets which increases the size and cost of these devices. For miniaturization of circulators, designers are encouraged to use planar technologies (eg: microstrip) or pre-oriented materials [51, 54–56] to avoid the use of permanent magnets. For microstrip circulators, only one magnet is used to polarize the material. These topologies increase the non-homogeneity of the DC biasing fields in ferrite materials.

More realistic description of EM behavior of circulators requires accurate computation of permeability tensor components. A dynamic EM analysis of the structure, considering inhomogeneous internal fields and a generalized permeability tensor model would enable

us to understand the internal field distribution and the demagnetizing field effects on the performances of ferrite circulators. A magneto-static analysis is carried out to find the internal biasing field in the ferrite sample. Permeability tensor is described by generalized permeability tensor (GPT) model [36] considering the spatial variation of internal magnetic fields.

IV.4.1 Circulator Design

A microstrip Y-junction circulator is designed for an extended frequency range around X-band. The design procedure of microstrip Y-junction circulator is based on Bosma principles [57].

Radius of the junction resonator at the center of the circuit was estimated according to the first circulator equation. The circulator design is optimized by HFSS simulations.

The quarter wavelength lines are designed on the LTCC compatible substrate T950 and connected to the 50Ω access lines. The width of the quarter-wavelength line is tuned using HFSS for maximum isolation. The design does not show ternary symmetry as the branches of the junction are not identical.

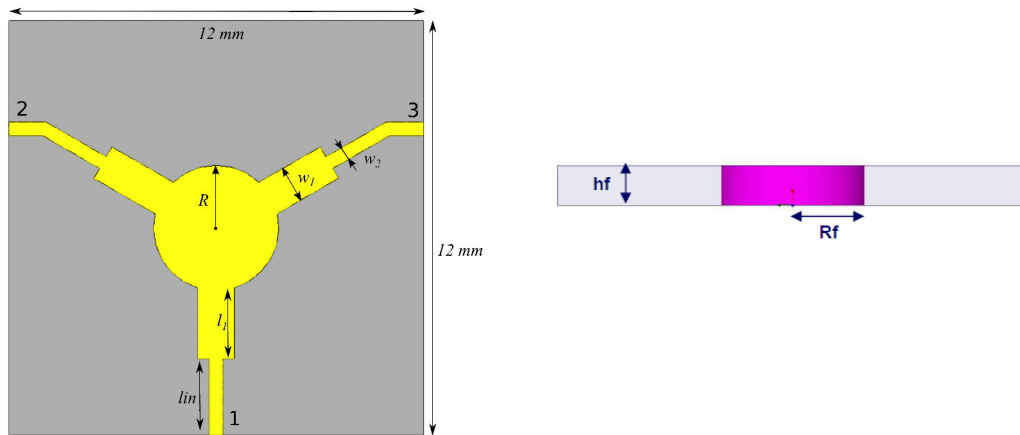


Figure IV.20: Y-junction microstrip circulator- Design parameters. Quarter wavelength line: $l_1=1.8$ mm, $w_1=0.93$ mm. 50Ω Access line: $l_{in}=2$ mm, $w_2=0.4$ mm. Ferrite sample: radius $R_f=1.82$ mm, thickness=1 mm. Thickness of substrate, $h_f=1$ mm.

A Yttrium iron garnet (YIG) ferrite substituted with bismuth, and copper cations, is used for the design and realization of microstrip Y-junction circulator. The ferrite puck at the center of the dielectric substrate material has a thickness of 1 mm and radius 1.82 mm.

The ferrite material has the following properties: relative permittivity $\epsilon_f=19$, $\tan\delta=0.003$, saturation magnetization $4\pi M_s=1710$ G, anisotropy field $H_a=50$ Oe, and resonance linewidth $\Delta H=10$ Oe.

The HFSS simulations are based on following material properties:

Material	ϵ	$\tan\delta * 1e^{-3}$	$4\pi M_s(G)$	$H_a(Oe)$	$\Delta H(Oe)$
Ferrite	19	3	1710	50	10
Dielectric substrate T950	21	3	-	-	-

In the EM simulations, applied DC magnetic field at the center of the ferrite is taken as 2800 Oe. The demagnetization coefficient is calculated to be 0.64, so the ferrite disk is assumed to be magnetized with uniform internal DC magnetic field ($H_{in}=H_{DC}-N.M_s=2800-0.636*1710=1712$ Oe).

The operation frequency of the circulator is chosen above the FMR resonance region. The optimized radius of the ferrite is 1.82 mm. The junction resonator is designed with the same radius as the ferrite puck. The substrate material used is a LTCC compatible dielectric T950 with a relative permittivity 21 and loss tangent, $\tan\delta=0.003$. The length and width of microstrip access line are 1.8 mm and 0.93 mm respectively. The 50 Ω access lines are optimized by HFSS simulations.

IV.4.2 Experimental results

The Y-junction microstrip circulator is fabricated with an additive multilayer process using LTCC technology (Low temperature co-fired ceramics). A bulk sample of substituted yttrium iron garnet (YIG) ferrite material (chemical composition $Y_{2.8}Cu_{0.05}Bi_{0.67}Fe_5O_{12}$ is chosen for the core of the circulator [50].

The circulator circuit is designed on top of the dielectric substrate. By substituting with bismuth and copper cations, the sintering temperature of the Yttrium garnet is considerably decreased from $\sim 1,450^\circ\text{C}$ to down to $\sim 950^\circ\text{C}$. This decrease allows the co-firing of compatible materials with silver or gold. The addition of bismuth ions increases the permittivity of the material and subsequently reduces the core size of the circulator. The ferrite puck has a radius of 1.82 mm and thickness 1 mm.

The DC biasing field is applied normal to the ferrite material by placing a permanent magnet above the junction. We use a Sintered Samarium Cobalt Magnet (SmCo magnet)-Recoma[®]20, with residual induction (B_r) 9000 G, and coercivity 8800 Oe for magnetizing the circulator junction.

The static field at the center of the ferrite is controlled by placing a dielectric in between the junction conductor and the magnet. The radius of the magnet is 1.91 mm. The static field provided by the magnet is enough to saturate the ferrite material. Usage of only one magnet, instead of two with conventional stripline technology, increases the DC biasing field non-uniformity in the junction.

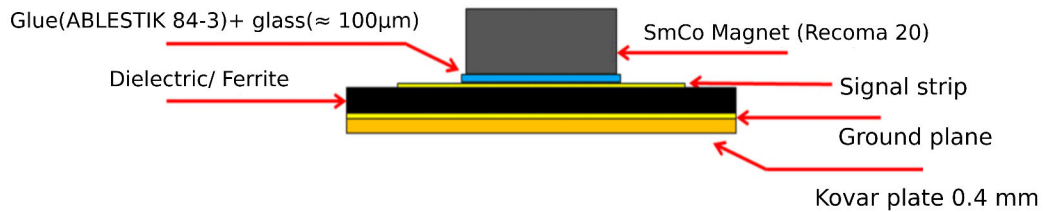
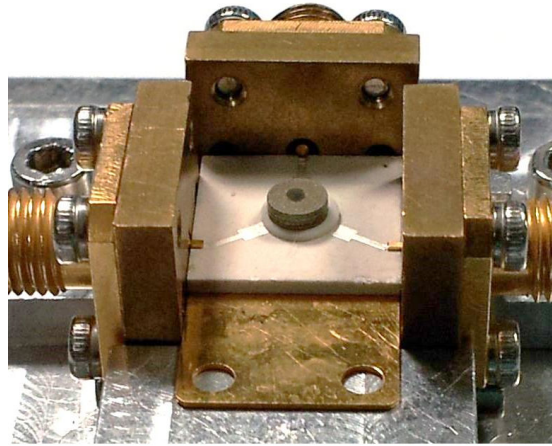


Figure IV.21: Y-junction microstrip circulator- Experimental setup and cutting view.

Circulator ground plane, conductive strips, and junction are realized by depositing thick layers of silver. The junction radius is 1.82 mm. The quarter wavelength lines are deposited on the substrate material and connected to the 50 Ω access lines.

The S-parameter measurements are done with Rohde & Schwarz ZVA24 (4 port) vector network analyzer in the frequency range from 6 GHz up to 14 GHz. Figure IV.21 shows the experimental setup of our microstrip Y-junction circulator biased by a single magnet.

Figure IV.22 shows the measured insertion loss, isolation and return loss of the microstrip circulator. The circulator shows an isolation of 23 dB with corresponding insertion loss of 0.6 dB and 39% bandwidth. The results show the dual band response which helps the broadband behavior of circulator.

The measured results show a shift in center frequency to the lower frequency region. The center frequency is shifted to lower frequency value compared to the HFSS simulations with uniform biasing fields assumption. The measured 20 dB isolation bandwidth is found to be higher than the simulated one. This difference is due to the fact that internal field in ferrite material is not homogeneous as assumed in classical HFSS simulations.

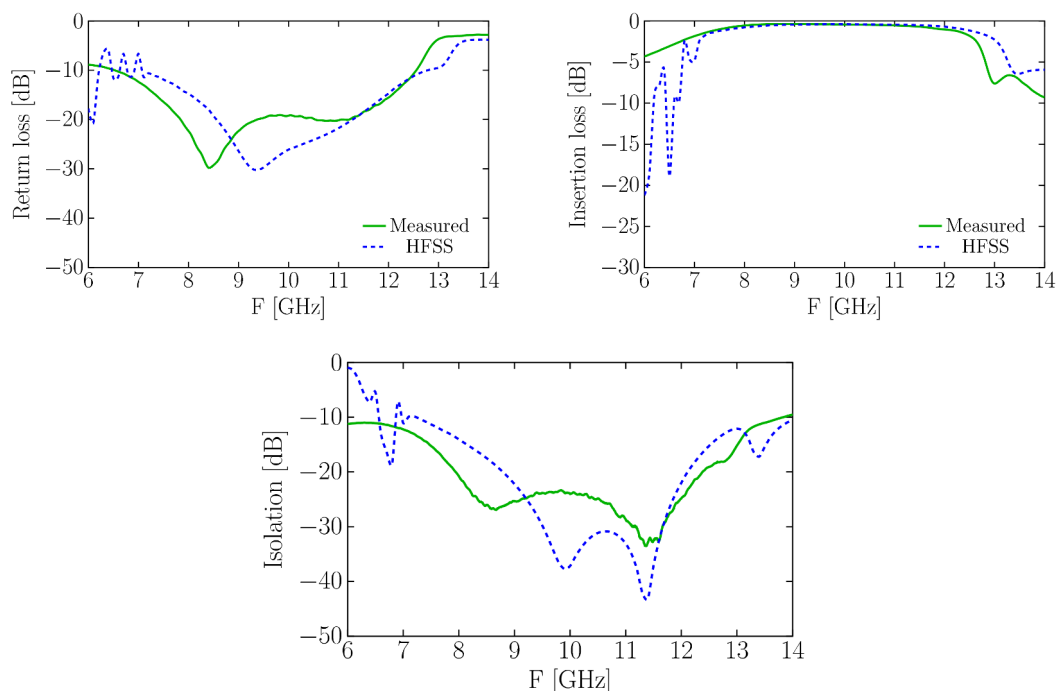


Figure IV.22: Measured (-) and simulated (-) S-parameters of Y-junction microstrip circulator: HFSS with uniform biasing fields assumption.

Different parts of the ferrite material may have different static biasing fields and different magnetization states. Some part of ferrite can be partially magnetized state where Polder model is no longer valid.

A static field analysis of the ferrite disk magnetized by a single permanent magnet will help us to understand the internal field polarization of ferrite material. An EM analysis of the structure considering the non-homogeneity of internal static fields and use of a generalized permeability model will enable us to better understand circulator performances.

IV.4.3 Non-uniform biasing fields- Electromagnetic analysis

The inhomogeneity of the internal static DC magnetic fields in the ferrites is studied using the magneto-static solver previously developed in Lab-STICC [47]. This magneto-static analysis presents a more realistic description of internal DC fields. For each mesh cell, this solver takes into account a hysteresis cycle based on Stoner-Wohlfarth energy model [38].

We used only one permanent magnet placed above the junction for biasing the ferrite in the circulator and this topology results in significant internal field non-homogeneity in the ferrite medium. The ferrite disk shows a variation in internal field along radial direction as well as along the thickness of the ferrite material.

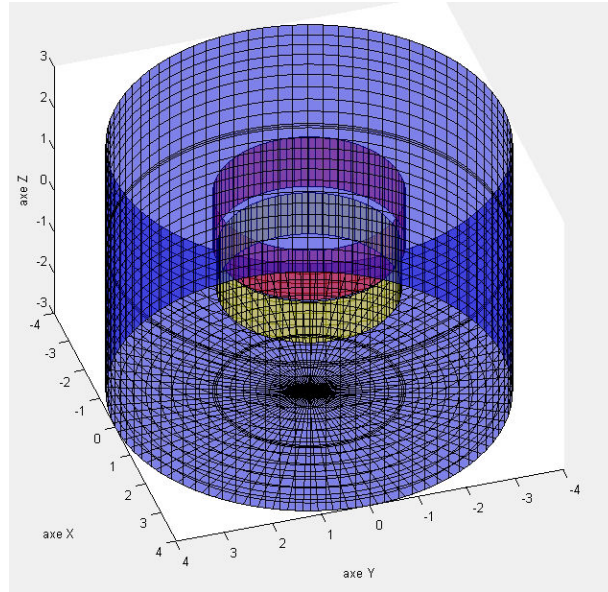


Figure IV.23: Magneto-static analysis of a ferrite disk magnetized by a permanent magnet- Mesh settings.

The ferrite material shows a variation of magnetization along the thickness with maximum field happens at the face closest to the magnet. The ferrite regions farther from the magnet show low internal biasing fields and this can possibly result in unsaturated areas in the ferrite disk.

The anisotropic properties of the material are dependent on the magnitude and direction of internal DC biasing fields. In order to take into account the non-homogeneity of the internal static fields, the ferrite disk is divided into different computational regions where the internal field is considered to be uniform.

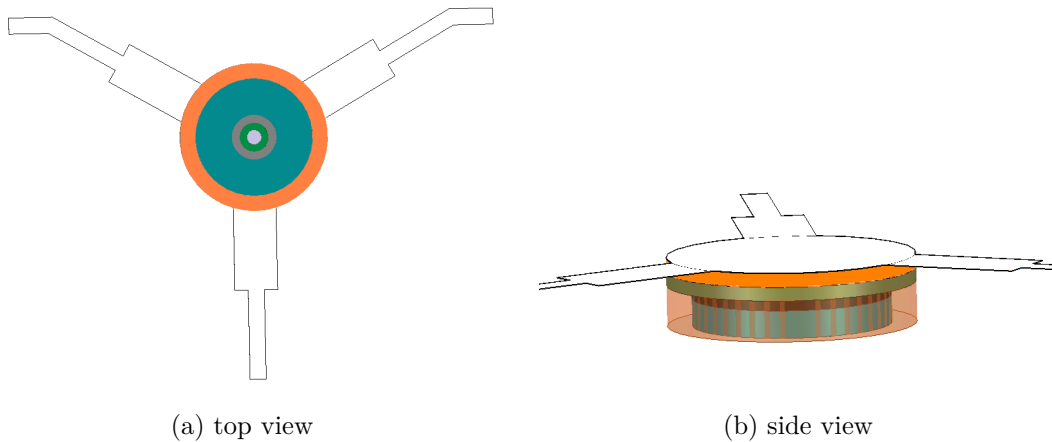


Figure IV.24: 3D modeling of ferrite puck – Ferrite material is divided into different annulus sectors.

The non-homogeneity in each layer is introduced by dividing the disk into several concentric annuli around a central cylinder. In each region the internal field is considered to be uniform in magnitude and direction. Each region is defined as a separate material with its own permeability tensor in HFSS simulations.

EM properties of these computational regions are characterized by permeability tensors. In each region the permeability tensor is calculated using the generalized permeability tensor (GPT) model considering the internal field polarization and hysteresis phenomenon. GPT model gives a more realistic representation of EM properties of the ferrite material in a predictive way whatever their magnetization state is.

For each region, all the input parameters of the GPT model are the same except for the internal field value. The predictive nature of the GPT model, make it possible to find permeability tensor components for all the regions in a single computation procedure. Real and imaginary parts of permeability tensor components are imported to HFSS as frequency dependent dataset points. Each of the annulus regions is defined as a new material in Ansys HFSS by using the frequency dependent functions obtained using inbuilt piecewise linear interpolation function.

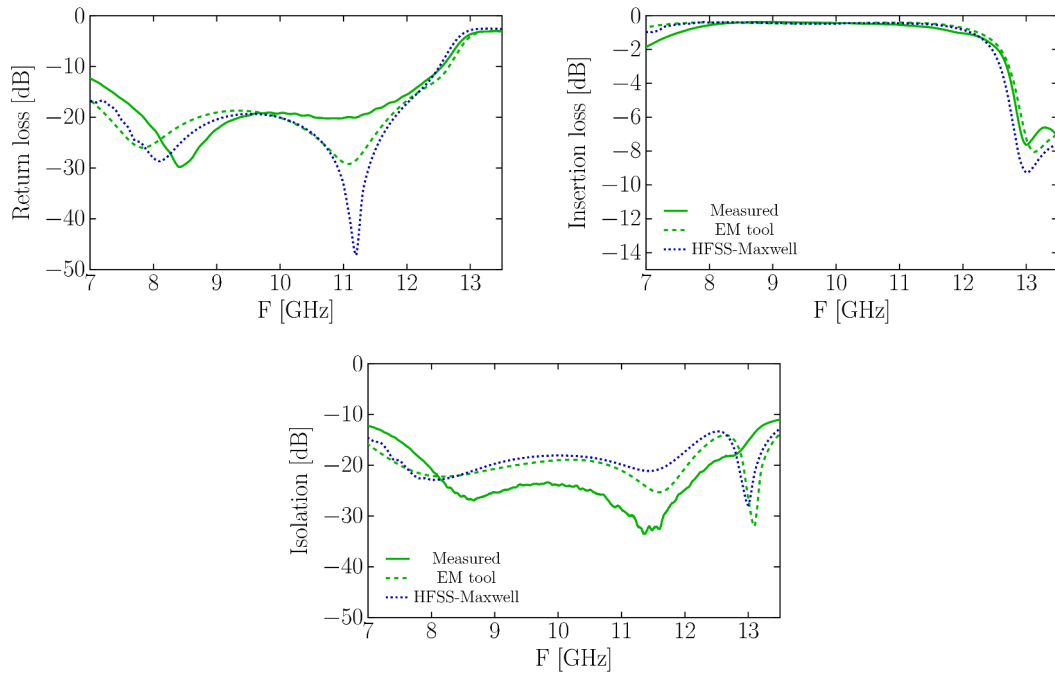


Figure IV.25: Measured and simulated S-parameters of Y-junction microstrip circulator: Non-uniform biasing fields assumption.

The frequency domain simulations are done for a frequency range from 6 GHz up to 14 GHz. The simulated S-parameters are then compared with the measured S parameters.

Measured and simulated S-parameters are shown in the Figure IV.25. Results are then also compared with Maxwell-HFSS combined simulations. Theoretical results show good agreement with the measurement results. These results validate the use of proposed theoretical tool in the limit case- saturated ferrites.

Our approach shows good agreement with the results obtained with HFSS-Maxwell combined simulations although these simulations use Polder model. This is due to the fact that GPT model gives similar results with polder model in saturated state. The integration of theoretical permeability tensor in Ansys HFSS made it possible to do the EM simulations as a function of intensity of applied biasing field, irrespective of their state of magnetization.

By taking into account the inhomogeneity of the internal polarizing fields, proposed theoretical tool can predict the dynamic behavior of ferrite devices more accurately, at all magnetization states. This new theoretical tool will be advantageous for the design of devices working in the partially magnetized states: self-biased circulators/Insulators [51], miniature antennas [58], tunable filters [59], phase shifters [60], etc.

IV.5 Conclusion

In this chapter, we presented a predictive EM tool to study the EM properties of ferrites in a predictive way, whatever their magnetization state is, and takes into account the inhomogeneity of the internal polarization fields. The proposed EM tool combines a theoretical magneto-static solver and generalized permeability tensor model with commercial EM simulation software Ansys HFSS.

Our theoretical EM tool is validated by modeling, and realizing a microstrip Y-junction circulator. This theoretical tool is validated in the limit case saturation by comparing the simulation results with measurements.

We discussed the non-homogeneous internal magnetic fields in anisotropic ferrite materials and their effect on the dynamic behavior of ferrite base devices. A magneto-static analysis of the structure considering inhomogeneous internal fields enabled us to understand the internal biasing field distribution and the demagnetizing field effects on the performances of ferrite based devices.

The integration of magneto-static analysis with EM simulations made it possible to predict the dynamic behavior of ferrite devices more accurately. By taking into account the inhomogeneity of the internal polarizing fields, proposed theoretical tool predict the dynamic behavior of ferrite devices more accurately, at all magnetization states.

This theoretical modeling approach combines experimental techniques to find the physical parameters of the ferrites, and theoretical model which will use these parameters to describe the dynamic behavior of ferrites at any magnetization state. Static input parameters of this theoretical tool are determined using standard material characterization methods. Only dynamic input parameter, damping factor is calculated using the coaxial line technique proposed in the first part of this thesis (Chapter II). Integration of GPT model coupled with magneto-static solver into a commercial EM simulator makes it possible to avoid the limitations of commercial magneto-static, and EM simulations softwares.

This association of theoretical tools with commercial simulation software opens up new perspectives for the study and the design of microwave ferrite based applications. Keeping in mind the fact that GPT model is valid at any magnetization state unlike Polder model which is only valid in the saturated state, the proposed approach show good advantage over conventional EM simulation methods.

Integration of magneto-static analysis enhances the predictive nature of GPT model. Thanks to universal nature of the GPT model, this EM tool will be applicable for the design of other ferrite devices regardless of their state of magnetization. This new theoretical tool will be more advantageous for the design of devices working in the partially magnetized states: tunable filters, phase shifters, self-biased circulators/insulators, miniature antennas, etc. This tool will allow us to understand influence of constituent material properties, and their geometrical parameters on the performance of these devices.

Chapitre 4. Résumé

Dans ce chapitre, nous discutons des champs magnétiques internes non homogènes dans les matériaux ferrites anisotropes et de leurs effets sur le comportement dynamique des dispositifs à ferrite. Le champ magnétique statique interne vu par les moments magnétiques dans l'échantillon est réduit par les effets du champ démagnétisant. Tout d'abord, pour estimer les effets démagnétisants macroscopiques dus à la forme de l'échantillon, nous avons mesuré les spectres d'absorption d'échantillons denses de composition identique (Yttrium Iron Garnet-YIG) mais d'épaisseurs différentes. Les pics d'absorption de puissance se déplacent vers des fréquences plus élevées lorsque le champ appliqué augmente. La variation de la fréquence du pic d'absorption en fonction du champ appliqué suit une relation linéaire de pente positive proche de la valeur du rapport gyromagnétique 2,8 MHz/Oe.

Les spectres d'absorption de puissance des matériaux ferrites denses montrent la présence de pics de résonance secondaires. Ces pics secondaires entraînent un élargissement de l'absorption à proximité de la résonance. Ces pics suivent un comportement attendu : lorsque le champ statique augmente, les pics de résonance se déplacent vers des fréquences plus élevées. Après la saturation, chaque pic de résonance montre une variation linéaire de la fréquence avec l'augmentation du champ statique. L'analyse EM initiale de la cellule de mesure dans l'approximation quasi-TEM ne prédit pas ces pics secondaires dans le spectre de puissance absorbée. La simulation HFSS utilisant une polarisation uniforme produit des résultats similaires à ceux de l'analyse quasi-TEM, et ne peut pas expliquer l'élargissement de l'absorption de puissance près de la fréquence de résonance. En effet, ces simulations considèrent une valeur approximative unique pour le coefficient démagnétisant et une aimantation uniforme dans l'échantillon. En réalité, le coefficient démagnétisant N est une quantité tensorielle qui varie suivant les directions de l'espace à l'intérieur de l'échantillon. Cela conduit à des champs internes inhomogènes à l'intérieur du matériau ferrite.

Une étude magnétostatique utilisant Maxwell 3DTM d'Ansys peut être utilisée pour trouver les champs internes non uniformes dans le matériau de ferrite. Les spectres d'absorption de puissance simulés à l'aide de la combinaison de Maxwell 3D et de HFSS montrent des pics multiples en accord avec les résultats de mesure. A partir de ces résultats, il est clair que les pics multiples et l'élargissement des pertes dans les spectres d'absorption sont dus

à la non-uniformité des champs internes à l'intérieur du matériau de ferrite. Cette étude conclut que les effets des champs démagnétisants sont importants dans les échantillons non ellipsoïdaux. Il est donc nécessaire d'évaluer les effets du champ démagnétisant et de calculer avec précision les champs internes non homogènes dans le matériau de ferrite pour obtenir de meilleurs résultats avec des simulations EM.

L'association de Maxwell 3D avec HFSS produit des résultats satisfaisants dans le cas de matériaux ferrites saturés. Cette description de l'aimantation est suffisante pour les matériaux à l'état saturé mais ne convient pas à la description d'autres états d'aimantation. Le comportement dynamique du ferrite dans les états rémanent ou partiellement aimanté ne peut être décrit par cette approche théorique.

Dans la suite nous présentons un outil prédictif pour étudier les propriétés EM des ferrites de manière prédictive, quel que soit leur état d'aimantation, et prenant en compte l'inhomogénéité des champs internes. L'outil proposé combine un solveur théorique magnétostatique et un modèle tensoriel généralisé de perméabilité avec un logiciel commercial de simulation Ansys HFSSTM. L'analyse magnétostatique de la structure en considérant des champs internes inhomogènes nous a permis de comprendre la distribution du champ de polarisation interne et les effets du champ démagnétisant sur les performances des dispositifs à ferrite. L'intégration de l'analyse magnétostatique avec des simulations EM a permis de prédire plus précisément le comportement dynamique de ces dispositifs.

Cette approche de modélisation théorique combine des techniques expérimentales pour trouver les paramètres physiques des ferrites et un modèle théorique qui utilisera ces paramètres pour décrire le comportement dynamique à n'importe quel état d'aimantation. Les paramètres statiques de cet outil théorique sont déterminés à l'aide de méthodes standards de caractérisation des matériaux. Seul le paramètre dynamique, le facteur d'amortissement « α », est calculé en utilisant la technique en ligne coaxiale proposée dans la première partie de cette thèse (Chapitre II). L'intégration du modèle GPT couplé au solveur magnétostatique dans un simulateur commercial EM permet d'éviter les limites des logiciels commerciaux de simulation magnétostatique et EM. En considérant l'inhomogénéité des champs internes de polarisation, l'outil théorique proposé sera capable de prédire le comportement dynamique des dispositifs à ferrite de manière plus précise, à tous les états d'aimantation.

Le tenseur de perméabilité est calculé dans plusieurs zones du matériau en utilisant un modèle généralisé de tenseur de perméabilité prenant en compte le tenseur de coefficients démagnétisants correspondant et l'amplitude et la direction du champ interne. Dans la conception HFSS, ces zones sont définies comme des matériaux différents ou simplement comme des régions de calcul dans lesquelles le matériau est le même mais avec différents champs internes de polarisation magnétique. Pour chaque région, les parties réelles et

imaginaires des composantes du tenseur de perméabilité sont définies comme des fonctions dépendantes de la fréquence dans HFSS. Les paramètres S sont ensuite calculés en utilisant le solveur dans le domaine fréquentiel. En tenant compte de l'inhomogénéité des champs internes de polarisation, l'outil théorique proposé peut prédire le comportement dynamique des ferrites anisotropes plus précisément, à tous les états d'aimantation.

Afin de mettre en évidence l'efficacité de l'outil de simulation EM développé et de démontrer la nécessité d'un outil capable de prédire de manière réaliste leurs performances, nous l'avons appliqué à la conception d'un dispositif à ferrite. Notre outil EM théorique a été utilisé pour la modélisation et la réalisation d'un circulateur micro-ruban à jonction Y. Cet outil théorique a été validé dans des cas limites en comparant les résultats de simulation avec les mesures.

Cette association d'outils théoriques et de logiciels commerciaux de simulation ouvre de nouvelles perspectives pour l'étude et la conception de dispositifs micro-ondes à ferrite. En gardant à l'esprit le fait que le modèle GPT est valide à n'importe quel état d'aimantation contrairement au modèle de Polder qui n'est valable qu'à l'état saturé, l'approche proposée présente un bon avantage par rapport aux méthodes conventionnelles de simulation EM. L'intégration de l'analyse magnétostatique améliore la nature prédictive du modèle GPT. Grâce à la nature universelle du modèle GPT, cet outil EM s'applique à la conception d'autres dispositifs de ferrite indépendamment de leur état d'aimantation. Ce nouvel outil théorique sera plus avantageux pour la conception de dispositifs fonctionnant dans les états partiellement aimantés: filtres accordables, déphaseurs, circulateurs auto-polarisés, isolateurs, antennes miniatures, etc. Cet outil nous permettra de comprendre l'influence des propriétés du matériau constitutif et de sa forme géométrique sur les performances de ces dispositifs.

Conclusion and Perspectives

Ferrite materials are widely used in microwave electronics for many telecommunication applications due to their low insertion loss in the direction of propagation, and their high level of isolation in the other direction. Dynamic behavior of ferrite material can be represented by the tensor permeability $\hat{\mu}$, each component of which has a double dependence with respect to the frequency and the static magnetic field H_{dc} . Consequently, design and optimization of microwave devices using ferrite materials requires a realistic knowledge of its dynamic response, namely permittivity and permeability and, on the other hand, control of wave propagation that condition their performance. Commercial simulation software use different theoretical models to describe the permeability tensor, $\hat{\mu}$ according to the state of magnetization. However, most of the EM simulators remain limited to certain states of magnetization, due to the simplified assumptions on which their permeability models are based upon.

In this thesis work, we presented a predictive electromagnetic tool to study the EM properties of ferrites in a predictive way, whatever their magnetization state is, and takes into account the inhomogeneity of the internal polarization fields. This theoretical modeling approach combines experimental techniques to find the physical parameters of the ferrites, and theoretical model which will use these parameters to describe the dynamic behavior of ferrites at any magnetization state.

This thesis work is carried out mainly in two parts: in the first part, we worked on the characterization technique to find the unique dynamic input parameter of generalized permeability tensor model, and in the second step we worked on the integration of this theoretical permeability model and a magneto-static solver in a commercial EM simulator Ansys HFSS.

In the first part of the thesis, we presented a broadband coaxial line method for damping factor measurement. Theoretical S-parameters are calculated using the direct EM analysis of the measurement cell. In the inverse problem of the coaxial line method, an optimization procedure is developed to optimize the damping factor α by matching theoretical S-parameters with measured S-parameters. The results are validated by comparing with supplier's data sheets.

By avoiding the use of phases of S-parameters, uncertainties due to the dimensional resonances are avoided in the inverse problem. On the contrary, our inverse problem exploits these resonances to converge the spectra of the amplitudes of the S-parameters more rapidly and more precisely. Standard resonant cavity methods are limited to a single frequency corresponding to the resonant frequency of the measurement cavity, and these methods require the sample to be spherical in shape and sample length to be small compared to one quarter of the wavelength of the microwave radiation in the sample. The coaxial line method eliminates the shape and size constraints related to the resonant cavity and the samples imposed by the standard resonant cavity methods. This broadband characterization method can be implemented easily, and can be used from DC to millimeter wave frequencies. The damping factor α is a more realistic representation of dynamic losses of ferrites than the parameters currently used: ΔH and ΔH_{eff} . Knowledge of a unique parameter representing dynamic losses would assist engineers in optimizing design and adjustment procedures for ferrite-based microwave devices (Eg: circulators).

During the second part of the thesis, we developed an EM modeling tool which combines a theoretical magneto-static solver and generalized permeability tensor model with commercial simulation software Ansys HFSS. Static input parameters like saturation magnetization $4\pi M_s$, anisotropy field H_a , etc., are measured using standard material characterization methods. Only dynamic input parameter, damping factor is calculated using the coaxial line technique proposed in the first part of this thesis.

Our theoretical EM tool is validated by modeling, and realizing a microstrip Y-junction circulator. Integration of GPT model coupled with magneto-static solver into a commercial EM simulator made it possible to avoid the limitations of commercial magneto-static and EM simulations softwares. Keeping in mind the fact that GPT model is valid at any magnetization state unlike Polder model which is only valid in the saturated state, the proposed approach show very good advantage over conventional EM simulations. A magneto-static analysis of the structure considering inhomogeneous internal fields enabled us to understand the internal bias field distribution and the demagnetizing field effects on the performances of circulator. Integration of magneto-static analysis enhances the predictive nature of GPT model and enabled us to predict the dynamic behavior of ferrite devices more accurately. It will allow us to understand influence of constituent material properties, and their geometrical parameters, on the performance of these devices.

By taking into account the inhomogeneity of the internal polarizing fields, proposed theoretical tool can predict the dynamic behavior of ferrite devices more accurately, at all magnetization states. This association of theoretical tools with commercial simulation software opens up new perspectives for the study and the design of microwave ferrite based applications.

In conclusion, we have successfully developed a theoretical tool to fill the obvious void in the field of ferrite based device modeling which forces the designers to follow a trial and error approach. This theoretical and experimental tools we have developed, which give direct access to the only dynamic input parameter (damping factor) of the GPT model and association of theoretical models with commercial simulation software, constitute a serious alternative to the conventional procedure (resonant cavity methods) and the use of Polder formulations. Thanks to universal nature of the GPT model, this EM tool will be applicable for the design of other ferrite devices regardless of their state of magnetization. This design tool will help the designers to reduce the cost and time for the development of new ferrite devices.

Furthermore, it will be interesting to use the coaxial line method for the determination of damping factor of ferrite materials in the millimeter wave frequencies. New theoretical EM tool will be more advantageous for the ferrite devices in the partially magnetized states like tunable filters, phase shifters, self-biased circulators/insulators, miniature antennas, etc. It will be interesting to use this theoretical tool in the case of devices which uses pre-oriented ferrite materials and for frequency-agile antennas.

Bibliography

- [1] *Magnetism: Fundamentals, Materials and Applications*. Springer Science & Business Media, Oct. 2002. Google-Books-ID: 2w840sO28pAC.
- [2] M. Pardavi-Horvath, “Microwave applications of soft ferrites,” *Journal of Magnetism and Magnetic Materials*, vol. 215-216, pp. 171–183, June 2000.
- [3] C. A. Balanis, *Advanced Engineering Electromagnetics, 2nd Edition*. Wiley, Jan. 2012. Google-Books-ID: 2eMbAAAAQBAJ.
- [4] L. F. Chen, C. K. Ong, C. P. Neo, V. V. Varadan, and V. K. Varadan, *Microwave Electronics: Measurement and Materials Characterization*. John Wiley & Sons, Nov. 2004. Google-Books-ID: 1vmUdUXIBNIC.
- [5] A. Aharoni, *Introduction to the Theory of Ferromagnetism*. Oxford University Press, 2000. Google-Books-ID: 9RvNuIDh0qMC.
- [6] J. A. Osborn, “Demagnetizing Factors of the General Ellipsoid,” *Physical Review*, vol. 67, pp. 351–357, June 1945.
- [7] E. C. Stoner, “The demagnetizing factors for ellipsoids,” *The London, Edinburgh, and Dublin Philosophical Magazine and Journal of Science*, vol. 36, pp. 803–821, Dec. 1945.
- [8] M. Beleggia, D. Vokoun, and M. De Graef, “Demagnetization factors for cylindrical shells and related shapes,” *Journal of Magnetism and Magnetic Materials*, vol. 321, pp. 1306–1315, May 2009.
- [9] S. G. Sandomirskii, “Calculation of short hollow cylinders under magnetization parallel to the generatrix,” *Russian Electrical Engineering*, vol. 80, pp. 109–112, Feb. 2009.
- [10] L. D. Landau and E. Lifshitz, “On the theory of the dispersion of magnetic permeability in ferromagnetic bodies,” *Phys. Z. Sowjetunion*, vol. 8, no. 153, pp. 101–114, 1935.
- [11] G. T.L, “A Lagrangian formulation of the gyromagnetic equation of the magnetic field,” *Physical Review*, vol. 100, no. 4, p. 1235, 1955.
- [12] T. L. Gilbert, “A phenomenological theory of damping in ferromagnetic materials,” *IEEE Transactions on Magnetics*, vol. 40, pp. 3443–3449, Nov. 2004.

- [13] A. G. Gurevich and G. A. Melkov, *Magnetization Oscillations and Waves*. CRC Press, Sept. 1996. Google-Books-ID: YgQtSvFIvFQC.
- [14] D. M. Pozar, *Microwave engineering*. Hoboken, NJ: Wiley, 2012.
- [15] D. Polder and J. Smit, “Resonance Phenomena in Ferrites,” *Reviews of Modern Physics*, vol. 25, pp. 89–90, Jan. 1953.
- [16] *Gyromagnetic materials intended for application at microwave frequencies -Measuring methods for properties*, vol. 60556. International Electrotechnical Commission std., 2006.
- [17] V. G. Harris, A. Geiler, Y. Chen, S. D. Yoon, M. Wu, A. Yang, Z. Chen, P. He, P. V. Parimi, X. Zuo, C. E. Patton, M. Abe, O. Acher, and C. Vittoria, “Recent advances in processing and applications of microwave ferrites,” *Journal of Magnetism and Magnetic Materials*, vol. 321, pp. 2035–2047, July 2009.
- [18] W. Weir, “Automatic measurement of complex dielectric constant and permeability at microwave frequencies,” *Proceedings of the IEEE*, vol. 62, no. 1, pp. 33–36, 1974.
- [19] A. M. Nicolson and G. F. Ross, “Measurement of the Intrinsic Properties of Materials by Time-Domain Techniques,” *IEEE Transactions on Instrumentation and Measurement*, vol. 19, no. 4, pp. 377–382, 1970.
- [20] P. Queffelec, P. Gelin, J. Gieraltowski, and J. Loaec, “A microstrip device for the broad band simultaneous measurement of complex permeability and permittivity,” *IEEE Transactions on Magnetics*, vol. 30, pp. 224–231, Mar. 1994.
- [21] P. Queffelec, M. Le Floc’h, and P. Gelin, “New method for determining the permeability tensor of magnetized ferrites in a wide frequency range,” *IEEE Transactions on Microwave Theory and Techniques*, vol. 48, pp. 1344–1351, Aug. 2000.
- [22] P. Queffelec, S. Mallegol, and M. LeFloc’h, “Automatic measurement of complex tensorial permeability of magnetized materials in a wide microwave frequency range,” *IEEE Transactions on Microwave Theory and Techniques*, vol. 50, pp. 2128–2134, Sept. 2002.
- [23] J. E. Lezaca, P. Queffelec, and A. Chevalier, “Generalized Measurement Method for the Determination of the Dynamic Behavior of Magnetic Materials in Any Magnetization State,” *IEEE Transactions on Magnetics*, vol. 46, pp. 1687–1690, June 2010.
- [24] P. Queffelec, M. Le Floc’h, and P. Gelin, “Nonreciprocal cell for the broadband measurement of tensorial permeability of magnetized ferrites: direct problem,” *IEEE Transactions on Microwave Theory and Techniques*, vol. 47, pp. 390–397, Apr. 1999.

- [25] E. K. Chong and S. H. Zak, *An introduction to optimization*, vol. 76. John Wiley & Sons, 2013.
- [26] J. E. Lezaca, P. Queffelec, and A. Chevalier, “Broadband permeability measurement method for ferrites at any magnetization state: direct problem,” *International Journal of Microwave and Wireless Technologies*, vol. 3, pp. 289–294, June 2011.
- [27] P. Gelin, P. Queffelec, and F. Le Pennec, “Effect of domain and grain shapes on the dynamical behavior of polycrystalline ferrites: Application to the initial permeability,” *Journal of Applied Physics*, vol. 98, no. 5, p. 053906, 2005.
- [28] A. Chevalier, J. Cortes, J. Lezaca, and P. Queffelec, “Broadband permeability measurement method for ferrites at any magnetization state: Experimental results,” *Journal of Applied Physics*, vol. 114, no. 17, 2013.
- [29] A. Guennou, P. Queffelec, P. Gelin, and J. L. Mattei, “Coupled Magneto-static/Electromagnetic Studies of Nonuniformly Biased $\lambda/4$ -Junction Circulator: Application to Transmission Bandwidth Increase,” *IEEE Transactions on Magnetics*, vol. 43, pp. 3645–3651, Sept. 2007.
- [30] E. Schloemann, “Microwave Behavior of Partially Magnetized Ferrites,” *Journal of Applied Physics*, vol. 41, pp. 204–214, Jan. 1970.
- [31] G. T. Rado, “Theory of the Microwave Permeability Tensor and Faraday Effect in Nonsaturated Ferromagnetic Materials,” *Physical Review*, vol. 89, pp. 529–529, Jan. 1953.
- [32] J. Green and F. Sandy, “Microwave Characterization of Partially Magnetized Ferrites,” *IEEE Transactions on Microwave Theory and Techniques*, vol. 22, pp. 641–645, June 1974.
- [33] M. Igarashi and Y. Naito, “Tensor permeability of partially magnetized ferrites,” *IEEE Transactions on Magnetics*, vol. 13, pp. 1664–1668, Sept. 1977.
- [34] M. Igarashi and Y. Naito, “Parallel Component μ_z of Partially Magnetized Microwave Ferrites,” *IEEE Transactions on Microwave Theory and Techniques*, vol. 29, pp. 568–571, June 1981.
- [35] D. Polder, “On the theory of ferromagnetic resonance,” *Physica*, vol. 15, no. 1, pp. 253–255, 1949.
- [36] P. Gelin and P. Queffelec, “Generalized Permeability Tensor Model: Application to Barium Hexaferrite in a Remanent State for Self-Biased Circulators,” *IEEE Transactions on Magnetics*, vol. 44, no. 1, pp. 24–31, 2008.

- [37] C. Kittel, "On the theory of ferromagnetic resonance absorption," *Physical Review*, vol. 73, no. 2, p. 155, 1948.
- [38] E. Stoner and E. Wohlfarth, "A mechanism of magnetic hysteresis in heterogeneous alloys," *IEEE Transactions on Magnetics*, vol. 27, pp. 3475–3518, July 1991.
- [39] K. S. Cole and R. H. Cole, "Dispersion and Absorption in Dielectrics II. Direct Current Characteristics," *The Journal of Chemical Physics*, vol. 10, pp. 98–105, Feb. 1942.
- [40] M. L. Kales, "Modes in Wave Guides Containing Ferrites," *Journal of Applied Physics*, vol. 24, pp. 604–608, May 1953.
- [41] P. S. Epstein, "Theory of Wave Propagation in a Gyromagnetic Medium," *Reviews of Modern Physics*, vol. 28, pp. 3–17, Jan. 1956.
- [42] M. E. Brodwin and D. A. Miller, "Propagation of the Quasi-TEM Mode in Ferrite-Filled Coaxial Line," *IEEE Transactions on Microwave Theory and Techniques*, vol. 12, no. 5, pp. 496–503, 1964.
- [43] T. Lewis, "Propagation constant in a ferrite-filled coaxial waveguide," *Proceedings of the IEEE*, vol. 55, pp. 241–242, Feb. 1967.
- [44] R. S. Mueller and F. J. Rosenbaum, "Propagation in Ferrite-Filled Coaxial Transmission Lines," *IEEE Transactions on Microwave Theory and Techniques*, vol. 16, no. 10, pp. 835–842, 1968.
- [45] T. F. Coleman and Y. Li, "An Interior Trust Region Approach for Nonlinear Minimization Subject to Bounds," *SIAM Journal on Optimization*, vol. 6, pp. 418–445, May 1996.
- [46] J. R. Baker-Jarvis, M. D. Janezic, B. F. Riddle, R. T. Johnk, C. L. Holloway, R. G. Geyer, and C. A. Grosvenor, "Measuring the Permittivity and Permeability of Lossy Materials: Solids, Liquids, Metals, and negative-Index Materials," *Technical Note (NIST TN) - 1536*, Feb. 2005.
- [47] A. Le Gouellec, G. Verissimo, V. Laur, P. Queffelec, I. Albert, and T. Girard, "Modeling non-saturated ferrite-based devices: Application to twin toroid ferrite phase shifters," *Journal of Applied Physics*, vol. 120, p. 073902, Aug. 2016.
- [48] J. D. Adam, L. E. Davis, G. F. Dionne, E. F. Schloemann, and S. N. Stitzer, "Ferrite devices and materials," *IEEE Transactions on Microwave Theory and Techniques*, vol. 50, pp. 721–737, Mar. 2002.

- [49] V. G. Harris, “Modern Microwave Ferrites,” *IEEE Transactions on Magnetics*, vol. 48, pp. 1075–1104, Mar. 2012.
- [50] L. Qassym, G. Cibien, R. Lebourgeois, G. Martin, and D. Colson, “New ferrimagnetic garnets for ltcc-technology circulators,” *International Symposium on Microelectronics*, vol. 2016, no. 1, pp. 000586–000590, 2016.
- [51] V. Laur, G. Vérissimo, P. Quéffélec, L. A. Farhat, H. Alaaeddine, E. Laroche, G. Martin, R. Lebourgeois, and J. P. Ganne, “Self-Biased Y-Junction Circulators Using Lanthanum- and Cobalt-Substituted Strontium Hexaferrites,” *IEEE Transactions on Microwave Theory and Techniques*, vol. 63, pp. 4376–4381, Dec. 2015.
- [52] V. Laur, J.-L. Mattei, G. Vérissimo, P. Queffelec, R. Lebourgeois, and J.-P. Ganne, “Application of Molded Interconnect Device technology to the realization of a self-biased circulator,” *Journal of Magnetism and Magnetic Materials*, vol. 404, pp. 126–132, Apr. 2016.
- [53] H. How, S. Oliver, S. McKnight, P. Zavracky, N. McGruer, C. Vittoria, and R. Schmidt, “Influence of nonuniform magnetic field on a ferrite junction circulator,” *IEEE Transactions on Microwave Theory and Techniques*, vol. 47, pp. 1982–1989, Oct. 1999.
- [54] M. A. Tsankov and L. G. Milenova, “Design of self-biased hexaferrite waveguide circulators,” *Journal of Applied Physics*, vol. 73, pp. 7018–7020, May 1993.
- [55] S. A. Oliver, P. Shi, N. E. McGruer, C. Vittoria, W. Hu, H. How, S. W. McKnight, and P. M. Zavracky, “Integrated self-biased hexaferrite microstrip circulators for millimeter-wavelength applications,” *IEEE Transactions on Microwave Theory and Techniques*, vol. 49, pp. 385–387, Feb. 2001.
- [56] B. K. O’Neil and J. L. Young, “Experimental Investigation of a Self-Biased Microstrip Circulator,” *IEEE Transactions on Microwave Theory and Techniques*, vol. 57, pp. 1669–1674, July 2009.
- [57] H. Bosma, “On the principle of stripline circulation,” *Proceedings of the IEE - Part B: Electronic and Communication Engineering*, vol. 109, no. 21S, pp. 137–146, 1962.
- [58] F. Canneva, F. Ferrero, A. Chevalier, J.-M. Ribero, J.-L. Mattei, P. Queffelec, and R. Staraj, “Miniature Reconfigurable Antenna with Magneto Dielectric Substrate for DVB-H Band,” *Microwave and Optical Technology Letters*, vol. 55, no. 9, pp. 2007–2011, 2013.

- [59] X. Yang, J. Wu, S. Beguhn, T. Nan, Y. Gao, Z. Zhou, and N. X. Sun, “Tunable Bandpass Filter Using Partially Magnetized Ferrites With High Power Handling Capability,” *IEEE Microwave and Wireless Components Letters*, vol. 23, pp. 184–186, Apr. 2013.
- [60] A. Abuelma’atti, I. Khairuddin, A. Gibson, I. Morgan, and A. Haigh, “A Twin Toroid Ferrite Phase Shifter,” in *2007 IEEE/MTT-S International Microwave Symposium*, pp. 2067–2070, June 2007.

Publications

1. Electromagnetic modeling of anisotropic ferrites - Application to microstrip Y-junction circulator design, V. V K Thalakkatukulathil, A. Chevalier, G. Verissimo, V.Laur, P. Queffelec, L. Qassym, and R. Lebourgeois, Journal of Applied Physics (under preparation)

Conferences

1. Modélisation et fabrication en technologie LTCC d'un circulateur microruban à jonction Y, Vinod V K Thalakkatukulathil, A. Chevalier et P. Queffelec, 15^{èmes} Journées de Caractérisation Microondes et Matériaux, Paris, 19-21 Mars 2018.
2. Caractérisation de matériaux magnétiques anisotropes en ligne coaxiale, Vinod V K Thalakkatukulathil, A. Chevalier et P. Queffelec, XX^{èmes} Journées Nationales Microondes, Saint-Malo, 2017.
3. Caractérisation électromagnétique des matériaux magnétiques anisotropes : vers une nouvelle approche de la détermination de la largeur de raie à mi-hauteur, Vinod V K Thalakkatukulathil, A. Chevalier et P. Queffelec, 14^{èmes} Journées de Caractérisation Microondes et Matériaux, Calais, 23-25 Mars 2016.

Modélisation et Caractérisation de matériaux ferrites anisotropes pour les dispositifs micro-ondes isolateurs/circulateurs

Les circulateurs et les isolateurs à ferrite sont couramment utilisés dans l'électronique hyperfréquence en raison de leur forte résistivité électrique et de leur aimantation spontanée élevée. La conception et l'optimisation des dispositifs micro-ondes à ferrites nécessitent d'une part la connaissance de leurs propriétés dynamiques, permittivité complexe et tenseur de perméabilité, et d'autre part le contrôle de la propagation de l'onde électromagnétique (EM) qui conditionne leurs performances. Les logiciels commerciaux de simulation utilisent différents modèles théoriques pour décrire le tenseur de perméabilité en fonction de l'état d'aimantation. Cependant la plupart de ces simulateurs EM restent limités à des états particuliers d'aimantation en raison des hypothèses simplificatrices des modèles de perméabilité utilisés.

Dans ce travail de thèse, nous présentons un outil prédictif pour l'étude des propriétés EM des ferrites quel que soit leur état d'aimantation et qui tient compte de l'inhomogénéité des champs internes de polarisation. Cette modélisation combine des techniques expérimentales de détermination des paramètres physiques des ferrites et un modèle théorique qui utilise ces paramètres pour décrire le comportement dynamique des ferrites quel que soit l'état d'aimantation.

Dans la première partie de la thèse nous présentons une méthode large bande en ligne coaxiale pour la mesure du coefficient d'amortissement. Les paramètres S théoriques sont calculés à partir d'une analyse EM (problème directe) de la cellule de mesure. Pour le problème inverse, une optimisation numérique a été développée pour calculer le coefficient d'amortissement (α) par comparaison des paramètres S calculés avec ceux mesurés.

Dans la seconde partie de la thèse, nous présentons un outil théorique de modélisation EM qui combine une analyse magnétostatique, un modèle du tenseur de perméabilité généralisé (GPT) et le simulateur Ansys HFSSTM. La majorité des paramètres d'entrée comme l'aimantation à saturation ou le champ d'anisotropie peuvent être mesurés à l'aide de techniques standards de caractérisation statique. Seul le paramètre dynamique, le coefficient d'amortissement, est déterminé à l'aide de la technique en ligne coaxiale proposée dans la première partie de la thèse. L'outil théorique développé est ensuite validé par la modélisation et la réalisation d'un circulateur micro-ruban à jonction Y. Grâce à la prise en compte de l'inhomogénéité des champs internes de polarisation, l'outil théorique proposé permet de mieux prédire le comportement dynamique des dispositifs à ferrites et cela pour tout état d'aimantation.

Mots-clés : Modélisation électromagnétique, caractérisation électromagnétique, tenseur de perméabilité généralisé, circulateurs, analyse magnétostatique, HFSS.

Electromagnetic modeling and characterization of anisotropic ferrite materials for microwave Isolators/Circulators

Ferrites are widely used in microwave electronics, particularly for circulators and insulators, because of their high electrical resistivity and high spontaneous magnetization. Design and optimization of microwave devices using ferrites requires realistic knowledge of its dynamic response, namely complex permittivity and permeability tensor and, on the other hand, control of wave propagation that condition their performance. Commercial simulation software use different theoretical models to describe the permeability tensor according to the state of magnetization. However, most of the electromagnetic (EM) simulators remain limited to certain states of magnetization, due to the simplified assumptions on which their permeability models are based upon.

In this thesis work, we presented a predictive electromagnetic tool to study the EM properties of ferrites, whatever their magnetization state is, and takes into account the inhomogeneity of the internal polarization fields. This theoretical modeling approach combines experimental techniques to find the physical parameters of the ferrites, and a theoretical model which will use these parameters to describe the dynamic behavior of ferrites at any magnetization state.

In the first part of the thesis, we presented a broadband coaxial line method for damping factor measurement. Theoretical S parameters are calculated using the EM analysis (direct problem) of the measurement cell. In the inverse problem, a numerical optimization procedure is developed to compute the damping factor (α) by matching theoretical S parameters with measured S parameters.

During the second part of the thesis, we developed a theoretical EM modeling tool which combines a magneto-static solver, generalized permeability tensor model and commercial simulation software Ansys HFSSTM. Most of the input parameters like saturation magnetization, anisotropy field, etc. can be measured using standard characterization methods, except the damping factor used to represent the dynamic losses. Static input parameters of this theoretical tool are determined using standard material characterization methods. Dynamic input parameter, damping factor is calculated using the coaxial line technique proposed in the first part of this thesis. Theoretical EM tool is validated by modeling, and realizing a microstrip Y-junction circulator. By taking into account the inhomogeneity of the internal polarizing fields, proposed theoretical tool can predict the dynamic behavior of ferrite devices more accurately, at all magnetization states.

Keywords: Electromagnetic modeling, damping factor, microwave characterization, generalized permeability tensor, circulators, magneto-static analysis, HFSS.